



The early Toarcian Oceanic Anoxic Event (Jenkyns Event) in the Alpine-Mediterranean Tethys, north African margin, and north European epicontinental seaway

G. Gambacorta ^{a,*}, H.-J. Brumsack ^b, H.C. Jenkyns ^c, E. Erba ^a

^a Dipartimento di Scienze della Terra, Università degli Studi di Milano, Milan, Italy

^b Institute for Chemistry and Biology of the Marine Environment (ICBM), University of Oldenburg, Oldenburg, Germany

^c Department of Earth Sciences, University of Oxford, South Parks Road, Oxford OX1 3AN, UK



ARTICLE INFO

Keywords:

Anoxia
Black shales
Chemostratigraphy
Jurassic
T-OAE
Toarcian

ABSTRACT

The early Toarcian Oceanic Anoxic Event (Jenkyns Event) was associated with major world-wide climatic changes with profound effects on the global carbon cycle. This review revisits the available literature covering the Jenkyns Event applying an updated common stratigraphic definition, allowing illustration of the development and evolution of anoxia in the Alpine-Mediterranean Tethys, north African margin, and North European epicontinental basins within a high-resolution temporal framework. The survey combines geographic and stratigraphic distribution of black shale, organic-matter properties (total organic carbon content and composition), variations in benthic fauna, distribution of euhedral and frambooidal pyrite, and redox conditions reconstructed on the basis of both inorganic and organic geochemical data. The compilation demonstrates that bottom waters were generally well oxygenated prior to the negative carbon-isotope excursion of the Toarcian Oceanic Anoxic Event whose onset was marked by the synchronous deterioration in bottom-water oxygen conditions at supra-regional scale. Persistent euxinia was dominantly confined to the north European epicontinental basins and sub-basins, paralleled by a supraregional decline in oxygen content at the seafloor also in the Alpine-Mediterranean Tethys area. In the interval of time represented by the core of the negative carbon-isotope excursion the most extreme redox conditions were reached along with intense euxinia extending periodically into the photic zone accompanied by deposition of black shales whose organic-matter content reached maximum values. Recovery to better oxygenated conditions was a diachronous process that started, in most places, at a time immediately following the end of the negative carbon-isotope excursion. The Alpine-Mediterranean Tethys became well oxygenated, while north European epicontinental areas experienced anoxia with less intense and intermittent sulphidic conditions interspersed with brief periods of oxygenation. $\Delta^{18}\text{O}$ variations reflect a progressive increase in fresh-water input to the northern European epicontinental basins and sub-basins that reached its acme in correspondence with the lowest values of the negative carbon-isotope anomaly. In these areas, the proximity to sources of fresh-water input and the local physiography or geographic restriction limited water exchange with the Tethys Ocean, favouring the onset of anoxia/euxinia and organic-matter preservation. These basins and sub-basins, due to their relatively closed physiography and redox conditions, acted as pools of dissolved divalent manganese associated with accumulation of iron sulphides. Part of the soluble manganese spilled out of these basins in oxygen minimum zones, being deposited/precipitated at the edge of the more oxygenated Tethys Ocean, and thereby leading to the formation of local manganese-rich carbonates deposited during the Jenkyns Event.

* Corresponding author.

E-mail address: gabriele.gambacorta@guest.unimi.it (G. Gambacorta).

1. Introduction

The Toarcian Oceanic Anoxic Event (T-OAE) was originally identified as a time of globally developed anoxia as indicated by the widespread deposition of lower Toarcian black shales associated with a positive carbon-isotope excursion (Jenkyns, 1985, 1988). Later investigations showed that the broad positive carbon-isotope excursion extending over much of the lower Toarcian is interrupted in its central portion by an abrupt negative carbonate and organic-carbon isotope anomaly (Jenkyns and Clayton, 1986, 1997). This negative carbon-isotope excursion (negative CIE) has now been globally observed both in shallow- and deep-marine records as well as in continental archives (Jenkyns and Clayton, 1986; Hesselbo et al., 2000, 2007; Schouten et al., 2000; Röhl et al., 2001; Jenkyns et al., 2001; Jenkyns et al., 2002; McElwain et al., 2005; Kemp et al., 2005; Emmanuel et al., 2006; van Breugel et al., 2006; Sabatino et al., 2009; Al-Suwaidi et al., 2010; Caruthers et al., 2011; Gröcke et al., 2011; Hesselbo and Pieńkowski, 2011; Izumi et al., 2012; Trabucho-Alexandre et al., 2012; Kafousia et al., 2011; Kafousia et al., 2014; Ikeda and Hori, 2014; Kemp and Izumi, 2014; Reolid, 2014; Xu et al., 2017; Them II et al., 2017; Fantasia et al., 2018; Ikeda et al., 2018; Filatova et al., 2020; Reolid et al., 2020b; Ruebsam and Al-Husseini, 2020; Remirez and Algeo, 2020a, 2020b; Hougård et al., 2021; Erba et al., 2022; Liu et al., 2022; Kemp et al., 2022a; Kunert and Kendall, 2023), and is thus a real phenomenon of the global carbon cycle.

The T-OAE was associated with a phase of extreme global climate change (Jenkyns, 2003; Jenkyns, 2010; Cohen et al., 2004; Ullmann et al., 2013; Percival et al., 2016; Them et al., 2017; Jenkyns and MacFarlane, 2021) characterized by extraordinary warmth (Dera et al., 2011; Korte and Hesselbo, 2011; Gómez et al., 2016; Ruebsam et al., 2020d), accelerated weathering (Jenkyns, 2003; Jenkyns, 2010; Cohen et al., 2004; Ullmann et al., 2013; Percival et al., 2016; Them et al., 2017; Jenkyns and MacFarlane, 2021; Liu et al., 2022), a major marine transgression (Hallam, 1981; Haq et al., 1987; Hesselbo and Jenkyns, 1998; Hardenbol et al., 1998; Hesselbo, 2008), and ocean acidification (Erba, 2004; Trecall et al., 2012; Casellato and Erba, 2015; Posenato et al., 2018; Müller et al., 2020; Ettinger et al., 2021). Widespread accumulation of black shales observed in the north European epicontinental seaway seems to have been associated with relatively low depositional rates of accompanying clastic and carbonate, leading to a degree of enrichment in organic matter even if its flux to the sea floor was not in any way enhanced. In this case, improved preservation of organic matter was largely due to the frequent and prolonged presence of anoxia/euxinia extending upwards from the sea floor (Mattioli et al., 2004, 2009; Reolid et al., 2021a; Kemp et al., 2022b; Ruebsam et al., 2022b). These extreme palaeoenvironmental conditions impacted marine primary producers affecting the biocalcification of calcareous nanoplankton and induced palaeoecological shifts in the dinoflagellate cyst community (Bucefalo Palliani et al., 2002; Erba, 2004; Mattioli et al., 2004, 2008, 2009; Tremolada et al., 2005; Casellato and Erba, 2015; Erba et al., 2019; Reolid et al., 2020b).

Venting of large quantities of greenhouse gases related to the degassing of the Karoo–Ferrar Large Igneous Province (Percival et al., 2015; Heimdal et al., 2021; Ruhl et al., 2022), dissociation of gas hydrates along continental margins and/or terrestrial environments (Hesselbo et al., 2000; Pálfy and Smith, 2000; McElwain et al., 2005; Svensen et al., 2007; Percival et al., 2015; Them et al., 2017; Ruebsam et al., 2019), and/or input of thermogenic methane related to metamorphism of organic-rich sediments (Jenkyns, 2010; Fantasia et al., 2018; Xu et al., 2018) are identified as the main potential triggers of the extreme climatic conditions that existed during the negative carbon-isotope excursion of the T-OAE. The overarching broad positive carbon-isotope excursion is, instead, attributed to accelerated global marine and lacustrine carbon burial, for which an abundant globally distributed sedimentary record exists (Jenkyns, 1988; Jenkyns, 2010; Fantasia et al., 2018; Xu et al., 2018; Silva et al., 2021a).

This study presents an in-depth analysis of literature data available for the distribution of black shales and the stratigraphic variation in redox conditions inferred from both inorganic and organic materials as well as from benthic fauna (i.e., bioturbation, micro- and macro-benthos), during the T-OAE in the Alpine-Mediterranean Tethys, north African margin, and north European epicontinental seaway. Over the years, the lack of a consistent definition of the T-OAE has resulted in the identification of different stratigraphic intervals as diagnostic of the event. As a consequence, many palaeoenvironmental changes and depositional processes described as having occurred within the same time interval are, in fact, diachronous. It is, therefore, necessary to standardize definitions and subdivisions of the T-OAE and establish a unique stratigraphic framework for the analysis and correlation of the available datasets. The aim of this review is to gain a comprehensive picture of temporal changes within a solid stratigraphic framework, allowing the reconstruction of the surface- and bottom-water dynamics and evolution in synchronous time windows.

2. Definition and subdivision of the Toarcian Oceanic Anoxic Event

After the original identification of the T-OAE on the basis of the globally distributed and apparently coeval organic-rich black shales and an accompanying broad positive carbon-isotope excursion interrupted by a negative trough (Jenkyns, 1988; Jenkyns and Clayton, 1997), Bouila et al. (2014) and Bouila and Hinov (2017) identified the T-OAE as the negative CIE disrupting the long-term $\delta^{13}\text{C}$ variation, and divided this interval into two segments: a lower decreasing part and an upper increasing part. However, the identification of these two segments is not always consistent. In fact, only the Sancerre-Couy section shows a wedge-shaped $\delta^{13}\text{C}_{\text{carb}}$ curve, while all the other sections exhibit an intervening valley floor in the $\delta^{13}\text{C}_{\text{carb}}$ and/or $\delta^{13}\text{C}_{\text{org}}$ curves. Therefore, the two-fold subdivision seems inappropriate. Müller et al. (2017) suggested using the term Jenkyns Event as a synonym for the T-OAE and, consequently, the label Jenkyns Event was applied to the entire positive carbon-isotope excursion. Müller et al. (2017) subdivided the Jenkyns Event into three intervals, namely Interval 1, covering the positive plateau preceding the base of the negative CIE, Interval 2 covering the decreasing part and the valley floor of the negative CIE, and Interval 3 matching the rising limb of the negative CIE together with the lower part of the upper plateau in various sections (Fig. 1). Thibault et al. (2018) only considered the negative CIE subdivided in three intervals A, B, and C corresponding to the positive plateau below the negative CIE and a part of the decreasing limb, the valley floor, and the increasing limb, respectively. However, the application of this approach varies significantly from section to section and is thus inconsistent. In particular, the three-fold subdivision is not appropriate for the Sancerre-Couy section where the $\delta^{13}\text{C}_{\text{carb}}$ negative excursion is characterized by a wedge-shaped pattern (Fig. 1). Ruebsam et al. (2019) used the term ‘Toa-CIE’ for the negative $\delta^{13}\text{C}$ excursion and identified three stages: the Toa-CIE stage A being the decline in $\delta^{13}\text{C}$ values, the Toa-CIE stage B corresponding to the valley floor, and the Toa-CIE stage C representing the increase to pre-excursion values. Bouila et al. (2019) suggested that the T-OAE coincides with the negative CIE, although they placed the base as varying from the uppermost part of the lower plateau to the base of the decreasing limb (Fig. 1). Ruebsam and Al-Husseini (2020) did not specify the position of the T-OAE but named the negative CIE the T-CIE and subdivided it into a falling limb, a valley and a rising limb, preceded and followed by a lower and an upper plateau, respectively. Reolid et al. (2020b) used both the terms T-OAE and the ‘Jenkyns Event’ specifying that the former term applies to marine successions with evidence of oxygen-depleted conditions while the latter has to be used for the global changes that occurred during the Early Toarcian, including anoxia, enhanced organic-matter burial, biotic crises in marine and terrestrial ecosystems, warming and sea-level rise. However, precise definitions of the beginning and end of the T-OAE and the Jenkyns Event were not provided, preventing their unambiguous identification and

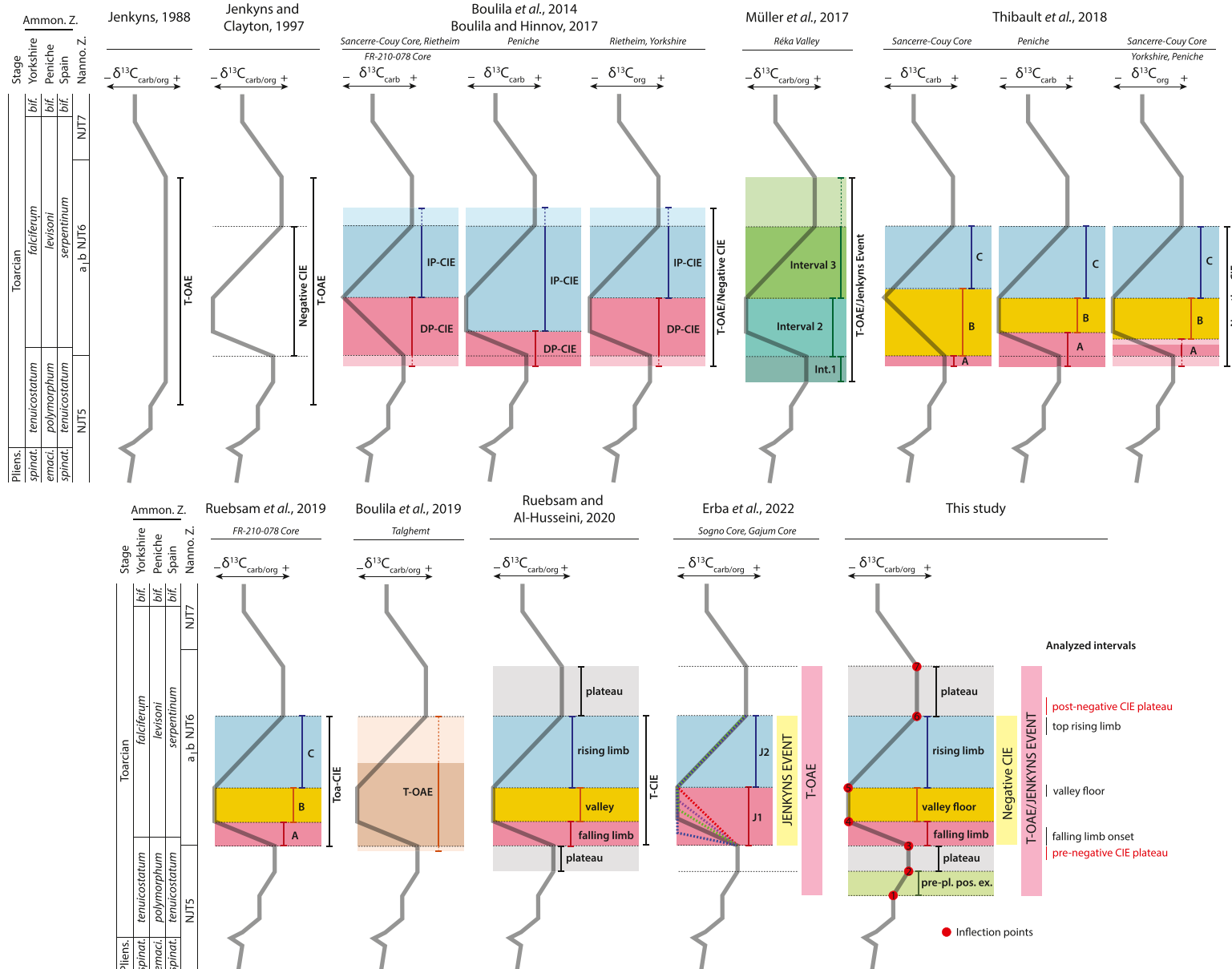


Fig. 1. Definitions and subdivisions proposed for the Toarcian Oceanic Anoxic Event (T-OAE). Schematic $\delta^{13}\text{C}$ reference curve for the latest Pliensbachian–Toarcian time interval is modified after Ruebsam and Al-Husseini, 2020. Ammonite biozones are after Elmi et al. (1997), Macchioni (2002), Page (2003), and Nikitenko et al. (2008). Calcareous nannofossil biozones are after Ferreira et al. (2019) and Visentin and Erba (2021). The vertical dashed lines represent the variability in the extent of the subdivisions. Definitions and subdivisions adopted in this study, and relative stratigraphic position of intervals analysed are reported in the bottom right of the figure. Inflection points, from bottom to top: 1. onset of the pre-plateau positive excursion; 2. onset of the pre-negative CIE plateau interval; 3. onset of the falling limb; 4. base of the falling limb; 5. onset of the rising limb; 6. top of the rising limb; 7. top of the post-negative CIE plateau interval. Negative carbon-isotope excursion: negative CIE; DP-CIE: decreasing part of the negative carbon-isotope excursion; IP-CIE: increasing part of the negative-carbon isotope excursion.

correlation on a regional, supra-regional and global scale. Erba et al. (2022) adopted the definition given by Jenkyns (1988) and used the term T-OAE for the entire overarching C isotopic positive excursion, inclusive of the negative CIE in its central part (Jenkyns, 2010). The term Jenkyns Event was solely applied to the negative CIE, which correlates with the ammonite uppermost *tenuicostatum* Zone–*exaratum* Subzone interval (Xu et al., 2018; Storm et al., 2020) and falling within the NJT6 nannofossil Zone (Ferreira et al., 2019; Visentin and Erba, 2021). Erba et al. (2022) subdivided the Jenkyns Event in two isotopic segments, namely the J1 from the base of the falling limb up to the top of the valley floor, and the J2 for the rising limb (Fig. 1).

In this paper, we adopt the definition of Jenkyns (1988) to identify the T-OAE corresponding to the broad $\delta^{13}\text{C}$ positive excursion, inclusive of the negative CIE in its central portion, and consider the term Jenkyns Event as a synonym for T-OAE, as initially proposed by Müller et al. (2017) (Fig. 1 and Fig. S1 in the Supplementary Material). The literature survey conducted on all the analysed sections shows that only three C isotopic records (Sancerre-Couy, FR-210-078 Core, and Rietheim) exhibit a wedge-shaped profile of the $\delta^{13}\text{C}_{\text{carb}}$ negative CIE but not of the associated $\delta^{13}\text{C}_{\text{org}}$ anomaly (Hermoso et al., 2009a; Ruebsam et al., 2014; Montero-Serrano et al., 2015), possibly as a result of diagenetic imprints on the carbonate record. These $\delta^{13}\text{C}_{\text{carb}}$ profiles, therefore, represent an exception while the typical negative CIE consists of an initial decrease, a valley, and a final increase. Consequently, in this review we adopt the three-fold subdivision of the negative CIE proposed by Ruebsam and Al-Husseini (2020) (Fig. 1). In particular, stratigraphically from bottom to top, we identify within the idealized T-OAE

carbon-isotope profile six isotopic segments: a pre-plateau positive excursion and a pre-negative CIE plateau that predates the negative CIE, a falling limb, a valley floor, and a rising limb forming the negative CIE, and a post-excursion plateau. These segments are separated by inflection points that mark the transition from one segment to the other. In particular, from bottom to top, we identify: an onset point of the pre-plateau positive excursion coincident with the onset of the T-OAE (onset of the pre-plateau positive excursion), an inflection point of the pre-negative CIE plateau (onset of the pre-negative CIE plateau interval); an onset point of the negative carbon-isotope anomaly (onset of the falling limb); an inflection point that marks the transition from the progressively decreasing carbon-isotope values to the valley interval characterized by preferentially light $\delta^{13}\text{C}$ values (base of the falling limb); a point that marks the end of the valley floor and the beginning of the progressive increase back to higher carbon-isotope values (onset of the rising limb); an onset point of the post-excursion plateau with relatively stable $\delta^{13}\text{C}$ values (top of the rising limb); and finally an inflection point that marks the end of the post-excursion plateau and the end of the T-OAE (top of the post-negative CIE plateau interval).

3. Methodology

In the present study we considered only those sections with an available carbon-isotope record, either inorganic or organic, and with a resolution sufficient for identifying the negative carbon-isotope anomaly of the T-OAE. A total of 89 sections offer the above-mentioned characteristics and were used for this review (Fig. 2 and Table 1).

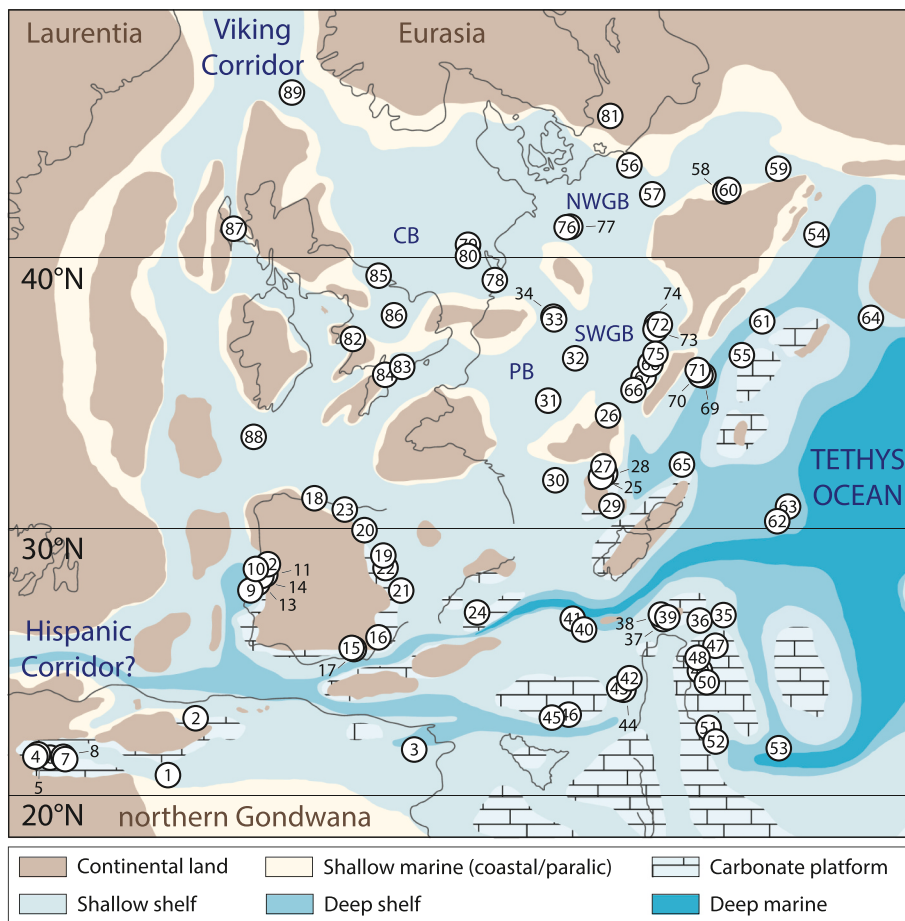


Fig. 2. Palaeogeographic map of Alpine-Mediterranean Tethys and north European epicontinental basins and sub-basins during the Toarcian (modified after Ruebsam et al., 2018) and relative position of locations with known record of the negative carbon-isotope excursion of the T-OAE. CB: Cleveland Basin; PB: Paris Basin; NWGB: Northwestern German Basin; SWGB: Southwestern German Basin.

Table 1

List of sites considered in the study with the relative numerical code used in the text and figures for their identification.

1	Raknet El Kahla	31	Sancerre-Couy Core	61	Réka Valley
2	Mellala	32	Andra HTM 102	62	Úrkút
3	Cháabet El Attaris	33	Bascharage	63	Tölgyhát
4	Dades Valley	34	FR-210-078 Core	64	Dobrávitsa-1
5	Boumardoul n'Imazighn composite section	35	Monte Mangart	65	Creux de l'Ours
6	Amelago	36	Dogna Core	66	Gipf
7	Foum Tilicht	37	Madonna della Corona	67	Riniken
8	Talghemt	38	Colma di Malcesine	68	Rietheim
9	Peniche	39	Sega d'Ala	69	Scheibelberg
10	Figueira da Foz	40	Sogno Core	70	Bächental
11	Fonte Coberta/Rabaçal	41	Gajum Core	71	Sachrang
12	Ribeiro (Coimbra composite section)	42	Valdorbia	72	Dotternhausen
13	Porto de Mós	43	Pozzale	73	Denkingen borehole (BEB 1012)
14	Maria Pares	44	Somma	74	Dormettingen
15	La Cerradura	45	Mercato San Severino	75	Aubach
16	Fuente Vidriera	46	Monte Sorgenza	76	Core L1
17	Arroyo Mingarrón	47	Kovk	77	Schandelah Core
18	West Rodiles-Santa Mera	48	Gornje Jelenje	78	Rijswijk-1 Core
19	La Almunia-Ricla	49	Velebit-A	79	F11-01
20	Castrovido	50	Velebit-B	80	L05-04
21	Sierra Palomera (Rambla del Salto)	51	Petousi	81	Bornholm
22	Barranco de la Cañada	52	Toka	82	Mochras Farm Borehole
23	Castillo de Pedroso	53	Kastelli	83	Winterborne (Kingstone)
24	Es Cosconar (section 4)	54	Zárvá	84	Seavington St Michael
25	Roqueredonde	55	Skladana Skala	85	Yorkshire composite section*
26	Beaujolais (Lafarge quarry)	56	Mechowo IG 1	86	Holwell Quarries
27	Truc de Balduc	57	Gorzów Wielkopolski IG 1	87	Raasy
28	Fontaneilles	58	Sulisowice 38 BN	88	Well 18/25-1
29	Cuers	59	Brody-Lubienica BL 1	89	Gulfaks 34/10-35 Core
30	Penne Château-Granier section	60	Parkoszowice		

* Hawskers Bottoms, Port Mulgrave, Runswick Bay, Kettleness, Saltwick Bay, Old Nabb, Ravenscar, Staithes, Robin Hood's Bay, Blea Wyke (Peak), Saltwick Nab, Dove's Nest borehole, Whitby.

Stratigraphically from bottom to top, the Jenkyns Event was analysed in five time intervals (Fig. 1): a) a 'pre-negative CIE plateau interval' corresponding to the interval directly preceding the onset point of the negative carbon-isotope anomaly of the T-OAE; b) an interval right above the onset point of the negative CIE ('falling limb onset') identified by the basal part of the negative CIE; c) an interval called 'valley floor' associated with the most negative values reached by the negative carbon-isotope anomaly prior to the steady increase back to heavier $\delta^{13}\text{C}$ values, i.e. close to the onset of the rising limb; d) an upper part that features the final interval of the gradual increase back to pre-anomaly values ('top rising limb'); and finally e) the interval immediately following the end of the negative CIE, called 'post-negative CIE plateau interval'.

For each time interval, a series of different parameters were considered in order to map the regional distribution of specific properties within the Alpine-Mediterranean Tethys and in basins/sub-basins of epicontinental northern Europe. The initial review of the stratigraphy available for individual sections resulted in the identification of hiatuses in the interval preceding the negative CIE of the T-OAE based on sedimentological, biostratigraphic and chemostratigraphic criteria.

Based on the lithological description, we mapped the presence or absence of black shales or dark grey shales within each interval, either covering part or the entire interval of interest. However, it should be noted that, for the sake of readability, in those cases where both black shales and dark grey shales were recorded, we report on the maps exclusively the presence of black shales. Moreover, for each interval we reported, where present, the occurrence of dominant terrestrial organic matter (i.e., woody fragments, coaly horizons, etc.). As far as the average total organic carbon (TOC) is concerned, we distinguished six different discrete TOC classes ($\text{TOC} \leq 0.5\%$, $0.5 < \text{TOC} \leq 1.0\%$, $1.0 < \text{TOC} \leq 2.5\%$, $2.5 < \text{TOC} \leq 5.0\%$, $5.0 < \text{TOC} \leq 10.0\%$, and $\text{TOC} > 10.0\%$).

We mapped the relative stratigraphic variation in oxygen-isotope ratios from the onset of the falling limb up to the inflection point at the onset of the rising limb. Most oxygen-isotope data utilized were measured on bulk carbonate, with the exception of the Portuguese

Peniche section (Site 9), the Spanish Barranco de la Cañada (Site 22), and the Yorkshire record in the UK (Site 85) where, in the absence of bulk carbonate data, measurements on belemnites, brachiopods and bivalves were used. For the sake of completeness, we highlighted those records in which a moderate to severe diagenetic overprint was recorded in the oxygen-isotope values. The $\Delta^{18}\text{O}$ were estimated for each interval by subtracting the $\delta^{18}\text{O}$ value at the onset of the rising limb from the $\delta^{18}\text{O}$ value at the onset of the falling limb, the latter used as a background value against which the shift is measured. $\Delta^{18}\text{O}$ is computed as follows:

$$\Delta^{18}\text{O} = \delta^{18}\text{O}_{\text{rising limb onset}} - \delta^{18}\text{O}_{\text{falling limb onset}}$$

Consequently, negative $\Delta^{18}\text{O}$ values indicate a shift to lower oxygen-isotope ratios, while positive $\Delta^{18}\text{O}$ values represent a rise to higher oxygen-isotope ratios.

The presence or absence of benthic fauna (i.e., bioturbation, micro- and macro-benthos) was divided into three major classes: a) intervals with 'no benthic fauna', i.e. intervals completely devoid of benthic fossils and/or bioturbation, in some cases associated with the presence of well-defined laminations; b) intervals with a 'limited benthic fauna', i.e. where benthic fossils are rare to very rare, and/or bioturbation is uncommon; c) intervals where a 'benthic fauna' is present with the persistent presence of benthic fossils and/or intense bioturbation. Moreover, for each site the presence/absence of pyrite either euhedral (nodules, laminae, etc.) or in the form of framboids was plotted. Where available, we also report the average dimension of pyrite framboids, separating three classes: $\leq 5\ \mu\text{m}$, between 5 and $10\ \mu\text{m}$, and $> 10\ \mu\text{m}$.

The redox conditions were reconstructed based both on inorganic and organic data, adopting the classification of redox facies proposed by Tyson and Pearson (1991), with oxic conditions associated with oxygen levels $> 2.0\ \text{ml/l}$, dysoxic conditions characterized by values between 2.0 and $0.2\ \text{ml/l}$, suboxic conditions between 0.2 and $\sim 0\ \text{ml/l}$, anoxic when oxygen content is equal to $0\ \text{ml/l}$, and euxinic when the complete lack of oxygen is accompanied by the presence of free H_2S . As regards inorganic data, the redox conditions were distinguished into four main

classes based on bulk elemental data and isotopic data (e.g., Mo isotopes). In particular, based on inorganic data, we distinguished: a) intervals characterized by fully oxic conditions; b) intervals that reached suboxic conditions; c) intervals that experienced phases of fully anoxic conditions; and d) intervals of anoxia alternated with either short or prolonged interludes of euxinia. Redox conditions were classified also by using CNS data (total organic carbon (TOC), nitrogen and sulfur) and, more precisely, on the basis of molecular biomarkers. Using these data we distinguished oxic–suboxic intervals from those recording anoxic or anoxic–euxinic conditions. The documentation of lipids derived from anaerobic photoautotrophic bacteria (e.g. chlorobactane, okenone, isorenieratane) was used to map the presence of photic-zone euxinia (Summons and Powell, 1986; Sinninghe Damsté et al., 1993; Ruebsam et al., 2018). For each site plotted on the maps the most intense conditions experienced during the specific stratigraphic interval are reported. This approach means that, for example, an interval characterized by pulses of suboxia alternating with oxic conditions was classified as ‘suboxic’, and in cases of fully anoxic or even euxinic conditions alternating with suboxic or oxic conditions the interval was classified as ‘anoxic–euxinic’.

Average Mn and Fe concentrations, where available from elemental data, were reported for each interval. In particular, for Mn we distinguished four classes: a) concentrations ≤ 500 ppm; b) between 500 and 1000 ppm; c) between 1000 and 2000 ppm; and d) concentrations > 2000 ppm. Moreover, the presence of Mn-nodules, Mn-hardgrounds, and general descriptions of Mn-rich carbonates were plotted. As regards Fe, seven classes of average concentrations were defined: a) concentrations $\leq 1\%$; b) between 1 and 2%; c) between 2 and 3%; d) between 3 and 4%; e) between 4 and 5%; f) between 5 and 6%; and g) average concentrations $> 6\%$.

Different proxies may either record processes that operated at different time-scales or have a different sensitivity to changes in redox conditions. For example, short-lived intervals of pore water re-oxygenation could have been recorded by benthic fauna without being resolved by geochemical data. Analogously, minor changes in oxygen availability could have been recorded by variations in the benthic fauna without inducing any significative change in the geochemical record. In order to bypass these limitations, redox conditions were estimated combining data on benthic fauna and bioturbation with inorganic and organic geochemical data. Different numerical values were attributed for the various discrete classes as follows: a) for benthic fauna (i.e. bioturbation, micro- and macro-benthos) a value of 0 was assigned when present, 1 for limited benthic fauna, and 2 for absence of benthic fauna; b) a combined redox indicator based on inorganic and/or organic geochemical data where a value of 0 was assigned for oxic conditions (i.e., oxic conditions on inorganic data and/or oxic–suboxic conditions on organic data), 1 for suboxic conditions (i.e., suboxia on inorganic data), 2 for anoxic, and 3 for euxinic. A ‘Redox Index’ (RI) was subsequently estimated combining the two separate numbers above for those sites where both data on benthic fauna and inorganic and/or organic geochemical data were available. Such indices can vary from 0 to 5, with 0 representing completely oxygenated conditions and 5 corresponding to euxinic conditions with total absence of benthic fauna.

4. Sedimentological and geochemical variations across the Toarcian Oceanic Anoxic Event

4.1. Palaeobathymetry

During the early Toarcian, the Alpine-Mediterranean Tethys was separated from the proto-Atlantic Ocean by a deeper marine area branching from the Hispanic Corridor. To the north a relatively shallow-water epicontinental sea, connected to the Arctic Ocean by the Viking Corridor, extended from about 30°N to about 50°N (Fig. 2). This shelfal region was characterized by the presence of relatively deeper epicontinental basins and sub-basins, such as the Cleveland Basin, Paris Basin,

and the Northwestern and Southwestern German basins. Sedimentological evidence, such as current-bedded clastic sediments as well as the local presence of silt-grade sedimentary structures in black shales, suggest generally shallow-water depths (e.g., Trabucho-Alexandre et al., 2012). Water palaeodepths of about 15 to 30 m were estimated for the lower Toarcian black shales in Yorkshire (Site 84), north-east England (Hallam, 1967). Frimmel et al. (2004) and Röhl et al. (2001) reconstructed water palaeodepths of about 50 m and 100–150 m, respectively, for coeval facies in south-west Germany. A paralic environment, ranging from fluvial to marginal marine was associated with the deposition of the Bornholm record (Site 81) in the Eastern Danish Basin (Hesselbo et al., 2000; Percival et al., 2015). Moving south, lower than 30°N, a series of tropical carbonate systems developed both attached to continental landmasses and as isolated platforms (e.g., Winterer, 1998; Woodfine et al., 2008; Sabatino et al., 2009; Ettinger et al., 2021). Water-depth estimates for pelagic and hemipelagic settings in the southern portion are scarce. Bjerrum et al. (2001) suggested a water palaeodepth of about 200 m for the shallow westerly dipping homoclinal ramp of the Lusitanian Basin at the margin of the proto-Atlantic Ocean (Site 9). Erba et al. (2022), on the basis of previous paleobathymetric reconstructions for the Jurassic troughs in present-day Northern Italy (Bernoulli and Jenkyns, 1974; Bosellini and Winterer, 1975; Bernoulli et al., 1979), estimated a paleobathymetry of about 1000 and 1500 m water depth for the Tethyan pelagic records of Gajum (Site 41) and Sogno (Site 40) in the Lombardy Basin (northern Italy), respectively. These values are in agreement with estimates given by Winterer (1998) for the East Sebino Basin in the easternmost part of the Lombardy Basin and the adjacent Belluno Basin in the Southern Alps. Relatively great palaeodepths are implied also for the so-called Kastelli Pelites (Site 53) in the Pindos Zone (northern Peloponnese, Greece), based on the occurrence of radiolarites stratigraphically associated with organic-rich T-OAE shales (Kafousia et al., 2011).

4.2. Occurrence of a pre-negative carbon-isotope anomaly hiatus

Evidence of a hiatus in the *tenuicostatum* Zone immediately preceding the interval of the negative CIE of the T-OAE was documented in many sections (Fig. 3) deposited at shallow depths, with a pattern of sedimentation ranging from shallow marine to hemipelagic. In particular, a major erosion surface was observed in the interval directly preceding the negative CIE in the Dades Valley section (Site 4) in the Moroccan Central High Atlas (Krencker et al., 2015; Krencker et al., 2019). The shallow-marine record of the Roqueredonde section (Site 25) in the Grands Causses Basin in France (Bomou et al., 2021) also shows the presence of a significant hiatus at the onset level of the negative CIE, as confirmed by the absence of ammonites characteristic of the lower part of the *tenuicostatum* Zone. The occurrence of a packstone unit with tempestites associated with an erosional surface, overlain by sediments with chaotically organized fossils and capped by low-angle ripples, marks the base of the negative CIE in the Andra Core HTM 102 (Site 32) in the Paris Basin (van Breugel et al., 2006). In the Penne Château-Granier section (Site 30) (Quercy Basin, France) the upper Pliensbachian to basal Toarcian (lower *tenuicostatum* Zone) bioclastic carbonates are separated by a hardground from the lower Toarcian (upper *tenuicostatum* Zone) “Schistes Carton” (Emmanuel et al., 2006). At the Monte Mangart section (site 35) in the Julian Alps (Sabatino et al., 2009), a hardground consisting of ferromanganese oxyhydroxide nodules is present at the base of the negative CIE interval. A hiatus at the base of the negative CIE has been proposed by Ruebsam et al. (2020d) for the Valdorbia record (Site 42) in the Umbria-Marche Basin, even if here the actual occurrence of a gap is somewhat ambiguous. A gap at the same stratigraphic position has been identified also in the shelfal successions of Gipf (Site 66) and Riniken (Site 67) (Fantasia et al., 2018) and at Rietheim (Site 68) (Montero-Serrano et al., 2015) in the Swiss Tabular Jura based on ammonite biostratigraphy (Wiedenmayer, 1980). Nannofossil biostratigraphy highlighted a hiatus within the *tenuicostatum* Zone at the base

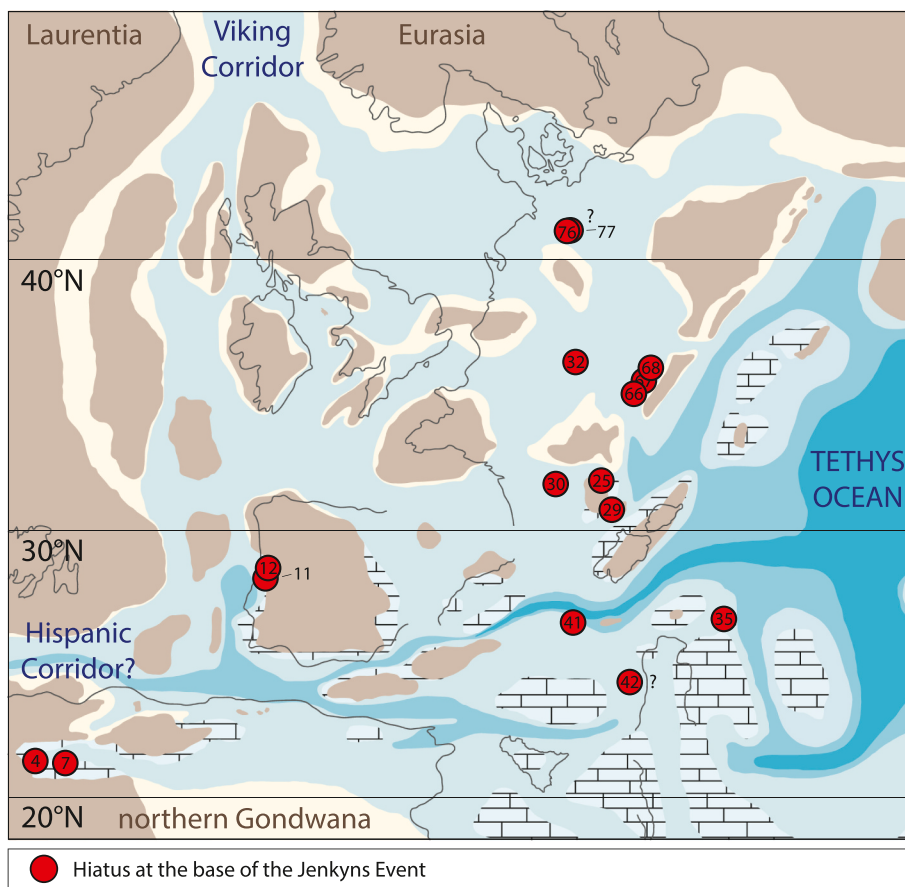


Fig. 3. Palaeogeographic position of sites with the evidence of a hiatus in the interval directly preceding the negative carbon-isotope excursion of the T-OAE ('pre-negative CIE plateau interval'). See Appendix A for data used to produce this map.

of the negative CIE interval in the L1 (Site 76) and Schandelah (Site 77) cores in the North German Basin (van de Schootbrugge et al., 2019; Visentin et al., 2021). The hemipelagic succession of the Cuers section (Site 29) in the Dauphinois Basin (France) is characterized within the *tenuicostatum* Zone by a hardground at the top of a breccia overlain by marly limestones and marls within the *tenuicostatum* Zone (Léonide et al., 2012). On the basis of carbon-isotope data, Pittet et al. (2014) identified a hiatus in correspondence with the interval immediately below the onset level of the negative CIE of the T-OAE (interval 2 in their work) in the Rabaçal (Site 11) and Ribeiro (Site 12) sections in the Lusitanian Basin (Portugal). Also a few sections deposited at greater water depths exhibit a hiatus: for example, the Foum Tillicht section (Site 7) in the deeper water domain of the Central High Atlas Basin (Morocco) (Bodin et al., 2016), and the pelagic record of the Gajum Core (Site 41) in the Lombardy Basin (northwestern Italy) deposited at about 1000 m of water depth (Visentin and Erba, 2021; Erba et al., 2022).

As suggested by Pittet et al. (2014), in offshore localities of the Lusitanian Basin, a combination of a major drop of sea level and a subsequent rapid transgression probably explains the observed marine erosion in the 'pre-negative CIE plateau interval'. A rapid sea-level fall preceding the negative CIE was also suggested by Krencker et al. (2019), based on the observation of coeval deeply incised valleys in marine sections cropping out in Greenland and Morocco. The presence of gaps before and after the negative CIE of the T-OAE has also been explored in the study by Ruebsam and Al-Husseini (2020). Their research, along with investigations conducted by Röhl et al. (2001), Hermoso et al. (2013), Pittet et al. (2014), Krencker et al. (2019), Ruebsam et al. (2019), and Ruebsam et al. (2020c), has provided evidence indicating that these gaps coincide with periods of sea-level falls and lowstands. Glacio-eustasy has been proposed as a potential driver of sea-level

fluctuations, with lowstands aligned with colder climatic conditions (e.g., Suan et al., 2010; Korte and Hesselbo, 2011; Krencker et al., 2019; Ruebsam et al., 2019, 2020e). However, while sea-level variations of few tens of metres during the Toarcian (Haq, 2017) can be invoked for shallow-water settings, they cannot explain the occurrence of hiatuses in deeper water settings. A supra-regional early Toarcian tectonic phase associated with the opening of the Alpine and Ligurian Tethys starting from about 185 Ma (Schettino and Turco, 2011) was probably responsible for gaps and massive re-sedimentation observed during the interval preceding the negative CIE of the T-OAE.

4.3. Black shales and TOC content

The distribution of black shales/dark grey shales and their TOC content for the 89 studied sites are reported in Figs. 4 and 5, respectively. A detailed review of TOC data was recently presented by Kemp et al. (2022b). Our examination of TOC data differs from theirs by illustrating the greater number of sections considered in our compilation. Furthermore, while Kemp et al. (2022b) presented the average TOC distribution within the negative CIE of the T-OAE, in our study we captured the evolution of the TOCs before, during and after this isotopic phenomenon.

Available data indicate that, except for very few localities, deposition of black shales during the 'pre-negative CIE plateau interval' did not take place (Fig. 4a). Only very few sections, probably reflecting very local conditions, were characterized by the deposition of black shales over this interval of time. Very dark grey to black mudstones and silty mudstones were observed in the L05-04 well in the Dutch Central Graben (Site 80) (Trabucho-Alexandre et al., 2012), and black shales were described by Suan et al. (2018) for the interval directly below the

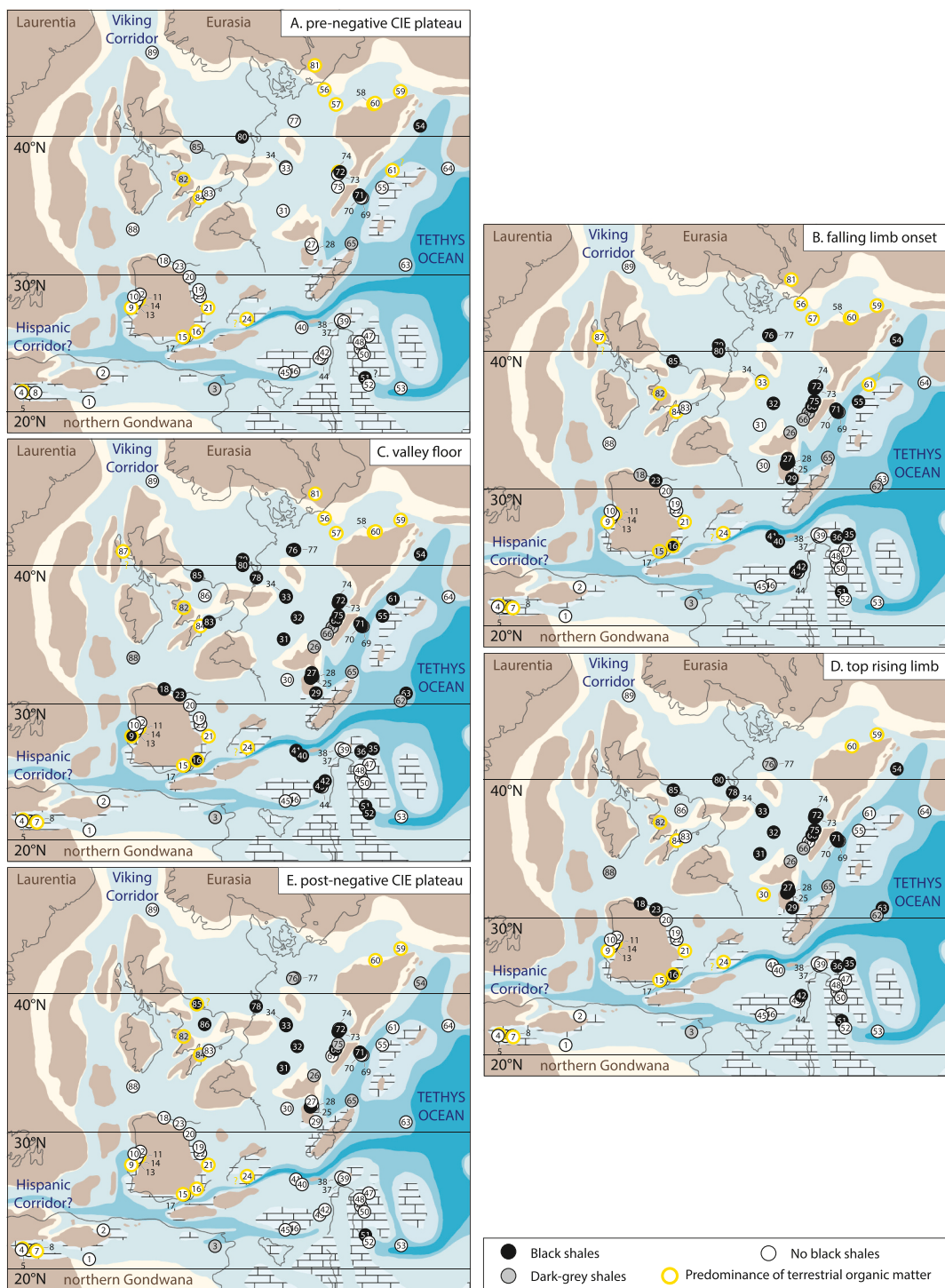


Fig. 4. Palaeogeographic distribution of black shales and dark grey shales across the T-OAE. Sites dominated by terrestrial organic matter (woody fragments, coaly horizons, etc.) are highlighted with a yellow circle. See Fig. 1 for identification of different stratigraphic intervals and Appendix A for data used to produce this map. (For interpretation of the references to colour in this figure legend, the reader is referred to the web version of this article.)

negative CIE of the Jenkyns Event at Zázrivá in Slovakia (Site 54) at middle shelf depths. From a lithological point of view, black shales associated with the ‘pre-negative CIE plateau interval’ are reported at the Petousi section in the Ionian Zone in Greece (Site 51) (Kafousia et al., 2013, 2014). These shales are indeed characterized by generally very low TOC values from about 0.1 to 1.8% (Fig. 5a). Relatively higher values, from about 3 to 4.5%, were observed at Châabet El Attaris in Tunisia (Site 3) (Ruebsam et al., 2022a; Reolid et al., 2023), Castrovido section in Spain (Site 20) (Danise et al., 2019, and the L05-04 well in the

Dutch Central Graben (Site 80) (Trabucho-Alexandre et al., 2012). Relatively high average TOC values of about 3% documented in the Spanish Sierra Palomera (Rambla del Salto) section (Site 21) are related to dispersed continental organic matter rather than the presence of black shales (Gómez and Arias, 2010; Gómez and Goy, 2011; Danise et al., 2019). Discrete black-shale intervals, i.e., Seegrasschiefer and Tafel-fleins horizons, with high TOC content of about 6% and 9%, respectively, are also known from the Dotternhausen section (Site 72) (Schouten et al., 2000; Frimmel et al., 2004; Schwark and Frimmel,

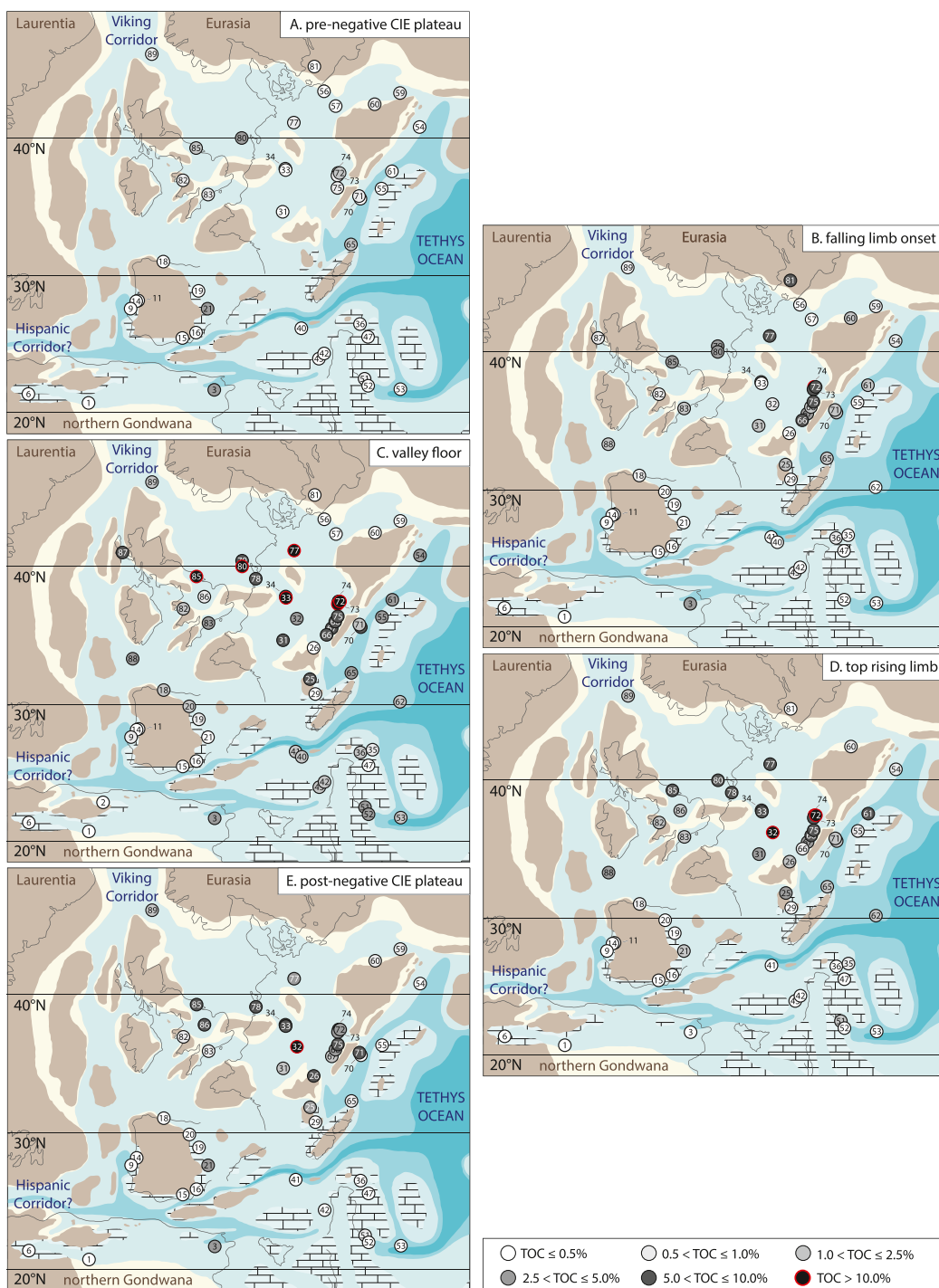


Fig. 5. Palaeogeographic distribution of average total organic carbon (TOC) content across the T-OAE. Locations without TOC data are not reported on maps. See Fig. 1 for identification of different stratigraphic intervals and Appendix A for data used to produce this map.

2004; Dickson et al., 2017; Wang et al., 2021).

At the onset of the negative CIE ('falling limb onset interval'), deposition of black shales became widespread from shallow- to deep-water settings throughout epicontinental northern Europe and the Alpine-Mediterranean Tethys (Fig. 4b). In this stratigraphic interval, average TOC values range from less than 1% to about 10.5% (Fig. 5b), with the highest average values from 7 to 10.5% observed in the SW German Basin at Dotternhausen (Site 72) (Schouten et al., 2000; Frimmel et al., 2004; Röhl and Schmid-Röhl, 2005; Dickson et al., 2017; Wang et al., 2020, 2021), Denkingen borehole (BEB 1012) (Site 73)

(Suan et al., 2015), Dormettingen (Site 74) (Ajuaba et al., 2022), and Aubach section (Site 75) (Hougaard et al., 2021). At Gipf (Site 66) in the Swiss Tabular Jura the average value is 5.5% (Fantasia et al., 2018, 2019b), and the FR-2010-078 core (Site 34) in the Paris Basin shows average values of 4.5% and 5%, respectively (Ruebsam et al., 2022b). An average TOC value of 5.9% occurs at Bornholm (Site 81) in the Eastern Danish Basin associated with the presence of coaly horizons (McElwain et al., 2005).

The deposition of black shales reached its maximum extent in correspondence with the lowest part of the $\delta^{13}\text{C}$ negative trough ('valley

floor interval') in most basins and sub-basins from northern Europe to the Alpine-Mediterranean Tethys (Fig. 4c). Generally, the highest TOC values are observed in correspondence with this interval, with average values ranging from less than 0.5% up to 17.5% (Fig. 5c). The highest average values of 17.5% were observed in the Paris Basin at Bascharge (Site 33) (Hermoso et al., 2014). Very high values were measured also in the L05–04 borehole (Site 80) in the Dutch Central Graben with average values of 15.5% (Trabucho-Alexandre et al., 2012), in the Rijswijk-1 Core (Site 78) in the Netherlands with average values of 13.5% (Dickson et al., 2017; Houben et al., 2021), and in the Yorkshire composite section (Site 85) in UK with average values of about 12% (Sælen et al., 1996, 2000; McArthur et al., 2008; Kemp et al., 2011; Percival et al., 2015; Dickson et al., 2017). The Tethyan section of Bächental in Austria (Site 70), unlike other coeval Tethyan sections, exhibits high TOC average values of about 6% and peaks up to about 9.5% (Neumeister et al., 2015).

In the highest part of the negative CIE interval ('top rising limb interval') a progressive decrease in the black shale distribution is observed at a regional scale (Fig. 4d). In this interval, apart from a few sections, average TOC contents decrease (Fig. 5d). Noteworthy exceptions are the Andra HTM 102 record (Site 32) in the Paris Basin with a rise from an average TOC value of 3% (in the lowest part of the negative carbon-isotope trough) to average TOC values of 16% (van Breugel et al., 2006) in the 'top rising limb interval', and the Hungarian Réka Valley section (Site 61) with a change from 5 to 7% (Ruebsam et al., 2018). Excluding the Andra HTM 102 record, characterized by very high TOC average values in the 'top rising limb interval', TOC values range from less than 0.5% up to 10.5%. High average TOC values were measured at Dormettingen (Site 74) in the South German Basin with average values of 10.5% (Ajuaba et al., 2022), in the Shandelah Core (Site 77) in the North German Basin with an average TOC of 10% (Baroni et al., 2018), in the Rijswijk-1 Core (Site 78) in the West Netherlands Basin with average values of 9.5% (Dickson et al., 2017; Houben et al., 2021), and in the L05-04 Core (Site 80) from the Dutch Central Graben with average values of 9% (Trabucho-Alexandre et al., 2012).

In correspondence with the 'post-negative CIE plateau interval', deposition of black shales occurred on a local to regional scale and organic-rich facies persisted mainly in the northern European epicontinental basins and sub-basins (Fig. 4e). In particular, black-shale deposition continued in the Paris Basin at Sancerre (Site 31) (Hermoso et al., 2009a), Andra HTM 102 (Site 32) (van Breugel et al., 2006), Bascharge (Site 33) (Hermoso et al., 2014), in the SW German Basin at Dotternhausen (Site 72) (Schouten et al., 2000; Frimmel et al., 2004; Schark and Frimmel, 2004; Dickson et al., 2017), Denkingen borehole (Site 73) (Suan et al., 2015), in the North German Basin in the L1 (Site 76) and Schandalah (Site 77) cores (Visentin et al., 2021), both characterized by medium brown shales rather than black shales *sensu stricto*, and in the Cleveland Basin in Yorkshire (Site 85) (Sælen et al., 1996, 2000; Jenkyns and Clayton, 1997; Hesselbo et al., 2000; Kemp et al., 2005; Dickson et al., 2017). Black-shale deposition persisted also in Tethyan areas in the Petousi section in Greece (Site 51) (Kafousia et al., 2013, 2014). Average TOC values during the 'post-negative CIE plateau interval' range from <0.5% to about 16% (Fig. 5e). Highest values occur in the Paris Basin, in particular at the Andra HTM 102 site (Site 32) with average values of 16% (van Breugel et al., 2006), and at Bascharge (Site 33) with average values of about 7.5% (Hermoso et al., 2014). TOC values in the SW and North German Basin are characterized by values of about 5%, rather lower than the 6–10% observed in the 'top rising limb Interval', as for example at Dotternhausen (Site 72) (Schouten et al., 2000; Frimmel et al., 2004; Röhl and Schmid-Röhl, 2005; Dickson et al., 2017; Wang et al., 2020, 2021), Denkingen borehole (Site 73) (Suan et al., 2015), Aubach (Site 75) (Hougaard et al., 2021), and Schandalah Core (Site 77) (Baroni et al., 2018), with the exception of the Dormettingen record (Site 74) characterized by average values of 8% (Ajuaba et al., 2022). The Yorkshire section of the Cleveland Basin (Site 85) shows the same average values of about 5.5% in both intervals

(Sælen et al., 1996, 2000; McArthur et al., 2008; Kemp et al., 2011; Percival et al., 2015; Dickson et al., 2017). High TOC values were measured also in the Netherlands in the Rijswijk-1 Core (Site 78) with average values of 9% (Dickson et al., 2017; Houben et al., 2021), and in the English East Midlands Shelf at the Holwell Quarries (Site 86) where black shales are present exclusively following the negative CIE with an average TOC value of 8.5% (Caswell and Coe, 2012). In contrast to other coeval Tethyan records, high TOC values were observed also in the Sachrang section in Bavaria, Germany (Site 71) with average TOC values of 7.6% (Ebli et al., 1998).

Overall, through the whole of the T-OAE interval, a contribution from land-derived organic matter is significant in all those records from sites proximal to palaeocoastlines (Fig. 4). In particular, the palynofacies composition of the sedimentary organic matter at the Boumardoul n'Imazighn composite section (Site 5) and Foum Tilicht record (Site 7) in the Moroccan Atlas (Bodin et al., 2016) is dominated by continent-derived particles including opaque and translucent phytoclasts as well as sporomorphs. In the Portuguese section of Peniche (Site 9) organic matter is dominated by small phytoclasts with the occurrence in some intervals of large wood fragments (Fantasia et al., 2019a; Rodrigues et al., 2020a). Dominance of terrestrially derived palynomorphs is observed also in the Spanish records of Fonte Coberta/Rabaçal (Site 11) (Rodrigues et al., 2020a), La Cerradura (Site 15) and Fuente Vidriera (Site 16) (Rodrigues et al., 2019), Sierra Palomera (Rambla del Salto) (Site 21) (Barrón et al., 1999), and Es Cosconar (section 4) (Site 24) (Rosales et al., 2018). The organic content of the Mechowo IG 1 (Site 56), Gorzów Wielkopolski IG 1 (Site 57), Suliszowice 38 BN (Site 58), Brody-Lubienia BL 1 (Site 59), Parkoszowice (Site 60) records, deposited in the Polish Basin at shallow water depths in an environment proximal to the palaeocoastline, is made up of material that originates almost entirely from the terrestrial environment (wood, cuticles, and spores), with a negligible content of marine organic matter (Hesselbo and Pieńkowski, 2011; Pienkowski et al., 2016). The Bornholm record (Site 81) in the Eastern Danish Basin is characterized by coaly intervals deposited in a fluvial to marginal marine environment (Hesselbo et al., 2000; McElwain et al., 2005). In the Mochras Farm Borehole (Site 82) in the Cardigan Bay Basin, UK terrestrial material with abundant macrofossil wood accounts for a relatively elevated percentage of the total organic matter (van de Schootbrugge et al., 2005; Xu et al., 2018). Finally, weakly laminated sediments with preserved wood were observed in the English Seavington St Michael record in the Wessex Basin (Site 84) (Boomer et al., 2021).

4.4. Variation in oxygen-isotope data

The variation in the oxygen-isotope ratios ($\Delta^{18}\text{O}$) calculated from the onset of the falling limb to the onset of the rising limb is reported in Fig. 6. Sections characterized by evidence of moderate to significant diagenetic overprint of the $\delta^{18}\text{O}$ signal are highlighted with a pinkish circle on Fig. 6 and reported in detail on tables in the Appendix A. Indeed, some of the analysed micrites show evidence of diagenetic alteration of the $\delta^{18}\text{O}$ signal (e.g., Gómez and Goy, 2011; Suan et al., 2015; Jenkyns and MacFarlane, 2021). However, the fact that long time series of oxygen-isotope data from different localities show parallel trends suggest that - although absolute values are untrustworthy - the trends captured by $\Delta^{18}\text{O}$ values are likely meaningful in terms of palaeotemperature and/or salinity variation.

The most negative $\Delta^{18}\text{O}$ values are observed in the French sections of Roqueredonde (Site 25) and Bascharge (Site 33) with values of $-13\text{\textperthousand}$ and $-11\text{\textperthousand}$, respectively (Hermoso et al., 2014; Bomou et al., 2021). In some sections, an anomalous rise in the oxygen-isotope ratios is marked by positive $\Delta^{18}\text{O}$ values. The highest value is recorded in the Tunisian Châabet El Attaris section (Site 3) with values of 3\textperthousand (Ruebsam et al., 2022a). Positive $\Delta^{18}\text{O}$ values, from about 1 to $\sim 0\text{\textperthousand}$, were observed also in the Algerian Mellala section (Site 2) (Reolid et al., 2014b), and in the Portuguese and Spanish records of Figueira da Foz (Site 10), Fonte

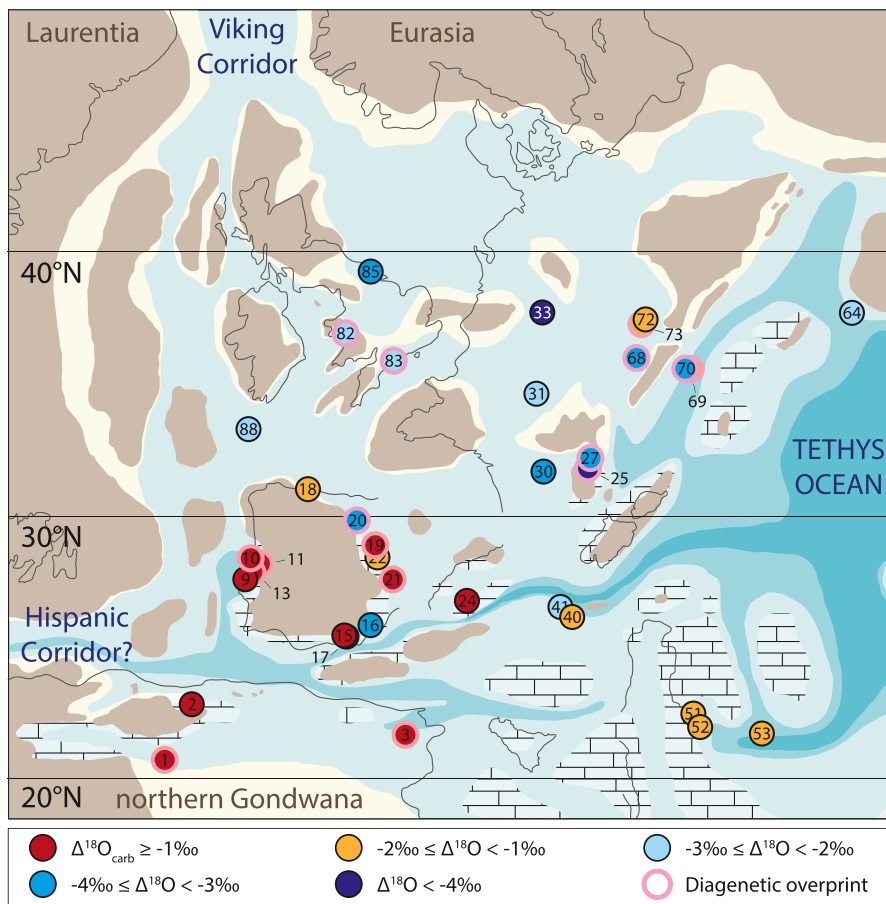


Fig. 6. Palaeogeographic distribution of $\Delta^{18}\text{O}$ values, computed as the difference in the oxygen-isotope composition at the onset of the rising limb and at the onset of the falling limb of the negative carbon-isotope excursion of the T-OAE. Locations without $\delta^{18}\text{O}$ data are not reported on maps. See Appendix A for data used to produce this map. Isotopic records characterized by a moderate to significant diagenetic overprint are highlighted with a pinkish circle.

Coberta/Rabaçal (Site 11), La Cerradura (Site 15), and Arroyo Minguarrón (Site 17) (Duarte et al., 2007; Reolid et al., 2014a; Reolid et al., 2020a). These results probably reflect some local diagenetic trends. Apart from these sections, $\Delta^{18}\text{O}$ values range from about $-4.5\text{\textperthousand}$ to about $-0.5\text{\textperthousand}$. Although diagenetic overprints are to be expected in sediments of this age, common patterns at supra-regional scale seem indicative of at least a partial primary signal. In particular, $\Delta^{18}\text{O}$ values $\geq -2\text{\textperthousand}$ are mainly located in the southernmost part of the studied area at latitudes lower than 30°N . On the contrary, the most negative $\Delta^{18}\text{O}$ values, indicative of a greater relative decrease in $\delta^{18}\text{O}$ ratios, are mainly confined to higher latitudes, in the northern European continental shelf.

4.5. Spatio-temporal redox variations

'Redox Indexes' estimated for the considered sites are reported in Appendix B and plotted on palaeogeographic maps in Fig. 7. It should be noted that redox conditions estimated from inorganic and organic geochemical data, when both present, are always in agreement. A speculative distribution of redox conditions far from the locations of the investigated records is also tentatively illustrated on the maps. The variation in benthic fauna, distribution of euhedral and frambooidal pyrite, inorganic and organic geochemical data within the various stratigraphic intervals, here used to estimate the various 'Redox Indexes', are discussed in detail in the Supplementary Material.

During the 'pre-negative CIE plateau interval' (Fig. 7a) estimated RI mainly range from 0 to 2, with most of the sites being characterized by values equal to 0, indicating stable well-oxygenated conditions. An exception is represented by the Tunisian Châabet El Attaris record (Site

3) and the German Dotternhausen record (Site 72), both with a value of 4, and the L05-04 Core (Site 80) with a value of 3. In particular, at Châabet El Attaris, anoxic conditions are paralleled by the absence of macro-benthos and benthic foraminifera and by the occurrence of plane-parallel sedimentary structures (Reolid et al., 2021b; Ruebsam et al., 2022a). At Dotternhausen, the discrete TOC-rich intercalations (i.e., Seegrasschiefer and Tafelfleins horizons) lack benthic communities (e.g., Röhl et al., 2001) and, as captured by organic geochemical data (Frimmel et al., 2004; Schwark and Frimmel, 2004), reflect time intervals characterized by suboxic–anoxic conditions. In the L05-04 Core, however, anoxia as reconstructed by elemental data, was probably interrupted by brief episodes of re-oxygenation, as illustrated by common traces of bioturbation within the thin beds (Trabucho-Alexandre et al., 2012).

During the 'falling limb onset interval' (Fig. 7b) most of the records from the northern epicontinental basins and sub-basins are characterized by RI values of 5, indicative of euxinic conditions with the complete lack of benthic fauna. Based on available data, the Dutch Central Graben experienced peculiar conditions, as recorded in the F11-01 (Site 79) and L05-04 (Site 80) cores. Here, even though geochemical data point to predominantly anoxic bottom waters (Houben et al., 2021), the observation of reworked sediment by strong currents and bioturbation suggests that oxic conditions prevailed (Trabucho-Alexandre et al., 2012). It is thus possible that, during this stratigraphic interval, anoxia in the Dutch Graben was frequently interrupted by storm activity and geostrophic flows capable of mixing and re-oxygenating the water-column. RI values of 5 can be observed also at Valdorbia (Site 42) in the Umbria-Marche Basin, and at Zázrivá in Slovakia (Site 54), thereby

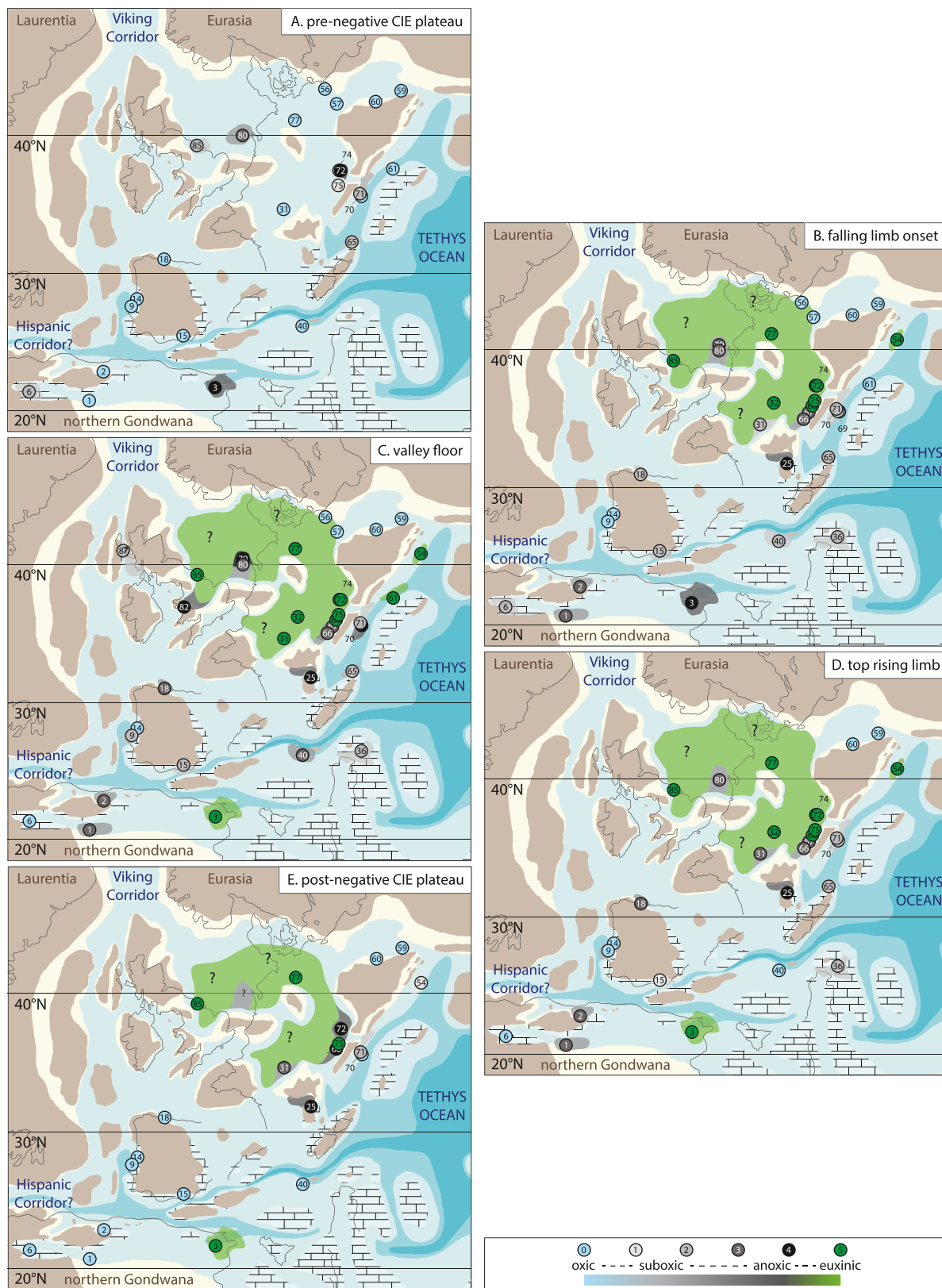


Fig. 7. Palaeogeographic distribution of prevailing dysoxic-anoxic conditions and euxinic conditions in the Alpine-Mediterranean Tethys and north European epicontinental basins and sub-basins across the T-OAE. Redox conditions at each site are estimated on the basis of Redox Indexes computed by combining data on benthic fauna and bioturbation with inorganic and organic geochemical data. The areal extent of redox conditions far from available records is speculative. See text for details.

indicating that relatively stable euxinia was established locally away from the northern shelfal area. Anoxia with lack of benthic fauna (Bomou et al., 2021) was established in the French Roqueredonde record (Site 25) and continued to persist also in the Tunisian Châabet El Attaris section (Site 3) (Reolid et al., 2021b; Ruebsam et al., 2022a). Less severe or less continuous anoxia can be inferred for records such as the Swiss Gipf (Site 66) and Riniken (Site 67) successions where, even if geochemical data suggest the occurrence of anoxia, some limited bioturbation is recorded (Fantasia et al., 2018, 2019b). In particular, in the Algerian Raknet El Kahla (Site 1) and Mellala (Site 2) records, and at La Cerradura (Site 15) and West Rodiles (Site 18) in Spain the complete lack of bioturbation (Fig. S2 in the Supplementary Material) supports the presence of suboxia, as suggested by geochemical data (Figs. S4 and S5 in the Supplementary Material).

In correspondence with the ‘valley floor interval’ (Fig. 7c) RI values equal to 5 continued to persist in most of the northern epicontinental basins and sub-basins and at Valdorbia in central Italy (Site 42) and Zázrivá in Slovakia (Site 54), extending also to the Châabet El Attaris section in Tunisia (Site 3) and the Hungarian Réka Valley (Site 64). Anoxic conditions with no benthic fauna (RI equal to 4) were recorded at Roqueredonde (Site 25), Bächental (Site 70), and the Mochras Farm Borehole (Site 82), indicating the extension of stable anoxic conditions to these areas. On the contrary, records such as the Swiss Gipf (Site 66) and Riniken (Site 67) sections were probably characterized by less continuous anoxic conditions, as suggested by the occurrence of minor bioturbation (Fantasia et al., 2018, 2019b). Sedimentological data indicate that the Dutch Central Graben continued to be subjected to frequent reworking by bottom currents that probably fostered some re-oxygenation of bottom waters (Trabucho-Alexandre et al., 2012).

In correspondence with the ‘top rising limb interval’ estimated RI do not exhibit major changes with respect to the ‘valley floor interval’. However, variations can be observed in some records. In particular, at La Cerradura (Site 15) the RI falls from 3 to 2, associated with the establishment of suboxic conditions (Reolid et al., 2014a; Rodrigues et al., 2019; Silva et al., 2021b) and evidence for some limited recovery of benthic fauna (Reolid et al., 2014a; Baeza-Carratalá et al., 2017; Reolid et al., 2018; Rodríguez-Tovar, 2021; Šimo and Reolid, 2021). The Sogno Core (Site 40) in the Lombardy Basin records a shift of RI from 3 to 0, indicating that, during the ‘top rising limb interval’, conditions in this part of the basin were already fully oxygenated. Similarly, the Bachental section (Site 70) records a shift of RI from 4 to 2, associated with a change from anoxic conditions with no benthic fauna to dominant suboxia and the occurrence of some limited bioturbation.

In the ‘post-negative CIE interval’, RI values of 5 persist exclusively in some sections located in the northern epicontinental area and at Châabet El Attaris (Site 3). In the latter locality, organic geochemical data (Ruebsam et al., 2022a) suggest that PZE was apparently more intense at times following the negative CIE than during it. By contrast, most of the records outside of the northern epicontinental shelfal area exhibit values of 0, indicating fully oxygenated conditions. An exception is the La Cerradura section in Spain (Site 15), with an RI value of 1 during this stratigraphic interval, likely deposited under feeble and discontinuous dysoxic conditions, as suggested by minor enrichments in redox-sensitive elements (Reolid et al., 2014a; Silva et al., 2021b) and evidence of bioturbation (Reolid et al., 2014a; Baeza-Carratalá et al., 2017; Reolid et al., 2018; Rodríguez-Tovar, 2021; Šimo and Reolid, 2021). A change to lower RI values can be observed also at Zázrivá (Site 54) from 5 to 2, indicating a shift to suboxic conditions witnessed by a recovery of benthic foraminifera in a depositional setting characterized by improved oxygenation with transient episodes of lower oxygenation (Suan et al., 2018). A clear change to lower RI values can be observed also within the northern epicontinental area, as in the Swiss Tabular Jura at Rietheim (Site 68) and in the SW German Basin at Dotternhausen (Site 72), both with a change in the RI from 5 to 4. In both these records, the anoxic to euxinic conditions indicated by geochemical data are accompanied by the occurrence of several thin bioturbated layers with

moderately diverse benthic fauna (e.g., bivalves) showing a progressive moderate increase in abundance and diversity (Schouten et al., 2000; Röhl et al., 2001; Bailey et al., 2003; Schwark and Frimmel, 2004; Röhl and Schmid-Röhl, 2005; Montero-Serrano et al., 2015; Dickson et al., 2017; Baroni et al., 2018; Fantasia et al., 2018; Fantasia et al., 2018; Wang et al., 2020). Such evidence suggests that during the ‘post-negative CIE interval’ anoxia-euxinia was less persistent and frequently interrupted by phases of re-oxygenation.

4.6. Variations in manganese and iron concentrations

Manganese and iron contents within sediments are strongly dependent on variations in bottom-water redox conditions (Calvert and Pedersen, 1996; Canfield et al., 1996; Wijsman et al., 2001; Lyons and Severmann, 2006; Tribouillard et al., 2006; Raiswell and Canfield, 2012). Changes in Mn and Fe concentrations in the investigated records across the negative CIE of the T-OAE are reported in Figs. 8 and 9. Additionally, in Fig. 9 the presence of Mn nodules and hardgrounds (i.e., Mn-oxyhydroxides), indicative of low sedimentation rates and oxidizing conditions (Jenkyns, 1970, 1971), and Mn-rich carbonates, associated with reducing pore waters (Calvert and Pedersen, 1993, 1996), are reported.

In the ‘pre-negative CIE plateau interval’ many successions are characterized by a rise of Mn concentration compared to background levels (Fig. 8a). A clear rise is observed in the French Sancerre-Couy succession (Site 31) (Hermoso et al., 2009b, 2013), the Sogno Core in the Lombardy Basin (Site 40) (Gambacorta et al., 2023), the Monte Sorgenza succession in the Campania-Lucania Platform (Site 46) (Lu et al., 2010), the Croatian Adriatic Platform in the Velebit-A record (Site 49) (Sabatino et al., 2013), and the German Dotternhausen record (Site 72) (Bailey et al., 2003; Dickson et al., 2017; Baroni et al., 2018; Wang et al., 2020). The average Mn concentrations range from <100 ppm to >3000 ppm (Fig. 8b), with elevated values principally observed in the northern epicontinental seaway at Sancerre-Couy (Site 31) (Hermoso et al., 2009b, 2013), the German Sachrang (Site 71) (Ebli et al., 1998) and Dotternhausen (Site 72) (Bailey et al., 2003; Dickson et al., 2017; Baroni et al., 2018; Wang et al., 2020) records, and in the Schandelah Core (Site 77) in the North German Basin (Baroni et al., 2018). High average concentrations of about 3300 ppm were observed also in the Tethyan Sogno Core (Site 40) (Gambacorta et al., 2023). Fe-Mn hardgrounds (i.e., Mn-oxyhydroxides) are documented in the ‘pre-negative CIE interval’ of the Monte Mangart succession (Site 35) (Sabatino et al., 2009, 2011), and at Kovk in the Slovenian Adriatic Platform (Ettinger et al., 2021). Manganese nodules (i.e., Mn-oxyhydroxides) are described in the ‘pre-negative CIE interval’ also for the Tölgyhát succession (Site 63) in the Hungarian Gerecse Basin (Müller et al., 2021). As for Mn, increased Fe concentrations with respect to background values are reported in Fig. 9a. In particular, a rise is observed in the Sancerre-Couy record (Site 31) (Hermoso et al., 2009b), at Dotternhausen (Site 72) (Baroni et al., 2018; Wang et al., 2020), in the German Schandalah Core (Site 77) (Baroni et al., 2018), and in the Dutch L05-04 Core (Site 80) (Trabucho-Alexandre et al., 2012). Fe average concentrations range from less than 1% to more than 6%, with higher values clustered in the northern epicontinental area, as in the L05-04 Core (Trabucho-Alexandre et al., 2012) and in the Mochras Farm (Site 82) (Xu et al., 2018) (Fig. 9b).

With the onset of the negative CIE (‘falling limb onset interval’) (Fig. 8c), and across the valley floor (Fig. 8d and e), the average Mn concentrations in the northern epicontinental basins and sub-basins decrease to lower values, whereas higher concentrations are observed at sites located either further south towards the open ocean, as in the Sogno Core (Site 40) (Gambacorta et al., 2023), at Monte Mangart (Site 35) (Sabatino et al., 2011), and in the extremely Mn-enriched succession of the Hungarian Úrkút section (Site 62) (Vető et al., 1997; Suan et al., 2016), or close to the proto-Atlantic in the Raknet El Kahla (Site 1) and Peniche (Site 9) sections (Hermoso et al., 2009b; Silva and Duarte, 2015;

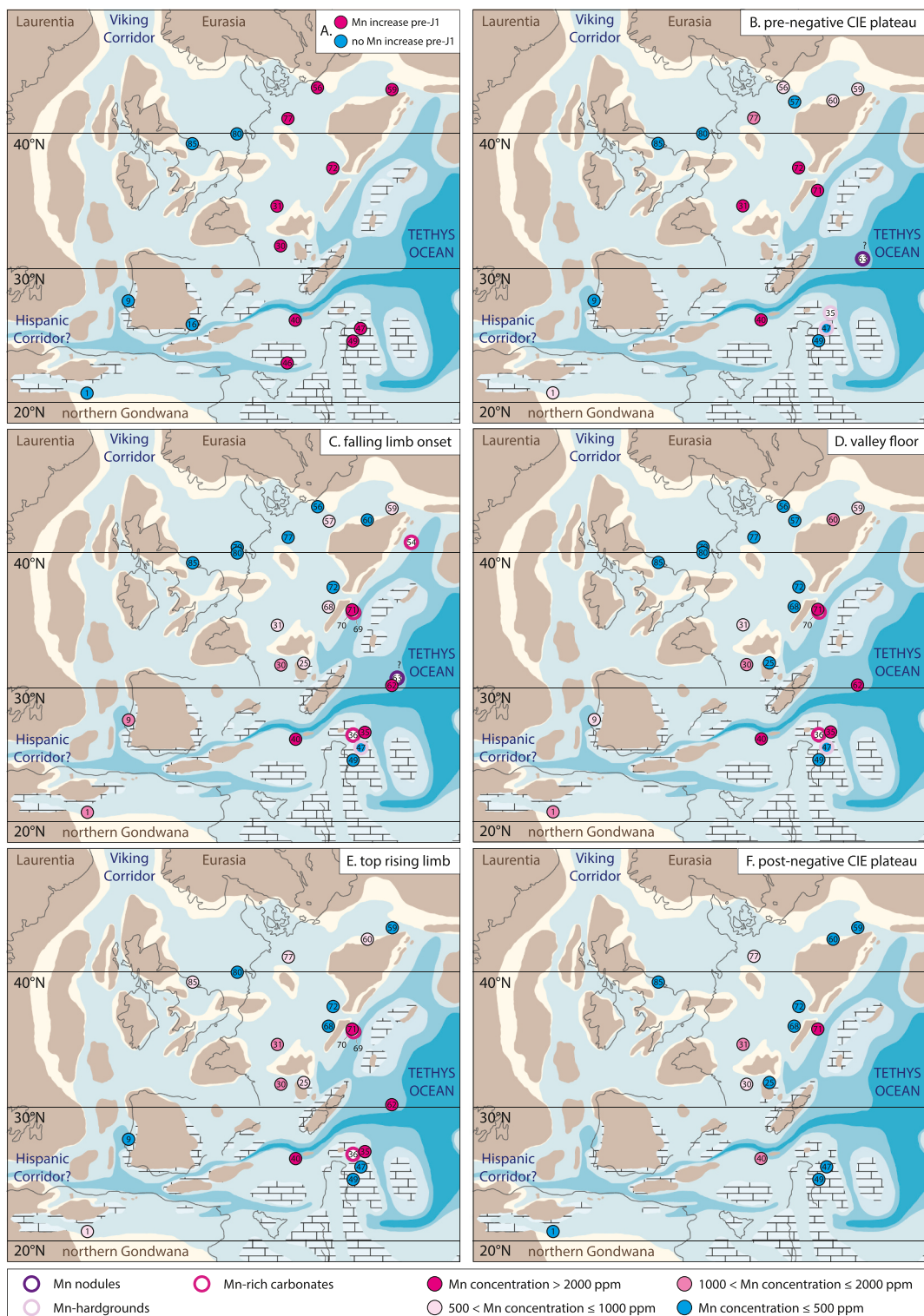


Fig. 8. Palaeogeographic distribution of Mn nodules, Mn-hardgrounds, Mn-rich carbonates (indicated with different colour borders), and Mn elemental concentrations (reported using different colour fillings) across the T-OAE. Locations without Mn data are not reported on maps. See Fig. 1 for identification of different stratigraphic intervals and Appendix A for data used to produce this map.

Reolid et al., 2012; Ruebsam et al., 2020b). However, it should be noted that in the ‘top rising limb interval’ some sections of the north European epicontinental sea show a limited increase in Mn concentrations (Fig. 8e), such as at Sancerre-Couy (Site 31) (Hermoso et al., 2009b, 2013), in the Schadelah Core (Site 77) (Baroni et al., 2018), and in Yorkshire (Site 85) (Bailey et al., 2003; McArthur et al., 2008; Pearce

et al., 2008; Dickson et al., 2017; Baroni et al., 2018; Thibault et al., 2018; McArthur, 2019; Remirez and Algeo, 2020a). The negative CIE interval of many successions is characterized by the presence of Mn-rich carbonates, such as the Dogna Core (Site 36) drilled next to the Longarone section in the Belluno Basin in Northwestern Italy (Jenkyns et al., 1985; Bellanca et al., 1999), the Zárvá record in the basin within the

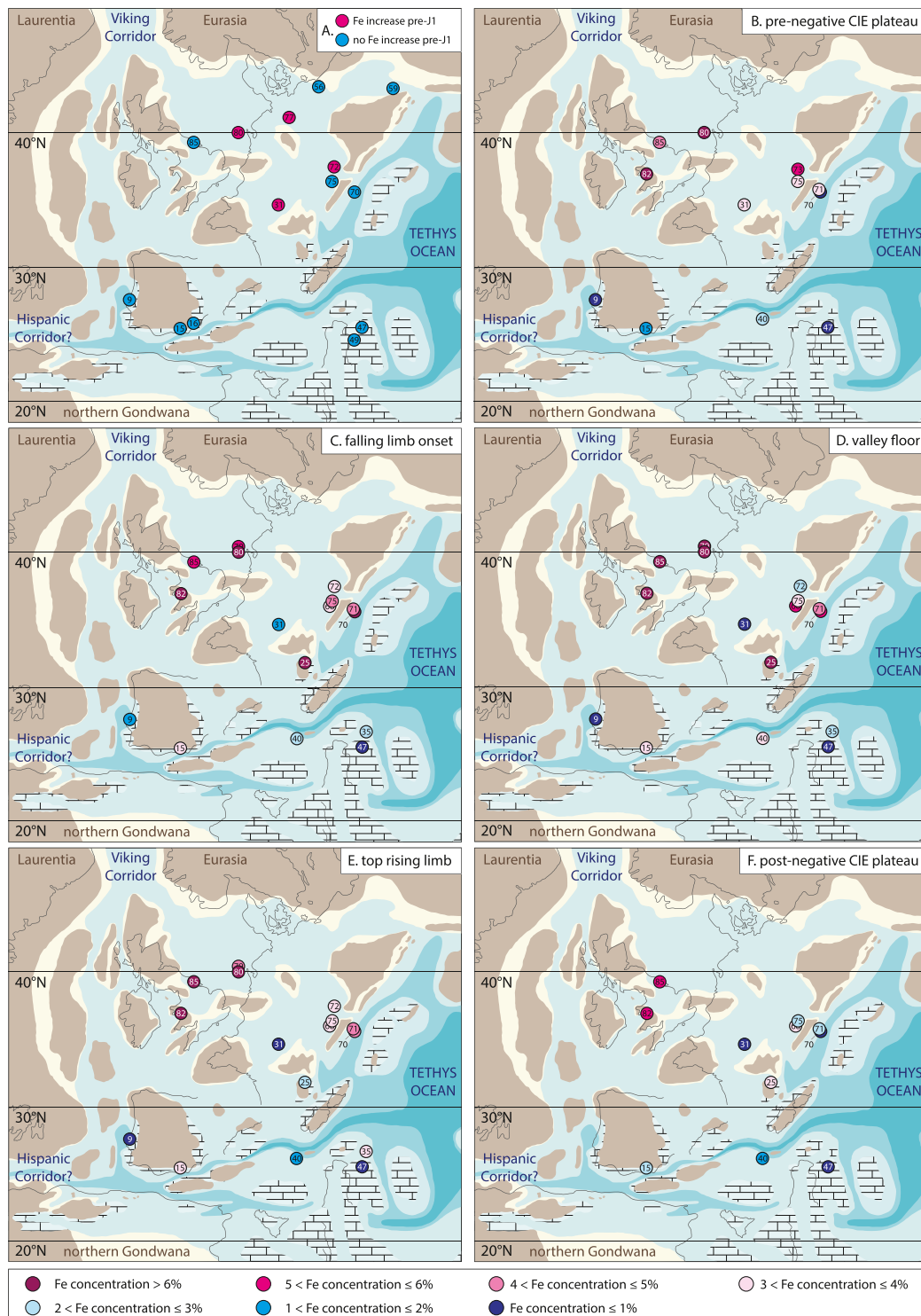


Fig. 9. Palaeogeographic distribution of Fe elemental concentrations across the T-OAE. Locations without Fe data are not reported on maps. See Fig. 1 for identification of different stratigraphic intervals and Appendix A for data used to produce this map.

Oravicium crustal block and the Bohemian Massif (Site 54) where common manganese-rich carbonates are documented (Suan et al., 2018), and in the Austrian Bächental (Site 70) site (Kodina et al., 1988; Neu-meister et al., 2015, 2016; Suan et al., 2016). Fe-Mn crusts (hardground, i.e., Mn-oxyhydroxides) are described from Kovik in Slovenia (Site 47) (Ettinger et al., 2021), while in the Tölgyhát section in the Gerecse Basin (Site 63) the occurrence of manganese nodules dispersed in a thin-

layered clayey marl is reported (Müller et al., 2021). Differently from Mn, an increase in Fe average concentrations is reported across the negative CIE interval in the north European epicontinental seaway, while relatively low Fe values still persist outside of this area (Fig. 9c, d, and e). High Fe average concentrations were observed in the north European epicontinental seaway in the French record of Roqueredonde (Site 25) (Bomou et al., 2021), in the Dutch Central Graben in the F11-01

(Site 79) and L05-04 (Site 80) cores (Trabucho-Alexandre et al., 2012), the Cardigan Basin in the Mochras Farm Borehole (Site 82) (Xu et al., 2018), and the Cleveland Basin in Yorkshire (Site 85) (McArthur et al., 2008; Baroni et al., 2018; Thibault et al., 2018). Relatively high concentrations occur also in the Swiss Tabular Jura at Rietheim (Site 68) (Montero-Serrano et al., 2015), the SW German Basin at Dotternhausen (Site 72) (Baroni et al., 2018; Wang et al., 2020), and the North German Basin at Aubach (Site 75) (Hougaard et al., 2021). Relatively high average Fe concentrations were observed also in the Alpine-Mediterranean Tethys in the Austrian Bächental section (Site 70) and Sachrang site (Site 71) (Ebli et al., 1998; Neumeister et al., 2016).

In the ‘post-negative CIE plateau interval’, with the exception of very few records, a general decrease in Mn average concentrations is documented throughout the investigated area (Fig. 8f). With the exception of the Sachrang record (Site 71), where only two data points suggest concentrations as high as about 5900 ppm (Ebli et al., 1998), all other records exhibit average concentrations lower than 2000 ppm. In particular, Mn average concentrations between 1000 and 2000 ppm were observed at Sancerre-Couy (Site 31) with average values of 1500 ppm (Hermoso et al., 2009b, 2013), and the Sogno Core (Site 40) with average values of 1700 ppm (Gambacorta et al., 2023). Similarly, a general decrease in Fe average concentrations is documented in the analysed records during the ‘post-negative CIE plateau interval’ (Fig. 9f). Relatively higher values continued to persist in the northern European epicontinental basins and sub-basins as opposed to the Alpine-Mediterranean area, although with lower values compared to those obtained for the negative CIE interval. Only the Mochras Farm Borehole (Site 82) and the Yorkshire succession (Site 85) exhibit relatively high average values of about 6% (Baroni et al., 2018; Thibault et al., 2018; Xu et al., 2018), while all the other records show Fe average concentrations lower than 4%.

5. Palaeoceanographic changes across the Toarcian Oceanic Anoxic Event

5.1. Evolution of redox conditions

The stratigraphic variation in estimated ‘Redox Indexes’ integrated with the other data presented herein shed light on the evolution of watermass conditions across the Jenkyns Event in the Alpine-Mediterranean Tethys and north European epicontinental seaway. Available data clearly indicate that just prior to the onset of the negative CIE (‘pre-negative CIE interval’) most of the considered records were characterized by well-oxygenated bottom waters (Fig. 7a) as indicated by widespread sediments hosting benthic fauna (e.g., trace fossils, bivalves, brachiopods, etc.), rare deposition of black shales, and lack of small pyrite framboids ($<5\text{ }\mu\text{m}$). Anoxia was confined to very local areas, such as some deeper parts of the Dutch Central Graben (RI = 3), in a limited part of the SW German Basin (RI = 4), and the Tunisian Atlas (RI = 4), as illustrated by black shales containing either continental or degraded marine organic matter, as suggested by average values of TOC $<5\%$. The common occurrence of euhedral pyrite and framboids larger than $5\text{ }\mu\text{m}$ has been attributed to early to late phases of diagenesis (Love and Amstutz, 1966; Wilkin and Barnes, 1996; Wilkin et al., 1996).

At the onset of the negative CIE (‘falling limb onset interval’) a general deterioration of bottom-water oxygen conditions occurred at supra-regional scale in all the investigated sites (Fig. 7b). The deposition of black shales and dark grey shales became widespread, typically associated with an increase in the average TOC content and HI values, although redox conditions were variable at different locations. Inorganic and organic geochemical proxies and the absence of benthic fauna (RI = 5) indicate that euxinia, and at times PZE, were confined to the north European epicontinental basins and sub-basins (Cleveland Basin, Paris Basin, North German and SW German basins). Local conditions might have hindered the establishment of stable anoxic/euxinic conditions, as in the Dutch Graben, where storms and geostrophic flows frequently

re-oxygenated the water-column during the interval represented by the entire negative CIE (Trabucho-Alexandre et al., 2012). Indeed, the widespread drastic transition to facies without bioturbation and benthic fossils in those areas where anoxia was never reached during the ‘falling limb onset interval’ indicates that the sediments were at least affected by lowered oxygen availability in pore waters, thus paralleling, albeit with lower intensity, what is observed on a supra-regional scale.

The most extreme intense anoxia/euxinia occurred in correspondence with the lowest point in the carbon-isotope trough (‘valley floor interval’) (Fig. 7c). The geographical distribution of black shales reached its maximum extent at different latitudes and palaeowater depths. In this stratigraphic interval, some sections present the only black shale occurrence of the entire succession, such as in the Lusitanian Basin at Peniche (Hesselbo et al., 2007). The organic matter content reached its maximum in most of the records with highest values up to more than 20%. Pyrite framboids reached their smallest sizes ($<5\text{ }\mu\text{m}$), further confirming a shift to the most extreme euxinic conditions in the water column, locally and temporarily extending into the photic zone as indicated by biomarkers for green sulfur bacteria. Based on available data, euxinia (RI = 5), although mainly confined to northern European areas, occurred locally also in other basins such as the Tunisian Atlas (Ruebsam et al., 2022b), the Slovakian Basin within the Oravicium crustal block and the Bohemian Massif (Suan et al., 2018), and the Mecsek Basin in Hungary (Ruebsam et al., 2018).

The latest phase of the negative CIE (‘top rising limb interval’) was characterized by persistent reducing conditions (Fig. 7d). Locally, the recovery from hypoxia started during the rising limb isotopic segment. In some sections, the deposition was characterized either by the absence of black shales, such as in the Lombardy Basin in the pelagic Sogno and Gajum records (Gambacorta et al., 2023), or a shift to lighter coloured shales as in the L1 and Schandelah cores in the North German Basin (Visentin et al., 2021). Some local changes to suboxic conditions occurred also in the euxinic north epicontinental basins, as in the Sancerre-Couy section (RI = 3) (Hermoso et al., 2009b, 2013) of the Paris Basin. TOC values decrease both in epicontinental areas and in the Alpine-Mediterranean Tethys. However, available data indicate that the recovery from anoxia was not synchronous with relatively milder conditions (RI equal to 1 or 2) or even a return to fully oxygenated conditions (RI = 0) occurring first in the Alpine-Mediterranean Tethys, north African margin, and proto-Atlantic areas and later in the north European epicontinental basins and sub-basins. As observed also by Silva et al. (2021b), the stratigraphic interval corresponding to the rising limb isotopic segment (partly covered by their organic-matter preservation interval T4 (OAE)) is characterized by widespread deposition of organic-rich facies, thus indicating that organic-carbon sequestration continued to occur also with the positive $\delta^{13}\text{C}$ trend of the Jenkyns Event.

While the progressive recovery from extreme redox conditions in the latest part of the negative CIE was in most cases subtle, a more drastic and widespread shift to more oxygenated bottom waters is documented for the ‘post-negative CIE plateau interval’ (Fig. 7e). All available data suggest that after the negative CIE anoxia/euxinia persisted exclusively in north European epicontinental areas. With the exceptions of the Petousi section in the Ionian Zone (Kafousia et al., 2013, 2014) and the Châabet El Attaris record in Tunisia (Reolid et al., 2021b), black shales and dark grey shales remained confined to north European basins and sub-basins with relatively high average TOC and HI values. An additional exception is represented by the Alpine-Mediterranean section of Sachrang in Bavaria (Germany), where the deposition of organic-rich marlstone persisted after the end of the negative CIE (Ebli et al., 1998). Apart from these areas, benthic fauna fully recovered as illustrated by RI equal to 0 in most of the sections with common bioturbation and high ichnodiversity (e.g., Fernández-Martínez et al., 2021), paralleled by the general absence of euhedral pyrite. Euxinia was likely confined to relatively smaller marine areas of the northern epicontinental basins and sub-basins. Overall, over the ‘post-negative CIE plateau interval’, sulphidic conditions became less intense and more

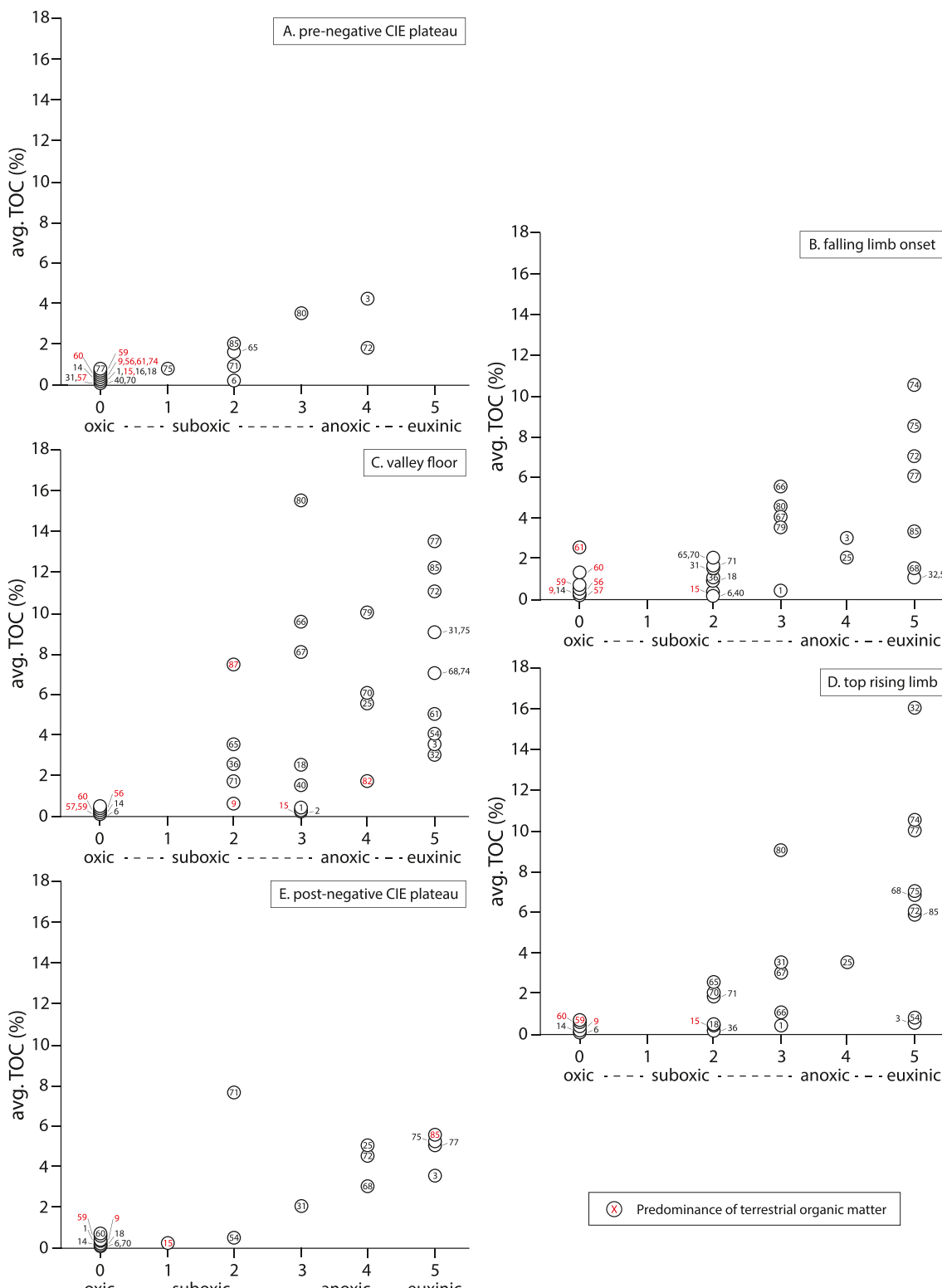


Fig. 10. Cross-plots of average total organic carbon (TOC) versus estimated redox conditions. Sites dominated by terrestrial organic matter (woody fragments, coaly horizons, etc.) are reported in red. For site identification and palaeogeographic location refer to Table 1 and Fig. 1. See text for details. (For interpretation of the references to colour in this figure legend, the reader is referred to the web version of this article.)

intermittent with brief periods of oxygenation that illustrate a gradual increase of oxygen availability and less stable and more seasonal PZE (Schwark and Frimmel, 2004; McArthur et al., 2008; Dickson et al., 2017; Baroni et al., 2018; Thibault et al., 2018; McArthur, 2019; Houben et al., 2021; Ajuaba et al., 2022). In summary, as shown also by Silva

et al. (2021b), enhanced organic-matter preservation, even if confined to a relatively smaller region, continued to take place also during the stratigraphic interval associated with the broad positive carbon-isotope excursion following the negative carbon-isotope anomaly.

Distribution of anoxia played a major role in the preservation of

organic matter during the T-OAE. The variation in TOC versus the ‘Redox Indexes’ estimated for each stratigraphic interval are reported in Fig. 10. Lower TOC values are recorded in correspondence with the generally well-oxygenated ‘pre-negative CIE interval’, while values rise in parallel with the negative CIE with maximum values at the level of the ‘valley floor interval’, confirming that, as observed also by Remirez and Algeo (2020b), local controls on carbon burial were amplified during the early Toarcian event. As expected, the rise in TOC content parallels the increase in the ‘Redox Index’, because of the more intense reducing conditions that favoured an enhanced preservation and also by the decrease in or lack of sediment reworking by benthic fauna.

5.2. Palaeoceanographic changes across the Toarcian Oceanic Anoxic Event in the Alpine-Mediterranean Tethys, north African margin, and north European epicontinental seaway

The causes of the observed widespread deoxygenation associated with the T-OAE, and, in particular, the mechanisms behind the establishment of intense anoxia/euxinia confined to north European epicontinental basins and sub-basins have been a matter of debate. An intensification of fresh-water runoff that favoured the establishment of a stronger pycnocline that prevented an efficient circulation has been suggested to explain the formation of anoxic/euxinic conditions in northern epicontinental basins (e.g., Sælen et al., 1996; Röhl et al., 2001; McArthur et al., 2008; Dera and Donnadieu, 2012; French et al., 2014; Dickson et al., 2017; Ruebsam et al., 2018; McArthur, 2019; Remirez and Algeo, 2020a).

The significant rise in $p\text{CO}_2$ concentrations reconstructed for the early Toarcian time interval (McElwain et al., 2005; Ruebsam et al., 2020a) presumably favoured an increase of average global temperatures (Bailey et al., 2003; Dera et al., 2011; Korte and Hesselbo, 2011; Gómez et al., 2016; Ruebsam et al., 2020d; Erba et al., 2022) and the acceleration of the hydrological cycle with increased weathering and runoff (Brumsack, 1991; Jones and Jenkyns, 2001; Bjerrum et al., 2001; Cohen et al., 2004; Dera et al., 2009a; Hermoso and Pellenard, 2014; Brazier et al., 2015; Montero-Serrano et al., 2015; Percival et al., 2015; Fantasia et al., 2018; Jenkyns and MacFarlane, 2021). Using a coupled ocean-atmosphere model (Fast Ocean Atmosphere Model – FOAM) Dera and Donnadieu (2012) estimated for the early Toarcian an average increase of 9 cm/yr in global precipitation rates and a 3.5 cm/yr rise in mean annual continental runoff. Higher volumes of fresh-water could then have entered particularly the northern epicontinental basins, perhaps extending as far south as the Austro-Alpine region (Sachrang and Bächental sections), thereby impacting the surface-water salinity and circulation.

A progressive warming of about 7–10 °C from the onset of the negative CIE to the interval characterized by the most negative carbon-isotope values at the inflection point marking the onset of the rising limb is well supported by TEX₈₆-based sea-surface temperatures from the Tethyan region (Ruebsam et al., 2020d). By considering the typical $\Delta^{18}\text{O}_{\text{carb}}$ gradients between 0.2–0.3 ‰ per °C for marine carbonates (Leng and Marshall, 2004; Maslin and Dickson, 2015), a decrease in $\delta^{18}\text{O}$ of about 2 ‰ is thus well explained by the shift to warmer conditions. Because oxygen isotopes can be greatly affected by diagenesis, their use as a reliable proxy for temperature reconstruction can be hindered (e.g., Marshall, 1992; Blanchet et al., 2012). However, the large number of records considered in this review allows a supra-regional smoothing of local distortions. The compilation of $\Delta^{18}\text{O}$ data presented in Fig. 6 offers some interesting considerations. Previous works (e.g., Sælen et al., 1996; Röhl et al., 2001; Dera and Donnadieu, 2012) demonstrated a systematic offset in the oxygen-isotope composition between records from northern European epicontinental basins and sub-basins and those from the Alpine-Mediterranean Tethys. Records located at higher latitudes, thus presumably cooler, exhibit counterintuitively lower $\Delta^{18}\text{O}_{\text{carb}}$ values than coeval records from lower latitudes (see tables in the Appendix A). In particular, many records

show a decrease in $\delta^{18}\text{O}$ larger than the hypothetical 2 ‰. Based on these observations, local variations in salinity might have influenced the lower $\Delta^{18}\text{O}_{\text{carb}}$ record in addition to temperature. In agreement with suggestions by previous authors, based both on bulk carbonate and belemnite oxygen-isotope data (e.g., Sælen et al., 1996; Röhl et al., 2001; Rosales et al., 2004 BEL; Dera and Donnadieu, 2012; Harazim et al., 2013), we speculate that on top of the global rise in temperature, the observed lower $\Delta^{18}\text{O}_{\text{carb}}$ values reflect a strong north-south gradient in salinity stratification, characterized by a progressive increase in runoff and fresh-water input to the northern European epicontinental basins and sub-basins that probably reached its acme in correspondence of the inflection point at the onset of the rising limb of the carbon-isotope curve (Fig. 11). Following Wei et al. (2018) and Wei and Algeo (2020), a recent study by Remirez and Algeo (2020a) used the B/Ga and S/TOC ratios to reconstruct watermass salinity in the Cleveland Basin (UK) and inferred a change from initially weakly brackish to strongly brackish conditions during the Jenkyns Event. Although some freshening did take place, Hesselbo et al. (2020) argued that the suggested degree of freshening (i.e., brackish or even freshwater conditions) proposed by Remirez and Algeo (2020a) is unrealistic. In particular, according to Hesselbo et al. (2020), reconstructed palaeo-salinities are not in agreement with the presence of organisms such as ammonites, benthic crinoids, belemnites, gastropods and bivalves typical of normal marine conditions. However, reconstruction of the possible sources of fresh-water input is difficult. Ruebsam et al. (2020c), based on organic geochemical and palynological data, suggested a massive increase in sediment delivery to the north European epicontinental basins from the hinterland. The presence of rivers located on emerged lands bounding the Causses and Quercy basins in France and SW German Basin capable of delivering fresh waters was suggested, based on oxygen-isotope data (Röhl et al., 2001; Emmanuel et al., 2006; Mailliot et al., 2009). A coeval Toarcian-Bajocian subsurface succession from the North German Basin was interpreted as a river-dominated deltaic system with typical delta plain (distributary deltaic channel belts and associated sheetsands) and delta-front (distributary mouth bar complexes) deposits (Zimmermann et al., 2017). Abundant phytoplankton in various basins were attributed to relatively proximal riverine inputs, as in the Mecsek Basin in Hungary (e.g., Baranyi et al., 2016; Suan et al., 2018; Rodrigues et al., 2020a, 2020b, 2021). As suggested by Baroni et al. (2018), continental runoff could have been paralleled by a southward flow through the Viking Corridor of brackish waters derived from the Arctic (Bjerrum et al., 2001) that could have reached northern epicontinental areas (Dera et al., 2009b; Korte et al., 2015) (Fig. 11).

Lowered surface-water salinities would have favoured the formation of a stable pycnocline that reduced the circulation efficiency, thereby inducing bottom-water deoxygenation. However, even if a common deterioration in bottom-water oxygenation can be observed at supra-regional scale, estimated redox conditions reported in Fig. 7 demonstrate that anoxia/euxina was not equally distributed. The physiography of the different basins and sub-basins might have played a major role in controlling the extent and intensity of bottom-water anoxia. The relatively open Alpine-Mediterranean Tethys and the regions close to the proto-Atlantic, with the exception of some local settings, were generally affected by relatively less severe redox conditions. The Austro-Alpine localities (i.e., Bächental, in particular, and Sachrang sections) are indeed anomalous compared with other Alpine-Mediterranean facies. Unlike other coeval Tethyan sections, these records are unusual in having relatively high TOC content, as well as Mn-rich carbonates (Ebli et al., 1998; Neumeister et al., 2015, 2016; Suan et al., 2016). The establishment of the peculiar redox conditions developed in this area were probably controlled by the relative proximity of this region to the epicontinental margin, which, further enhanced by local physiographic conditions, favoured the influence of a possible fresh-water input from the north. Unlike the Alpine-Mediterranean Tethys and north African margin, the articulated submarine physiography of the northern European area with shallow-water depths of about 15–150 m (Hallam, 1967;

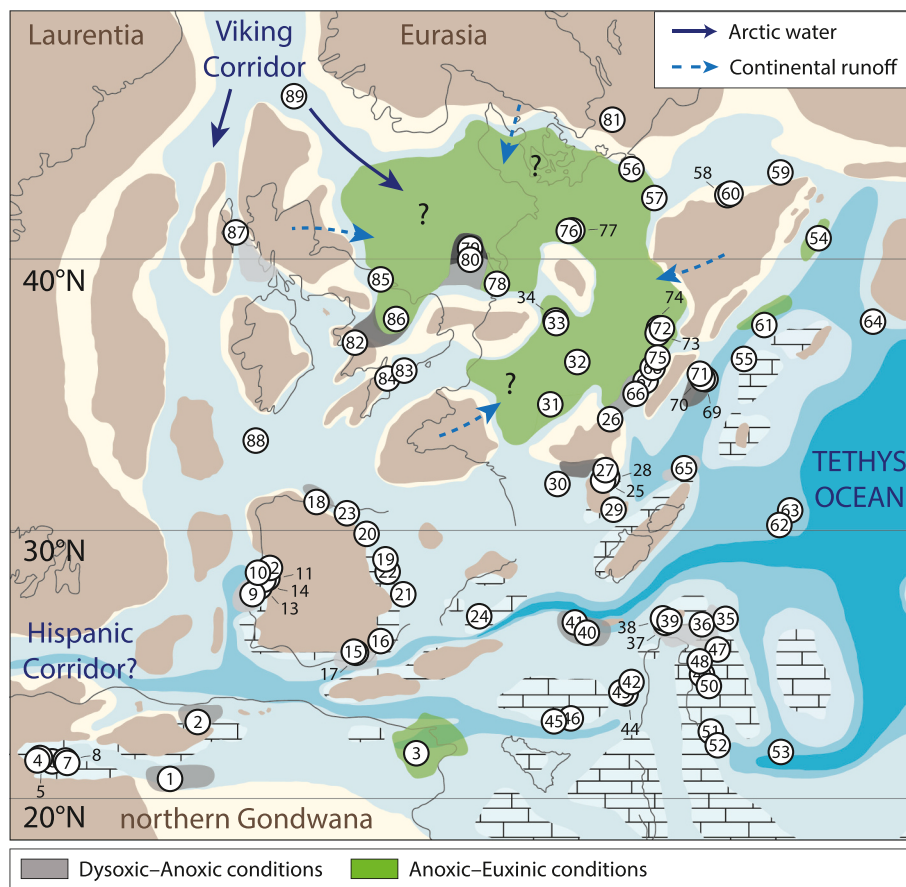


Fig. 11. Hypothetical fresh-water input of Arctic water masses and continental runoff into the epicontinental basins and sub-basins. See text for details.

(Röhl et al., 2001; Frimmel et al., 2004) and poor communication with the rest of the Tethys Ocean was likely favourable to the establishment of a relatively sluggish circulation (Remirez and Algeo, 2020b). Geochemical data are consistent with this interpretation. Changes in the Mo/TOC ratio in records from northern epicontinental basins, a proxy for reconstructing palaeohydrographic conditions (Algeo and Lyons, 2006; Algeo and Rowe, 2012), indicate aqueous Mo drawdown connected to severe watermass stagnation (e.g., McArthur et al., 2008; Pearce et al., 2008; Hermoso et al., 2013; Dickson et al., 2017; McArthur, 2019; Remirez and Algeo, 2020a, 2020b; Chen et al., 2021; Houben et al., 2021; Wang et al., 2021). The distribution of gammacerane, an organic geochemical proxy used to infer changes in water-column stratification, commonly related to hypersalinity (Sinninghe Damsté et al., 1995), is in agreement with a model of watermass restriction mainly confined to northern epicontinental basins and sub-basins. Evidence of gammacerane is reported for only a limited number of sites and, with the exception of the peculiar Austro-Alpine region (Neumeister et al., 2015), never thus far described in sections from the Alpine-Mediterranean Tethys and north African area. On the contrary, gammacerane is reported for the north European epicontinental shelf, with major concentrations reached in the ‘valley floor interval’ (Farrimond et al., 1989; French et al., 2014; Ruebsam et al., 2018; Xu et al., 2018; Ajuba et al., 2022). According to Baroni et al. (2018), the onset of bottom-water anoxia in the north European basins and sub-basins was amplified by large-scale ocean dynamics. Based on the results of FOAM models, they suggested the presence of a clockwise gyre over the Tethys Ocean capable of bringing oxygenated waters from the Equator. According to their models, due to the particular articulated physiography of the northern epicontinental seaway, the northward limb of the gyre was significantly weakened, thereby making this region highly sensitive to continental runoff and stratification. Indeed, available data suggest

that deposition of organic matter during the Jenkyns Event was mainly controlled by enhanced preservation favoured by persistent anoxia/euxinia with relatively modest flux rates of organic carbon but low supply of accompanying clastic and carbonate materials, thereby leading to stratigraphic condensation (Kemp et al., 2022b; Ruebsam et al., 2022b).

The recovery from anoxia occurred diachronously, with an earlier progressive re-oxygenation in the Alpine-Mediterranean Tethys and in the north African margin than in the north European epicontinental seaway. The establishment of less intense reducing conditions started during the rising limb isotopic segment. This timing is in agreement with global ocean redox trends, estimated by means of rhenium and molybdenum mass balance models, which depict a contraction of anoxia-euxinia before the end of the negative CIE (Kunert and Kendall, 2023). Geochemical data indicate that, with the end of the negative CIE, salinities moved progressively from strongly brackish back to weakly brackish (Remirez and Algeo, 2020a). The gradual cooling that accompanied the end of the negative CIE (Gambacorta et al., 2023) could have reduced weathering and runoff, thereby favouring the weakening of the pycnocline and the re-establishment of a more efficient circulation (Gambacorta et al., 2023) and a progressive termination of the event. van de Schootbrugge et al. (2020) interpreted the change in the dinoflagellate association from offshore Norway and the Yorkshire Coast (UK) as evidence of an enhanced connectivity between the Arctic and the Tethys through the Viking Corridor due to a relative sea-level rise. According to their interpretation, the arrival of low-salinity and oxygenated Arctic waters favoured the shift and establishment of dysoxic or even oxic conditions. However, this interpretation is not in agreement with the available sedimentologic and geochemical evidence, and a greater fresh-water input from the Arctic would have more likely favoured an intensification of watermass stratification rather than the

re-establishment of more oxygenated bottom-water conditions.

5.3. Variations in manganese and iron pools during the Toarcian Oceanic Anoxic Event

Lower Toarcian manganese-rich carbonates, with Mn contents reaching in some places very high concentrations of up to more than 20%, associated with organic-rich deposits, have been widely described in the literature (e.g., Jenkyns et al., 1985, 1991; Jenkyns, 1988; Neuemeister et al., 2016; Suan et al., 2016). However, their origin is still a matter of debate in part due to the stratigraphic control that may not be sufficiently precise to understand the possible causal link between the T-OAE and the observed enrichments. Indeed, most Mn-rich carbonates occur in the Alpine-Mediterranean Tethys, in particular in the Italian Lombardy Basin (e.g., Sogno Core) (Gambacorta et al., 2023), Belluno Basin (Dogna Core) and associated outcrop (Bellanca et al., 1999; Jenkyns et al., 2001), in the Julian Alps (Monte Mangart section) (Sabatino et al., 2009), and in the Austro-Alpine area (Bächental and Sachrang sections) (Germann, 1973; Ebli et al., 1998; Neuemeister et al., 2015, 2016; Suan et al., 2016) and the Bakony Mountains of western Hungary (e.g., Jenkyns et al., 1991; Polgári et al., 1991).

The major sources of manganese to the ocean are riverine inputs and, to a lesser extent, hydrothermal activity (Corbin et al., 2000; Tribouillard et al., 2006; van Hulten et al., 2017). The sedimentary geochemistry of manganese is strongly affected by changes in bottom-water redox conditions (Calvert and Pedersen, 1996; Tribouillard et al., 2006) (Fig. 12). Manganese, present in low concentrations in the dissolved phase, is scavenged as Mn(IV) in particulate Mn-

oxyhydroxides (Calvert and Pedersen, 1993, 1996). Under reducing conditions, however, oxyhydroxides are dissolved and Mn reduced to soluble Mn(II) that can diffuse either upward or downward within the sediments (Brumsack, 1986, 1989; Rajendran et al., 1992; Tribouillard et al., 2006). Upward diffusion of Mn(II) can lead either to the accumulation of Mn-oxyhydroxides in oxic pore waters or to the escape back into the water column if anoxic pore waters extend up to the sediment-water interface (Calvert and Pedersen, 1996; Cruse and Lyons, 2004). By contrast, the downward diffusion of Mn(II) can lead to MnCO₃ precipitation, a process that, with the exception of silled anoxic basins, becomes efficient under reducing pore waters but oxic bottom waters (Pedersen and Price, 1982; Calvert and Pedersen, 1993, 1996; Morford et al., 2001; Tribouillard et al., 2006). Generally, in the case of a poorly efficient fixation of Mn in carbonates, sediments are generally depleted in Mn under reducing conditions (Hild and Brumsack, 1998; Tribouillard et al., 2006). So, even if Mn-oxyhydroxides and Mn-carbonates are precipitated under opposite redox conditions in pore waters, their presence in open-marine settings suggests in both cases the occurrence of a surplus in Mn associated with oxic bottom-water conditions.

Higher fluxes of hydrothermally derived Mn could have been behind these enrichments in those areas close to the ridges of the Tethys Ocean (Jenkyns et al., 1991). Local hydrothermal sources of Mn were probably important in the Hungarian Úrkút deposit (Polgári et al., 1991, 2012), otherwise redox conditions were likely the governing factor responsible for the observed Mn enrichments. Such an origin is consistent with the spatial distribution of high Mn concentrations in the Lower Toarcian (Fig. 8). However, additional contributions from rivers should be taken into consideration. Fresh water associated with the increased runoff probably sourced additional amounts of Mn to shelfal and basinal areas (Gambacorta et al., 2023). However, as there is little evidence of rivers in the Alpine-Mediterranean Tethys, probably most of the Mn that reached this area was exported from epicontinental northern Europe. On top of these contributions to the Mn budget, an additional input from Arctic waters from the Viking Corridor cannot be excluded. In fact, due to the specific hydrographic configuration, the watermasses of the modern Arctic are enriched in Mn derived from rivers or coastal erosion (März et al., 2011; Macdonalds and Gobeil, 2011; Meinhardt et al., 2016a, 2016b). A similar process could have occurred also in Toarcian times, thereby transporting Mn-enriched waters from the Viking Corridor to northern epicontinent areas. Manganese delivered to the anoxic/euxinic north European epicontinent basins and sub-basins would have remained in solution and, when not fixed into Mn-carbonates, diffused from the sediment-water interface back to the water column. The epicontinent basins and, to a minor extent, the other anoxic/euxinic basins, likely acted as pools of dissolved manganese. Some of the dissolved Mn may have been reprecipitated in the Mn pool as Mn-carbonates or may have been transported from epicontinent basins into the Tethys Ocean where, upon encountering oxygenated conditions, it would have been deposited as Mn-oxyhydroxides or Mn-carbonates, according to the prevailing redox conditions (Fig. 13). Theoretically, as proposed in the idealized ‘bathtub ring’ model proposed by Force and Cannon (1988), Mn-rich sediments would then have formed all along the edge of the Mn-pool adjacent to the more oxygenated Tethys Ocean and in the northern part of the Adria microplate. However, available data, even if scattered, indicate that observed Mn-rich deposits do not form a continuous ring around the anoxic/euxinic north European epicontinent basins and sub-basins, but are limited to the southeast margin (i.e., Belluno Basin, Lombardy Basin, Julian Basin, Austro-Alpine nappes, Hungary) of the Alpine-Mediterranean Tethys and to the northern part of the Adria microplate. Some hypotheses can be advanced to explain the observed distribution. First, it is possible that truly oxic conditions were encountered only at the edge with the oxygenated Tethys Ocean while, in the rest of the surrounding areas, redox conditions were not favourable for the deposition of Mn. Otherwise, a major control by basin physiography could lie at the heart of the observed trends. In particular, the outflow of

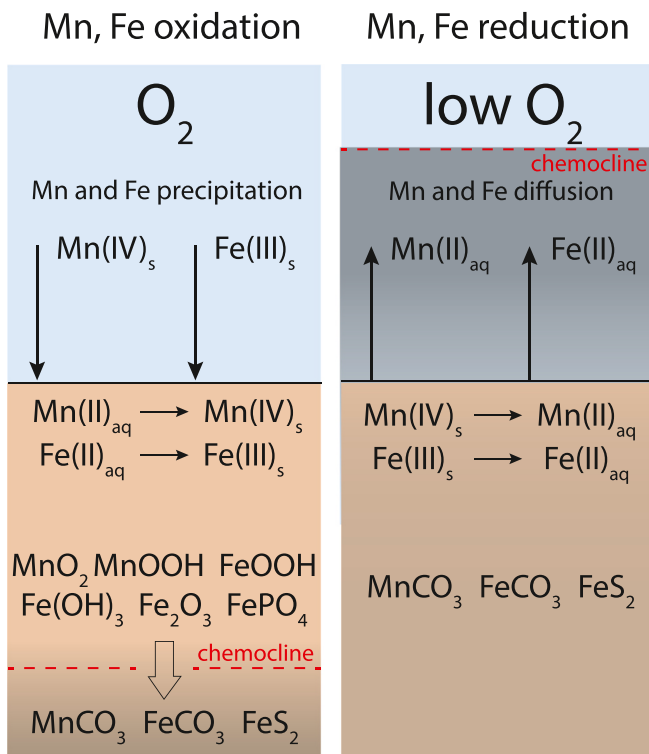


Fig. 12. Manganese and iron redox cycling. On the left: oxic bottom and pore waters favour the oxidation of Mn and Fe with the deposition of Mn and Fe oxides and hydroxides. Reducing pore-waters conditions occurring within the sediments below the chemocline favour instead the fixation of Mn in carbonates and of Fe in both carbonates and sulphides. On the right: under poorly-oxygenated bottom-water conditions (i.e., with the chemocline located in the water column above the sediment-water interface) reduced Mn and Fe are either fixed within the sediments in the form of Mn-carbonates, Fe-carbonates, and Fe-sulphides, or diffused back to the water column as divalent Mn and Fe.

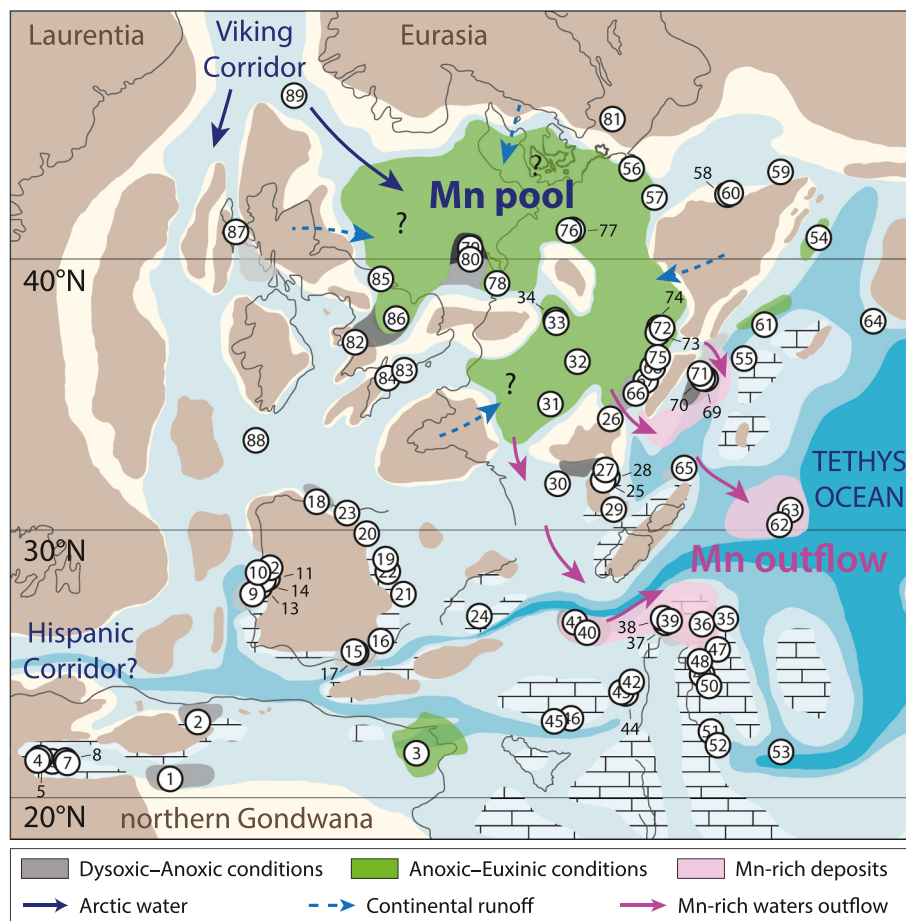


Fig. 13. Manganese cycling in the Alpine-Mediterranean Tethys and north European epicontinental basins and sub-basins during the T-OAE. See text for details.

large amounts of dissolved Mn could have been favoured only at the edges of the anoxic/euxinic basins where sills were sufficiently deep to allow the Mn-rich waters to pass through and exported elsewhere to be ultimately deposited, depending on the diagenetic pathway, as Mn-oxyhydroxides or Mn-carbonates. In present-day oceans, oxygen minimum zones are enriched in Mn (Calvert and Pedersen, 1993, 1996; Brumsack, 2006). As shown in some models proposed (Jenkyns, 1985, 1988; Jenkyns et al., 1991), oxygen-minima could have extended southwards during the T-OAE acting as a conveyor belt of divalent Mn from the north European epicontinental seaway to the Alpine-Mediterranean Tethys.

Interesting considerations also arise from reconstructed stratigraphic and palaeogeographic variations in Fe concentrations. Iron is delivered to the oceans mainly from rivers, aeolian dust and hydrothermal fluxes (Raiswell and Canfield, 2012). Under oxic conditions, Fe(III) is the thermodynamically stable geochemical species that tends to form mainly nanoparticulate Fe-oxyhydroxides. Conversely, Fe(II) is stable under anoxic conditions and either diffuses from reduced pore waters or forms FeCO_3 and Fe-sulfides (Raiswell and Canfield, 2012). Iron is recycled from shallow shelf sediments, either transported as Fe oxyhydroxides with oxic seawater towards the basin or diffused from pore waters, and laterally transported to adjacent marine basins (Fe shuttling) (Canfield et al., 1996; Wijsman et al., 2001; Lyons and Severmann, 2006; Dellwig et al., 2010; Raiswell and Canfield, 2012; Lenstra et al., 2019). In the presence of sulfidic (euxinic) waters mobilized Fe can be precipitated and trapped in the form of Fe sulfides (Lyons and Berner, 1992; Canfield et al., 1996; Lyons and Severmann, 2006; Raiswell and Canfield, 2012) (Fig. 9). Consequently, in an opposite way to Mn, sediments deposited under reducing conditions are commonly enriched in Fe.

Relatively high Fe concentrations are observed in the north European epicontinental basins and sub-basins (Fig. 9). Greater amounts of Fe were likely delivered to shelfal areas by the enhanced riverine supply, and then trapped into these basins as Fe sulphides. Hydrothermal fluxes from spreading ridges likely constituted an additional Fe source to Tethyan areas, although the generally mild redox conditions and open physiography did not allow accumulation of iron in great quantities.

Even if Mn and Fe data at high-resolution are still relatively limited, some common patterns can be outlined and a hypothetical evolution of Mn and Fe sketched out for the early Toarcian (Fig. 14). In most records, the ‘pre-negative CIE interval’ is characterized by a rise in Mn and Fe content (Figs. 8a, 9a) with respect to background values (Fig. 14b). In this stratigraphic interval, due to the prevailing oxic conditions, Mn diffusion from sediments was very limited and Mn and Fe accumulated mainly as oxyhydroxides. With the onset of anoxia/euxinia Mn transported to the epicontinental basins was rapidly remobilized, leaving Mn-depleted deposits (Fig. 8c) as a consequence of the dominance of Mn diffusion back into the water column. Part of this Mn could potentially have flowed out of the basins and reprecipitated, forming a rim of Mn-oxyhydroxides and Mn-carbonates at the contact with the better oxygenated waters of the Tethys Ocean, thus representing an additional contribution to the Mn sourced from hydrothermal ridges. By contrast, Fe was trapped as Fe-sulphide inside the anoxic/euxinic restricted basins (Figs. 9c, 14c). On a smaller scale, a similar process probably operated locally in some basins in the Alpine-Mediterranean Tethys (Figs. 8 and 9) as highlighted by the enrichments in Mn and Fe in these areas. Similarly, local suboxic to anoxic conditions and higher amounts of riverine-derived Mn and Fe favoured the fixation of Fe-sulphides and the remobilization of Mn and its reprecipitation downcurrent under oxic conditions. Such processes persisted throughout the interval of the negative

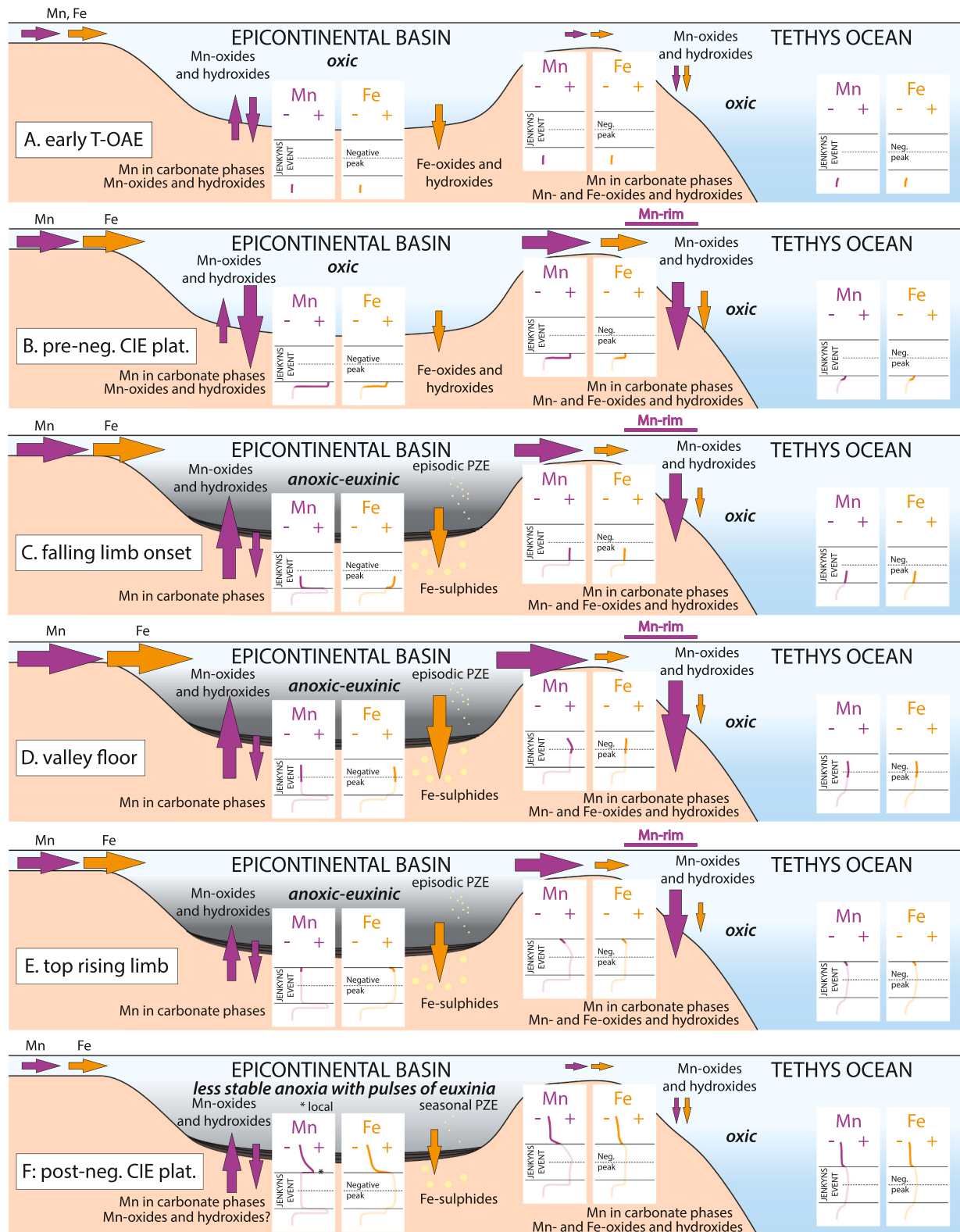


Fig. 14. Scheme representing the temporal and palaeogeographic variation in Mn and Fe in north European epicontinental basins and sub-basins across the T-OAE. See text for details.

CIE (Fig. 14d and e). With the end of the negative CIE ('post-negative CIE plateau interval'), the relative weakening of runoff could have resulted in lowered amounts of riverine-supplied Mn and Fe, and the consequent decrease in Mn and Fe concentrations (Figs. 8f, 9f, and 14f). The establishment of less intense and intermittent sulphidic conditions in northern epicontinental basins probably decreased the fixation of Fe into sulphide, although the environment remained unfavourable for the fixation of Mn in oxyhydroxides. However, it should be noted that some sites record a rise in Mn concentration right after the negative CIE, such as at Sancerre-Couy in the Paris Basin (Hermoso et al., 2009b), in the Schandeholz Core in the North German Basin (Baroni et al., 2018), and in the Cleveland Basin, Yorkshire (UK) (Baroni et al., 2018). Probably these local rises in Mn concentrations represent either intervals of transient oxic conditions favourable to the massive fixation of Mn-oxyhydroxides and Mn-carbonates, or a reduction in the outflow of Mn with the prevalent fixation into Mn-carbonates inside the North European epicontinental Mn-rich pool.

6. Conclusions

With this review we provide a detailed temporal and palaeogeographic characterization of the T-OAE in the Alpine-Mediterranean Tethys, north Africa and north European epicontinental basins. From this study, we conclude that:

1. In agreement with suggestions made by other authors in the past, with the exclusion of only three $\delta^{13}\text{C}_{\text{carb}}$ isotopic records characterized by a wedge-shaped profile, it is always possible to apply a three-fold subdivision of the negative CIE. In particular, from bottom to top, six isotopic segments can be recognized within the T-OAE isotopic excursion: a pre-plateau positive excursion and a pre-negative CIE plateau that predates the negative CIE, a falling limb, a valley floor, and a rising limb forming the negative CIE, and a post-negative CIE plateau.
2. In the stratigraphic interval immediately preceding the negative CIE of the T-OAE bottom waters were generally well-oxygenated, with anoxia confined to very local areas, such as some deeper parts of the Dutch Central Graben, in a limited part of the SW German Basin, and locally in the Tunisian Atlas and Moroccan High Atlas.
3. A synchronous shift to poorly oxygenated bottom waters correlates with the onset of the negative CIE and remained prevalent during this interval, with widespread deposition of organic-rich black shales on a supra-regional scale. Euxinia was mainly confined to the north European epicontinental basins and sub-basins, while a general decrease in oxygen availability occurred in certain basins of the Alpine-Mediterranean Tethys.
4. The most extreme palaeoceanographic conditions were reached in the core of the negative CIE when organic-matter preservation, and probably stratigraphic condensation, reached their maximum extent.
5. The widespread recovery to better oxygenated conditions started immediately after the end of the negative CIE, although the onset of improved bottom-water oxygenation is locally documented just before its end. With the end of the negative CIE, deposition of black shales and dark grey shales remained confined to north European basins and sub-basins. Apart from this area, excluding very few local exceptions, well-oxygenated conditions were fully re-established in the Alpine-Mediterranean Tethys and North African margin, as documented by the presence of benthic fauna, common bioturbation and high ichnodiversity, in agreement with geochemical data. At this time, the north European epicontinental seaway experienced brief periods of oxygenation with anoxia likely confined to more limited areas characterized by less intense and intermittent sulphidic conditions associated with more seasonal photic-zone euxinia. Evidently, while the onset of anoxia was a synchronous event, its termination was earlier in the Alpine-Mediterranean Tethys than in the north European epicontinental basins.

6. The presented compilation of $\Delta^{18}\text{O}_{\text{carb}}$ data clearly demonstrates, as observed by other authors in the past, a salinity-dependent systematic offset between the northern European epicontinental basins and sub-basins and Alpine-Mediterranean Tethys. Oxygen-isotope data show that the shift to lower ratios from the onset of the falling limb to the onset of the rising limb is different from section to section. In particular, higher $\Delta^{18}\text{O}_{\text{carb}}$ amplitudes are recorded at sites located in the northern epicontinental area, indicating that temperature cannot be the primary control behind the observed signal. We interpret these data as the evidence of a progressive increase in runoff and/or in Arctic fresh-water input to the northern European epicontinental basins and sub-basins that reached its acme in the core of the negative CIE. The increase in fresh-water flow coupled with the closed physiography of the north European epicontinental basins and sub-basins promoted the formation of a stronger pycnocline. The limited water exchange with the Tethys Ocean favoured the onset of anoxia/euxinia into these confined basins and the enhanced preservation of organic matter.
7. The limited exchange with surrounding areas, the proximity to the input of riverine-sourced Mn and Fe, and the peculiar redox conditions of the northern epicontinental basins and sub-basins favoured their role as pools for dissolved manganese that diffused into the water column, and the intense accumulation of iron into iron sulphides. We speculate that a part of the large amount of dissolved manganese present in epicontinental basins and sub-basins was exported and deposited at the interface with the more oxygenated waters of the Tethys Ocean. This input of manganese could have represented an additional contribution to the formation of the manganese-rich carbonates observed in correspondence with the T-OAE in the Alpine-Mediterranean region.

Declaration of Competing Interest

The authors declare that they have no known competing financial interests or personal relationships that could have appeared to influence the work reported in this paper.

Data availability

All data derived from published material. Data used for this review are summarized in the attached Supplementary files

Acknowledgments

This research was conducted within the PRIN 2017RX9XXX awarded to EE and the Italian Ministry of Education (MIUR) project "Dipartimenti di Eccellenza 2018–2022, Le Geoscienze per la Società: Risorse e loro evoluzione". The authors are grateful to both the Editor Guillaume Dupont-Nivet and an anonymous reviewer whose valuable comments contributed greatly to improving the quality of the manuscript.

Supplementary data

Data relative to variations in benthic fauna, distribution of euhedral and framboidal pyrite, inorganic and organic geochemical data are presented and discussed in detail in the Supplementary Material. Appendix A consists of spreadsheets reporting data and respective bibliographic sources used to produce the maps presented in this work. Separate spreadsheets are available for the intervals deposited below the negative CIE (pre-negative CIE plateau), onset of the negative CIE (falling limb onset), around the lowest point in the trough of the negative carbon-isotope anomaly (valley floor), the final interval of the gradual increase back to pre-anomaly values (top rising limb), and right above the negative CIE (post-negative CIE plateau). Appendix B consists of a spreadsheet summarizing all the available data and computed

'Redox Indexes' for each stratigraphic interval.

Supplementary data to this article can be found online at <https://doi.org/10.1016/j.earscirev.2023.104636>.

References

- Ajuaba, S., Sachsenhofer, R., Bechtel, A., Galasso, F., Gross, D., Misch, D., Schneebeli-Hermann, E., 2022. Biomarker and compound-specific isotope records across the Toarcian CIE at the Dormettingen section in SW Germany. *Int. J. Earth Sci.* 111, 1631–1661.
- Algeo, T.J., Lyons, T.W., 2006. Mo-total organic carbon covariation in modern anoxic marine environments: implications for analysis of paleoredox and paleohydrographic conditions. *Paleoceanography* 21. <https://doi.org/10.1029/2004PA001112>. PA1016.
- Algeo, T.J., Rowe, H., 2012. Paleoceanographic applications of trace-metal concentration data. *Chem. Geol.* 324, 6–18.
- Al-Suwaidi, A.H., Angelozzi, G.N., Baudin, F., Damborenea, S.E., Hesselbo, S.P., Jenkyns, H.C., Mancenido, M.O., Riccardi, A.C., 2010. First record of the Early Toarcian Oceanic Anoxic Event from the Southern Hemisphere, Neuquén Basin, Argentina. *J. Geol. Soc. Lond.* 167, 633–636.
- Baeza-Carratalá, J.F., Reolid, M., Joral, F.G., 2017. New deep-water brachiopod resilient assemblage from the South-Iberian Paleomargin (Western Tethys) and its significance for the brachiopod adaptive strategies around the Early Toarcian Mass Extinction Event. *Bull. Geosci.* 92, 233–256.
- Bailey, T.R., Rosenthal, Y., McArthur, J.M., van de Schootbrugge, B., Thirlwall, M.F., 2003. Paleoceanographic changes of the Late Pliensbachian-Early Toarcian interval: a possible link to the genesis of an Oceanic Anoxic Event. *Earth Planet. Sci. Lett.* 212, 307–320.
- Baranyi, V., Pálffy, J., Görög, A., Riding, J.B., Raucisik, B., 2016. Multiphase response of palynomorphs to the Toarcian Oceanic Anoxic Event (early Jurassic) in the Réka Valley section, Hungary. *Rev. Palaeobot. Palynol.* 235, 51–70.
- Baroni, I.R., Pohl, A., van Helmond, N.A.G.M., Papadomanolaki, N.M., Coe, A.L., Cohen, A.S., van de Schootbrugge, B., Donnadieu, Y., Slomp, C.P., 2018. Ocean Circulation in the Toarcian (Early Jurassic): a Key Control on Deoxygenation and Carbon Burial on the European Shelf. *Paleoceanogr. Paleoclimatol.* 33, 994–1012.
- Barrón, E., Comas-Rengifo, M.J., Trincão, P., 1999. Estudio palinológico del tránsito Pliensbachiense/Toarcicense en la Rambla del Salto (Sierra Palomera, Teruel, España). *Cuadernos Geol. Ibérico* 25, 181–187.
- Bellanca, A., Masetti, D., Neri, R., Venezia, F., 1999. Geochemical and sedimentological evidence of productivity cycles recorded in Toarcian black shales from the Belluno Basin, Southern Alps, Northern Italy. *J. Sediment. Res.* 69, 466–476.
- Bernoulli, D., Jenkyns, H.C., 1974. Alpine, Mediterranean, and Central Atlantic Mesozoic facies in relation to the early evolution of the Tethys. In: Dott, R.H., Shaver, R.H. (Eds.), *Modern and Ancient Geosynclinal Sedimentation*, Society of Economic Paleontologists and Mineralogists, Special Publication, vol. 19, pp. 129–160.
- Bernoulli, D., Homewood, P., Kälin, O., van Stijnenberg, J., 1979. Evolution of continental margins in the Alps. *Schweiz. Mineral. Petrogr. Mitt.* 59, 165–170.
- Bjerrum, C.J., Surlyk, F., Calmon, J.H., Slingerland, R.L., 2001. Numerical paleoceanographic study of the Early Jurassic transcontinental Laurasian Seaway. *Paleoceanography* 16, 390–404.
- Blanchet, C.L., Kasten, S., Vidal, L., Poulton, S.W., Ganeshram, R., Thouveny, N., 2012. Influence of diagenesis on the stable isotopic composition of biogenic carbonates from the Gulf of Tehuantepec oxygen minimum zone. *Geochem. Geophys. Geosyst.* 13. <https://doi.org/10.1029/2011GC003800>. Q04003.
- Bodin, S., Krencker, F.-N., Kothe, T., Hoffmann, R., Mattioli, E., Heimhofer, U., Kabiri, L., 2016. Perturbation of the carbon cycle during the late Pliensbachian – early Toarcian: New insight from high-resolution carbon isotope records in Morocco. *J. Afr. Earth Sci.* 116, 89–104.
- Bomou, S., Buan, G., Schlägl, J., Grosjean, A.-S., Suchéras-Marx, B., Adatte, T., Spangenberg, J.E., Fouché, S., Zacaí, A., Gilbert, C., Brazier, J.-M., Perrier, V., Vincent, P., Janneau, K., Martin, J.E., 2021. The palaeoenvironmental context of Toarcian vertebrate yielding shales of southern France (Hérault). In: Reolid, M., Duarte, L.V., Mattioli, E., Ruebsam, W. (Eds.), *Carbon Cycle and Ecosystem Response to the Jenkyns Event in the Early Toarcian (Jurassic)*, Geological Society, London, Special Publications, vol. 514, pp. 121–152.
- Boomer, I., Copestate, P., Page, K., Huxtable, J., Loy, T., Bown, P., Dunkley Jones, T., O'Callaghan, M., Hawkes, S., Halfacree, D., Reay, H., Caughey, N., 2021. Biotic and stable-isotope characterization of the Toarcian Ocean Anoxic Event through a carbonate-clastic sequence from Somerset, UK. In: Reolid, M., Duarte, L.V., Mattioli, E., Ruebsam, W. (Eds.), *Carbon Cycle and Ecosystem Response to the Jenkyns Event in the Early Toarcian (Jurassic)*. Geological Society, London, pp. 239–268. Special Publications 514.
- Bosellini, A., Winterer, E.L., 1975. Pelagic limestone and radiolarite of the Tethyan Mesozoic: a genetic model. *Geology* 3, 279–282.
- Boulila, S., Galbrun, B., Sadki, D., Gardin, S., Bartolini, A., 2019. Constraints on the duration of the early Toarcian T-OAE and evidence for carbon-reservoir change from the High Atlas (Morocco). *Global and Planetary Change* 175, 113–128.
- Boulila, S., Hinnov, L.A., 2017. A review of tempo and scale of the early Jurassic Toarcian OAE: implications for carbon cycle and sea level variations. *Newsl. Stratigr.* 50 (4), 363–389.
- Boulila, S., Galbrun, B., Huret, E., Hinnov, L.A., Rouget, I., Gardin, S., Bartolini, A., 2014. Astronomical calibration of the Toarcian Stage: Implications for sequence stratigraphy and duration of the early Toarcian OAE. *Earth Planet. Sci. Lett.* 386, 98–111.
- Brazier, J.-M., Suan, G., Tacail, T., Simon, L., Martin, J.E., Mattioli, E., Balter, V., 2015. Calcium isotope evidence for dramatic increase of continental weathering during the Toarcian oceanic anoxic event (early Jurassic). *Earth Planet. Sci. Lett.* 411, 164–176.
- van Breugel, Y., Baas, M., Schouten, S., Mattioli, E., Damsté, J.S.S., 2006. Isorenieratane record in black shales from the Paris Basin, France: Constraints on recycling of resired CO₂ as a mechanism for negative carbon isotope shifts during the Toarcian oceanic anoxic event. *Paleoceanography* 21. <https://doi.org/10.1029/2006PA001305>. PA4200.
- Brumsack, H.J., 1986. The inorganic geochemistry of Cretaceous black shales (DSDP leg 41) in comparison to modern upwelling sediments from the Gulf of California. In: Summerhayes, C.P., Shackleton, N.J. (Eds.), *North Atlantic Palaeoceanography*, vol. 21. *Geol. Soc. Spec. Publ.*, pp. 447–462.
- Brumsack, H.J., 1989. Geochemistry of recent TOC-rich sediments from the Gulf of California and the Black Sea. *Geol. Rundsch.* 78, 851–882.
- Brumsack, H.J., 1991. Inorganic geochemistry of the German 'Posidonia Shale': palaeoenvironmental consequences. In: Tyson, R.V., Pearson, T.H. (Eds.), *Modern and Ancient Continental Shelf Anoxia*, Geological Society Special Publication, vol. 58, pp. 353–362.
- Brumsack, H.J., 2006. The trace metal content of recent organic carbon-rich sediments: implications for cretaceous black shale formation. *Palaeogeogr. Palaeoclimatol. Palaeoecol.* 232, 344–361.
- Bucefalo Palliani, R., Mattioli, E., Riding, J.B., 2002. The response of marine phytoplankton and sedimentary organic matter to the early Toarcian (lower Jurassic) oceanic anoxic event in northern England. *Mar. Micropaleontol.* 46, 223–245.
- Calvert, S.E., Pedersen, T.F., 1993. Geochemistry of recent oxic and anoxic sediments: implications for the geological record. *Mar. Geol.* 113, 67–88.
- Calvert, S.E., Pedersen, T.F., 1996. Sedimentary geochemistry of manganese: implications for the environment of formation of manganeseiferous black shales. *Econ. Geol.* 91, 36–47.
- Canfield, D.E., Lyons, T.W., Raiswell, R., 1996. A model for iron deposition to euxinic Black Sea sediments. *Am. J. Sci.* 296, 818–834.
- Caruthers, A.H., Gröcke, D.R., Smith, P.L., 2011. The significance of an Early Jurassic (Toarcian) carbon-isotope excursion in Haida Gwaii (Queen Charlotte Islands), British Columbia, Canada. *Earth Planet. Sci. Lett.* 307, 19–26.
- Casellato, C.E., Erba, E., 2015. Calcareous nannofossil biostratigraphy and paleoceanography of the Toarcian Oceanic Anoxic Event at Colle di Sogno section (Southern Alps, Italy). *Riv. Ital. Paleontol. Stratigr.* 105, 343–376.
- Caswell, B.A., Coe, A.L., 2012. A high-resolution shallow marine record of the Toarcian (Early Jurassic) Oceanic Anoxic Event from the East Midlands Shelf, UK. *Palaeogeogr. Palaeoclimatol. Palaeoecol.* 365–366, 124–135.
- Chen, W., Kemp, D.B., He, T., Huang, C., Jin, S., Xiong, Y., Newton, R.J., 2021. First record of the early Toarcian Oceanic Anoxic Event in the Hebrides Basin (UK) and implications for redox and weathering changes. *Glob. Planet. Chang.* 207, 103685.
- Cohen, A.S., Coe, A.L., Harding, S.M., Schwark, L., 2004. Osmium isotope evidence for the regulation of atmospheric CO₂ by continental weathering. *Geology* 32, 157–160.
- Corbin, J.C., Person, A., Iatzoura, A., Ferré, B., Renard, M., 2000. Manganese in Pelagic carbonates: indication of major Tectonic events during the geodynamic evolution of a passive continental margin (the Jurassic European Margin of the Tethys-Ligurian Sea). *Palaeogeogr. Palaeoclimatol. Palaeoecol.* 156, 123–138.
- Cruse, A.M., Lyons, T.W., 2004. Trace metal records of regional paleoenvironmental variability in Pennsylvanian (Upper Carboniferous) black shales. *Chem. Geol.* 206, 319–345.
- Danise, S., Clémence, M.-E., Price, G.D., Murphy, D.P., Gómez, J.J., Twitchett, R.J., 2019. Stratigraphic and environmental control on marine benthic community change through the early Toarcian extinction event (Iberian Range, Spain). *Palaeogeogr. Palaeoclimatol. Palaeoecol.* 524, 183–200.
- Dellwig, O., Leipe, T., März, C., Glockzin, M., Pollehne, F., Schnetger, B., Yakushev, E.V., Böttcher, Brumsack, H.-J., 2010. A new particulate Mn-Fe-P shuttle at the redoxcline of anoxic basins. *Geochim. Cosmochim. Acta* 74, 7100–7115.
- Dera, G., Donnadieu, Y., 2012. Modeling evidences for global warming, Arctic seawater freshening, and sluggish oceanic circulation during the early Toarcian anoxic event. *Paleoceanogr. Paleoclimatol.* 27. <https://doi.org/10.1029/2012PA002283>.
- Dera, G., Pellenard, P., Neige, P., Deconinck, J.-F., Pucéat, E., Dommergues, J.-L., 2009a. Distribution of clay minerals in early Jurassic Peritethyan seas: Paleoclimatic significance inferred from multiproxy comparisons. *Palaeogeogr. Palaeoclimatol. Palaeoecol.* 271, 39–51.
- Dera, G., Pucéat, E., Pellenard, P., Neige, P., Delsate, D., Joachimski, M.M., Reisberg, L., Martinez, M., 2009b. Water mass exchange and variations in seawater temperature in the NW Tethys during the early Jurassic: evidence from neodymium and oxygen isotopes of fish teeth and belemnites. *Earth Planet. Sci. Lett.* 286, 198–207.
- Dera, G., Brigaud, B., Monna, F., Laffont, R., Pucéat, E., Deconinck, J.-F., Pellenard, P., Joachimski, M.M., Durlet, C., 2011. Climatic ups and downs in a disturbed Jurassic world. *Geology* 39, 215–218.
- Dickson, A.J., Gill, B.C., Ruhl, M., Jenkyns, H.C., Porcelli, D., Idiz, E., Lyons, T.W., van den Boorn, S.H.J.M., 2017. Molybdenum-isotope chemostratigraphy and paleoceanography of the Toarcian Oceanic Anoxic Event (early Jurassic). *Paleoceanography* 32, 813–829.
- Duarte, L.V., Oliveira, L.C., Rodrigues, R., 2007. Carbon isotopes as a sequence stratigraphic tool: examples from the lower and Middle Toarcian marly limestones of Portugal. *Bol. Geol. Min.* 118, 3–18.
- Ebli, O., Vétö, I., Lobitzer, H., Sajgó, C., Demény, A., Hetényie, M., 1998. Primary productivity and early diagenesis in the Toarcian Tethys on the example of the Mn-rich black shales of the Sachrang Formation, Northern Calcareous Alps. *Org. Geochem.* 29, 1635–1647.

- Elmi, S., Rulleau, L., Gabilly, J., Mouterde, R., 1997. 4. Toarcien. In: Cariou, E., Hantzpergue, P. (Eds.), Biostratigraphie du Jurassique ouest-européen et méditerranéen: zonations parallèles et distribution des invertébrés et microfossiles, Bulletin des Centres de recherches exploration-production Elf-Aquitaine, Pau, Mémoire, vol. 17, pp. 25–36.
- Emmanuel, L., Renard, M., Cubaynes, R., De Rafelis, M., Hermoso, M., Le Callonnec, L., Le Solleuz, A., Rey, J., 2006. The “Schistes Carton” of Quercy (Tarn, France): a lithological signature of a methane hydrate dissociation event in the early Toarcian. Implications for correlations between Boreal and Tethyan realms. *Bull. Soc. Géol. France* 177, 239–249.
- Erba, E., 2004. Calcareous nannofossils and Mesozoic oceanic anoxic events. *Mar. Micropaleontol.* 52, 85–106.
- Erba, E., Bottini, C., Faucher, G., Gambacorta, G., Visentin, S., 2019. The response of calcareous nannoplankton to Oceanic Anoxic events: the Italian pelagic record. *Boll. Soc. Paleontol. Ital.* 58, 51–71.
- Erba, E., Cavalheiro, L., Dickson, A.J., Faucher, G., Gambacorta, G., Jenkyns, H.C., Wagner, T., 2022. Carbon- and oxygen-isotope signature of the Toarcian Oceanic Anoxic Event: insights from two Tethyan pelagic sequences (Gajum and Sogno Cores – Lombardy Basin, northern Italy). *Newsl. Stratigr.* 55, 451–477.
- Ettinger, N.P., Larson, T.E., Kerans, C., Thibodeau, A.M., Hattori, K.E., Kacur, S.M., Martindale, R.C., 2021. Ocean acidification and photic zone anoxia at the Toarcian Oceanic Anoxic Event: Insights from the Adriatic Carbonate Platform. *Sedimentology* 68, 63–107.
- Fantasia, A., Föllmi, K.B., Adatte, T., Bernairdez, E., Spangenberg, J.E., Mattioli, E., 2018. The Toarcian Oceanic Anoxic Event in southwestern Gondwana: an example from the Andean Basin, northern Chile. *J. Geol. Soc. Lond.* 175, 883–902.
- Fantasia, A., Adatte, T., Spangenberg, J.E., Font, E., Duarte, L.V., Föllmi, K.B., 2019a. Global versus local processes during the Pliensbachian–Toarcian transition at the Peniche GSSP, Portugal: A multi-proxy record. *Earth Sci. Rev.* 198, 102932.
- Fantasia, A., Föllmi, K.B., Adatte, T., Spangenberg, J.E., Mattioli, E., 2019b. Expression of the Toarcian Oceanic Anoxic Event: New insights from a Swiss transect. *Sedimentology* 66, 262–284.
- Farrimond, P., Eglington, G., Brassell, S.C., Jenkyns, H.C., 1989. Toarcian oceanic anoxic event in Europe: an organic geochemical study. *Mar. Pet. Geol.* 6, 136–147.
- Fernández-Martínez, J., Rodríguez-Tovar, F.J., Piñuela, L., Martínez-Ruiz, F., García-Ramos, J.C., 2021. Bottom- and pore-water oxygenation during the early Toarcian Oceanic Anoxic Event (T-OAE) in the Asturian Basin (N Spain): Ichnological information to improve facies analysis. *Sediment. Geol.* 419, 105909.
- Ferreira, J., Mattioli, E., Sucherás-Marx, B., Giraud, F., Duarte, V.L., Pittet, B., Suan, G., Hassler, A., Spangenberg, J.E., 2019. Western Tethys early and Middle Jurassic calcareous nannofossil biostratigraphy. *Earth Sci. Rev.* 197, 1–19.
- Filatova, N.I., Konstantinovskaya, E., Vishnevskaya, V., 2020. Jurassic–Lower Cretaceous siliceous rocks and black shales from allochthonous complexes of the Koryak–Western Kamchatka orogenic belt, East Asia. *Int. Geol. Rev.* <https://doi.org/10.1080/00206814.2020.1848649>.
- Force, E.R., Cannon, W.F., 1988. Depositional model for shallow-marine manganese deposits around black shale basins. *Econ. Geol.* 83, 93–117.
- French, K.L., Sepúlveda, J., Trabucho-Alexandre, J., Gröcke, D.R., Summons, R.E., 2014. Organic geochemistry of the early Toarcian oceanic anoxic event in Hawsker Bottoms, Yorkshire, England. *Earth Planet. Sci. Lett.* 390, 116–127.
- Frimmel, A., Oschmann, W., Schwark, L., 2004. Chemostratigraphy of the Posidonia Black Shale, SW Germany: I. Influence of sea-level variation on organic facies evolution. *Chem. Geol.* 206, 199–230.
- Gambacorta, G., Cavalheiro, L., Brumsack, H.-J., Dickson, A.J., Jenkyns, H.C., Schnetger, B., Wagner, T., Erba, E., 2023. Suboxic conditions prevailed during the Toarcian Oceanic Anoxic Event in the Alpine-Mediterranean Tethys: the Sogno Core pelagic record (Lombardy Basin, northern Italy). *Glob. Planet. Chang.* 223, 104089.
- Germann, K., 1973. Deposition of Manganese and Iron Carbonates and Silicates in Liassic Marl of the Northern Limestone Alps (Kalkalpen). In: Amstutz, G.C., Bernard, A.J. (Eds.), Ores in Sediments. International Union of Geological Sciences, vol. 3. Springer, Berlin, Heidelberg, pp. 129–138. https://doi.org/10.1007/978-3-642-65329-2_11.
- Gómez, J.J., Arias, C., 2010. Rapid warming and ostracods mass extinction at the lower Toarcian (Jurassic) of Central Spain. *Mar. Micropaleontol.* 74, 119–135.
- Gómez, J.J., Goy, A., 2011. Warming-driven mass extinction in the early Toarcian (early Jurassic) of northern and Central Spain. Correlation with other time-equivalent European sections. *Palaeogeogr. Palaeoclimatol. Palaeoecol.* 306, 176–195.
- Gómez, J.J., Comas-Rengifo, M.J., Goy, A., 2016. Palaeoclimatic oscillations in the Pliensbachian (early Jurassic) of the Asturian Basin (Northern Spain). *Clim. Past* 12, 1199–1214.
- Gröcke, D.R., Horr, R.S., Trabucho-Alexandre, J., Kemp, D.B., Schwark, L., 2011. An open ocean record of the Toarcian oceanic anoxic event. *Solid Earth* 2, 245–257.
- Hallam, A., 1967. The depth significance of shales with bituminous laminae. *Mar. Geol.* 5, 481–493.
- Hallam, A., 1981. A revised sea-level curve for the early Jurassic. *J. Geol. Soc. Lond.* 138, 735–743.
- Haq, B.U., 2017. Jurassic Sea-Level Variations: a Reappraisal. *GSA Today* 28. <https://doi.org/10.1130/GSATG359A.1>.
- Haq, B.U., Hardenbol, J., Vail, P.R., 1987. Chronology of fluctuating sea-levels since the Triassic. *Nature* 235, 1156–1167.
- Harazim, D., Van de Schootbrugge, B., Sorichter, K., Fiebig, J., Weug, A., Suan, G., Oschmann, W., 2013. Spatial variability of watermass conditions within the Europea Epicontinent Seaway during the early Jurassic (Pliensbachian–Toarcian). *Sedimentology* 60, 359–390.
- Hardenbol, J., Thierry, J., Farley, M.B., Jacquin, T., de Graciansky, P.-C., Vail, P.R., 1998. Mesozoic and Cenozoic sequence chronostratigraphic framework of European basins. In: de Graciansky, P.-C., Hardenbol, J., Jacquin, T., Vail, P.R. (Eds.), Mesozoic and Cenozoic Sequence Stratigraphy of European Basins, vol. 60. Society for Sedimentary Geology, Tulsa, Oklahoma, pp. 3–13.
- Heimdal, T.H., Goddries, Y., Jones, M.T., Svensen, H.H., 2021. Assessing the importance of thermogenic degassing from the Karoo large Igneous Province (LIP) in driving Toarcian carbon cycle perturbations. *Nat. Commun.* 12 <https://doi.org/10.1038/s41467-021-26467-6>.
- Hermoso, M., Pellenard, P., 2014. Continental weathering and climatic changes inferred from clay mineralogy and paired carbon isotopes across the early to middle Toarcian in the Paris Basin. *Palaeogeogr. Palaeoclimatol. Palaeoecol.* 399, 385–393.
- Hermoso, M., Le Callonnec, L., Minoletti, F., Renard, M., Hesselbo, S.P., 2009a. Expression of the early Toarcian negative carbon-isotope excursion in separated carbonate microfractions (Jurassic, Paris Basin). *Earth Planet. Sci. Lett.* 277, 194–203.
- Hermoso, M., Minoletti, F., Le Callonnec, L., Jenkyns, H.C., Hesselbo, S.P., Rickaby, R.E.M., Renard, M., de Rafélis, M., Emmanuel, L., 2009b. Global and local forcing of early Toarcian seawater chemistry: a comparative study of different paleoceanographic settings (Paris and Lusitanian basins). *Paleoceanography* 24, PA4208. <https://doi.org/10.1029/2009PA001764>.
- Hermoso, M., Minoletti, F., Pellenard, P., 2013. Black shale deposition during Toarcian super-greenhouse driven by sea level. *Clim. Past* 9, 2703–2712.
- Hermoso, M., Delsate, D., Baudin, F., Le Callonnec, L., Minoletti, F., Renard, M., Faber, A., 2014. Record of early Toarcian carbon cycle perturbations in a nearshore environment: the Bascharage section (easternmost Paris Basin). *Solid Earth* 5, 793–804.
- Hesselbo, S.P., 2008. Sequence stratigraphy and inferred relative sea-level change from the onshore British Jurassic. *Proc. Geol. Assoc.* 119, 19–34.
- Hesselbo, S.P., Jenkyns, H.C., 1998. British lower Jurassic Sequence Stratigraphy. In: de Graciansky, P.-C., Hardenbol, J., Jaquin, T., Vail, P.R., Farley, M.B. (Eds.), Mesozoic and Cenozoic Sequence Stratigraphy of European Basins, Special Publication of the Society of Economic Paleontologists and Mineralogists, vol. 60, pp. 561–581.
- Hesselbo, S.P., Pieńkowski, G., 2011. Stepwise atmospheric carbon-isotope excursion during the Toarcian Oceanic Anoxic Event (early Jurassic, Polish Basin). *Earth Planet. Sci. Lett.* 301, 365–372.
- Hesselbo, S.P., Gröcke, D.R., Jenkyns, H.C., Bjerrum, C.J., Farrimond, P., Morgans Bell, H.S., Green, O.R., 2000. Massive dissociation of gas hydrate during a Jurassic Oceanic Anoxic Event. *Nature* 406, 392–395.
- Hesselbo, S.P., Jenkyns, H.C., Duarte, L.V., Oliveira, L.C.V., 2007. Carbon-isotope record of the early Jurassic (Toarcian) Oceanic Anoxic Event from fossil wood and marine carbonates (Lusitanian Basin, Portugal). *Earth Planet. Sci. Lett.* 253, 455–470.
- Hesselbo, S.P., Little, C.T.S., Ruhl, M., Thibault, N., Ullmann, C.V., 2020. Comments on “Paleosalinity determination in ancient epicontinental seas: a case study of the T-OAE in the Cleveland Basin (UK)” by Remírez, M. N. and Algeo, T. J. *Earth Sci. Rev.* 208, 103290.
- Hild, E., Brumsack, H.-J., 1998. Major and minor element geochemistry of lower Aptian sediments from the NW German Basin (core Hoheneggelsen KB 40). *Cretac. Res.* 19, 615–633.
- Houben, A.J.P., Goldberg, T., Slomp, C.P., 2021. Biogeochemical evolution and organic carbon deposition on the Northwest European Shelf during the Toarcian Ocean Anoxic Event. *Palaeogeogr. Palaeoclimatol. Palaeoecol.* 565, 110191.
- Hougård, I.W., Bojese-Koeoed, J.A., Vickers, M.L., Ullmann, C.V., Bjerrum, C.J., Rizzi, M., Korte, C., 2021. Redox element record shows that environmental perturbations associated with the T-OAE were of longer duration than the carbon isotope record suggests – the Aubach section, SW Germany. *Newsl. Stratigr.* 54, 229–246.
- van Hulten, M., Middag, R., Dutay, J.-C., de Baar, H., Roy-Barman, M., Gehlen, M., Tagliabue, A., Sterl, A., 2017. Manganese in the West Atlantic Ocean in the context of the first global ocean circulation model of manganese. *Biogeosciences* 14, 1123–1152.
- Ikeda, M., Hori, R.S., 2014. Effects of Karoo–Ferrar volcanism and astronomical cycles on the Toarcian oceanic anoxic events (Early Jurassic). *Palaeogeogr. Palaeoclimatol. Palaeoecol.* 410, 134–142.
- Ikeda, M., Hori, R.S., Ikebara, M., Miyashita, R., Chino, M., Yamada, K., 2018. Carbon cycle dynamics linked with Karoo–Ferrar volcanism and astronomical cycles during Pliensbachian–Toarcian (early Jurassic). *Glob. Planet. Chang.* 170, 163–171.
- Izumi, K., Miyaji, T., Tanabe, K., 2012. Early Toarcian (early Jurassic) oceanic anoxic event recorded in the shelf deposits in the northwestern Panthalassan: evidence from the Nishinakayama formation in the Toyora area, West Japan. *Palaeogeogr. Palaeoclimatol. Palaeoecol.* 15–316, 100–108.
- Jenkyns, H.C., 1970. Fossil manganese nodules from the west Sicilian Jurassic. *Ectogae Geol. Helv.* 63, 741–774.
- Jenkyns, H.C., 1971. The genesis of condensed sequences in the Tethyan Jurassic. *Lethaia* 4, 327–352.
- Jenkyns, H.C., 1985. The early Toarcian and Cenomanian–Turonian anoxic events in Europe: comparisons and contrasts. *Geol. Rundsch.* 74, 505–518.
- Jenkyns, H.C., 1988. The early Toarcian (Jurassic) Anoxic Event: stratigraphic, sedimentary and geochemical evidence. *Am. J. Sci.* 288, 101–151.
- Jenkyns, H.C., 2003. Evidence for rapid climate change in the Mesozoic–Palaeogene greenhouse world. *Philos. Trans. R. Soc. Lond. A* 361, 1885–1916.
- Jenkyns, H.C., 2010. Geochemistry of oceanic anoxic events. *Geochem. Geophys. Geosyst.* 11, Q03004. <https://doi.org/10.1029/2009GC002788>.
- Jenkyns, H.C., Clayton, C.J., 1986. Black shales and carbon isotopes in pelagic sediments from the Tethyan lower Jurassic. *Sedimentology* 33, 87–106.
- Jenkyns, H.C., Clayton, C.J., 1997. Lower Jurassic epicontinental carbonates and mudstones from England and Wales: chemostratigraphic signals and the early Toarcian anoxic event. *Sedimentology* 44, 687–706.

- Jenkyns, H.C., MacFarlane, S., 2021. The chemostratigraphy and environmental significance of the Marlstone and Junction Bed (Beacon Limestone, Toarcian, lower Jurassic, Dorset, UK). *Geol. Mag.* 159, 357–371.
- Jenkyns, H.C., Sarti, M., Masetti, D., Howarth, M.K., 1985. Ammonites and stratigraphy of lower Jurassic black shales and pelagic limestones from the Belluno Trough, Southern Alps, Italy. *Eclogae Geol. Helv.* 78, 299–311.
- Jenkyns, H.C., Géczy, B., Marshall, J.D., 1991. Jurassic manganese carbonates of Central Europe and the early Toarcian anoxic event. *J. Geol.* 99, 137–149.
- Jenkyns, H.C., Gröcke, D.R., Hesselbo, S.P., 2001. Nitrogen isotope evidence for water mass denitrification during the early Toarcian (Jurassic) oceanic anoxic event. *Paleoceanography* 16, 593–603.
- Jenkyns, H.C., Jones, C.E., Gröcke, D.R., Hesselbo, S.P., Parkinson, D.N., 2002. Chemostratigraphy of the Jurassic System: applications, limitations and implications for palaeoenvironmental studies. *J. Geol. Soc. Lond.* 159, 351–378.
- Jones, C.E., Jenkyns, H.C., 2001. Seawater strontium isotopes, Oceanic Anoxic events, and seafloor hydrothermal activity in the Jurassic and cretaceous. *Am. J. Sci.* 301, 112–149.
- Kafousia, N., Karakitsios, V., Jenkyns, H.C., Mattioli, E., 2011. A global event with a regional character: the early Toarcian Oceanic Anoxic Event in the Pindos Ocean (northern Peloponnese, Greece). *Geol. Mag.* 148, 619–631.
- Kafousia, N., Karakitsios, V., Mattioli, E., Jenkyns, H.C., 2013. Chemostratigraphy of the Toarcian Oceanic Anoxic Event from the Ionian Zone, Greece. In: *Bulletin of the Geological Society of Greece*, vol. XLVII, Proceedings of the 13th International Congress, Chania.
- Kafousia, N., KaraTkitis, V., Mattioli, E., Kenjo, S., Jenkyns, H.C., 2014. The Toarcian Oceanic Anoxic Event in the Ionian Zone, Greece. *Palaeogeogr. Palaeoclimatol. Palaeoecol.* 393, 135–145.
- Kemp, D.B., Izumi, K., 2014. Multiproxy geochemical analysis of a Panthalassic margin record of the early Toarcian oceanic anoxic event (Toyora area, Japan). *Palaeogeogr. Palaeoclimatol. Palaeoecol.* 414, 332–341.
- Kemp, D.B., Coe, A.L., Cohen, A.S., Schwark, L., 2005. Astronomical pacing of methane release in the early Jurassic period. *Nature* 437, 396–399.
- Kemp, D.B., Coe, A.L., Cohen, A.S., Weedon, G.P., 2011. Astronomical forcing and chronology of the early Toarcian (early Jurassic) oceanic anoxic event in Yorkshire, UK. *Paleoceanography* 26, PA4210. <https://doi.org/10.1029/2011PA002122>.
- Kemp, D.B., Chen, W., Cho, T., Algeo, T.J., Shen, J., Ikeda, M., 2022a. Deep-ocean anoxia across the Pliensbachian-Toarcian boundary and the Toarcian Oceanic Anoxic Event in the Panthalassic Ocean. *Glob. Planet. Chang.* 212, 103782.
- Kemp, D.B., Suan, G., Fantasia, A., Jin, S., Chen, W., 2022b. Global organic carbon burial during the Toarcian oceanic anoxic event: patterns and controls. *Earth Sci. Rev.* 231, 104086.
- Kodina, L.A., Bogatcheva, M.P., Lobitzer, H., 1988. An organic geochemical study of Austrian bituminous rocks. *Jahrb. Geol. Bundesanst.* 131, 291–300.
- Korte, C., Hesselbo, S.P., 2011. Shallow marine carbon and oxygen isotope and elemental records indicate icehousegreenhouse cycles during the early Jurassic. *Paleoceanography* 26, PA4219. <https://doi.org/10.1029/2011PA002160>.
- Korte, C., Hesselbo, S.P., Ullmann, C.V., Dietl, G., Ruhl, M., Schweigert, G., Thibault, N., 2015. Jurassic climate mode governed by ocean gateway. *Nat. Commun.* 6, 10015. <https://doi.org/10.1038/ncomms10015>.
- Krencker, F.-N., Bodin, S., Suan, G., Heimhofer, U., Kabiri, L., Immenhauser, A., 2015. Toarcian extreme warmth led to tropical cyclone intensification. *Earth and Planetary Science Letters* 425, 120–130.
- Krencker, F.-N., Lindström, S., Bodin, S., 2019. A major sea-level drop briefly precedes the Toarcian oceanic anoxic event: implication for early Jurassic climate and carbon cycle. *Sci. Rep.* 9, 12518. <https://doi.org/10.1038/s41598-019-48956-x>.
- Kurnet, A., Kendall, B., 2023. Global Ocean redox changes before and during the Toarcian Oceanic Anoxic Event. *Nat. Commun.* 14, 815. <https://doi.org/10.1038/s41467-023-36516-x>.
- Leng, M.J., Marshall, J.D., 2004. Palaeoclimate interpretation of stable isotope data from lake sediment archives. *Quat. Sci. Rev.* 23, 811–831.
- Lenstra, W.K., Hermans, M., Séguet, M.J.M., Witbaard, R., Behrends, T., Dijkstra, N., van Helmond, N.A.G.M., Kraal, P., Laan, P., Rijkenberg, M.J.A., Severmann, S., Teacă, A., Slomp, C.P., 2019. The shelf-to-basin iron shuttle in the Black Sea revisited. *Chem. Geol.* 511, 314–341.
- Leónide, P., Floquet, M., Durlet, C., Baudin, F., Pittet, B., Lécuyer, C., 2012. Drowning of a carbonate platform as a precursor stage of the early Toarcian global anoxic event (Southern Provence sub-Basin, South-east France). *Sedimentology* 59, 156–184.
- Liu, R., Hu, G., Cao, J., Yang, R., Liao, Z., Hu, C., Pang, Q., Pang, P., 2022. Enhanced hydrological cycling and continental weathering during the Jenkyns Event in a lake system in the Sichuan Basin, China. *Glob. Planet. Chang.* 216, 103915.
- Love, L.G., Amstutz, G.C., 1966. Review of microscopic pyrite from the Devonian Chattanooga shale and Rammelsberg Banders. *Fortschr. Mineral.* 43, 273–309.
- Lu, Z., Jenkyns, H.C., Rickaby, R.E.M., 2010. Iodine to calcium ratios in marine carbonate as a paleo-redox proxy during oceanic anoxic events. *Geology* 38, 1107–1110.
- Lyons, T.W., Berner, R.A., 1992. Carbon-sulfur-iron systematics of the uppermost Deepwater sediments of the Black Sea. *Chem. Geol.* 99, 1–27.
- Lyons, T.W., Severmann, S., 2006. A critical look at iron paleoredox proxies: new insights from modern euxinic marine basins. *Geochim. Cosmochim. Acta* 70, 5698–5722.
- Macchioni, F., 2002. Myths and legends in the correlation between the Boreal and Tethyan Realms. Implications on the dating of the early Toarcian mass extinctions and the Oceanic Anoxic Event. *Geobios* 35, 150–163.
- Macdonalds, R.W., Gobeil, C., 2011. Manganese sources and sinks in the Arctic Ocean with Reference to Periodic Enrichments in Basin Sediments. *Aquat. Geochem.* 18, 565–591.
- Mailliot, S., Mattioli, E., Bartolini, A., Baudin, F., Pittet, B., Guex, J., 2009. Late Pliensbachian-Early Toarcian (Early Jurassic) environmental changes in an epicontinental basin of NW Europe (Causse area, central France): A micropaleontological and geochemical approach. *Palaeogeogr. Palaeoclimatol. Palaeoecol.* 273, 346–364.
- Marshall, J.D., 1992. Climatic and oceanographic isotopic signals from the carbonate rock record and their preservation. *Geol. Mag.* 129, 143–160.
- März, C., Stratmann, A., Matthiessen, J., Meinhardt, A.-K., Eckert, S., Schnetger, B., Vogt, C., Stein, R., Brumsack, H.-J., 2011. Manganese-rich brown layers in Arctic Ocean sediments: Composition, formation mechanisms, and diagenetic overprint. *Geochim. Cosmochim. Acta* 75, 7668–7687.
- Maslin, M., Dickson, A.J., 2015. O-Isotopes. In: Harff, J., Meschede, M., Petersen, S., Thiede, J. (Eds.), *Encyclopedia of Marine Geosciences*. https://doi.org/10.1007/978-94-007-6644-0_81-1.
- Mattioli, E., Pittet, B., Bucefalo Palliani, R., Röhrl, H.-J., Schmid-Röhrl, A., Morettini, E., 2004. Phytoplankton evidence for timing and correlation of palaeoceanographical changes during the early Toarcian oceanic anoxic event (early Jurassic). *J. Geol. Soc. Lond.* 161, 685–693.
- Mattioli, E., Pittet, B., Suan, G., Mailliot, S., 2008. Calcareous nannoplankton across the early Toarcian Anoxic Event: implications for paleoceanography within the western Tethys. *Paleoceanography* 23, PA3208. <https://doi.org/10.1029/2007PA001435>.
- Mattioli, E., Pittet, B., Petitpierre, L., Mailliot, S., 2009. Dramatic decrease of the pelagic carbonate production by nannoplankton across the early Toarcian Anoxic Event (T-OAE). *Glob. Planet. Chang.* 65, 134–145.
- McArthur, J.M., 2019. Early Toarcian black shales: a response to an oceanic anoxic event or anoxia in marginal basins? *Chem. Geol.* 522, 71–83.
- McArthur, J.M., Algeo, T.J., van de Schootbrugge, B., Li, Q., Howarth, R.J., 2008. Basinal restriction, black shales, Re-Os dating, and the early Toarcian (Jurassic) oceanic anoxic event. *Paleoceanography* 23, PA4217. <https://doi.org/10.1029/2008PA001607>.
- McElwain, J.C., Wade-Murphy, J., Hesselbo, S.P., 2005. Changes in carbon dioxide during an oceanic anoxic event linked to intrusion into Gondwana coals. *Nature* 435, 479–482.
- Meinhardt, A.-K., Pahnke, K., Böning, P., Schnetger, B., Brumsack, H.-J., 2016a. Climate change and response in bottom water circulation and sediment provenance in the Central Arctic Ocean since the last Glacial. *Chem. Geol.* 427, 98–108.
- Meinhardt, A.-K., März, C., Schuth, S., Lettmann, K.A., Schnetger, B., Wolff, J.-O., Brumsack, H.-J., 2016b. Diagenetic regimes in Arctic Ocean sediments: Implications for sediment geochemistry and core correlation. *Geochim. Cosmochim. Acta* 188, 125–146.
- Montero-Serrano, J.-C., Föllmi, K.B., Adatte, T., Spangenberg, J.E., Tribouillard, N., Fantasia, A., Suan, G., 2015. Continental weathering and redox conditions during the early Toarcian Oceanic Anoxic Event in the northwestern Tethys: Insight from the Posidonia Shale section in the Swiss Jura Mountains. *Palaeogeogr. Palaeoclimatol. Palaeoecol.* 429, 83–99.
- Morford, J.L., Russell, A.D., Emerson, S., 2001. Trace metal evidence for changes in the redox environment associated with the transition from terrigenous clay to diatomaceous sediments. *Saanich Inlet, BC. Mar. Geol.* 174, 355–369.
- Müller, T., Price, G.D., Bajnai, D., Nyerges, A., Kesjár, D., Rauczik, B., Varga, A., Judik, K., Fekete, J., May, Z., Pálfy, J., 2017. New multiproxy record of the Jenkyns Event (also known as the Toarcian Oceanic Anoxic Event) from the Mecsek Mountains (Hungary): differences, duration and drivers. *Sedimentology* 64, 66–86.
- Müller, T., Jurikova, H., Gutjahr, M., Tomášových, A., Schlögl, J., Liebetrau, V., Duarte, L.V., Milovský, R., Suan, G., Mattioli, E., Pittet, B., Eisenhauer, A., 2020. Ocean acidification during the early Toarcian extinction event: evidence from boron isotopes in brachiopods. *Geology* 48, 1184–1188.
- Müller, T., Price, G.D., Mattioli, E., Leskó, M.Z., Kristály, F., Pálfy, J., 2021. Hardground, gap and thin black shale: Spatial heterogeneity of arrested carbonate sedimentation during the Jenkyns Event (T-OAE) in a Tethyan pelagic Basin (Gerecse Mts, Hungary). In: Reolid, M., Duarte, L.V., Mattioli, E., Ruebsam, W. (Eds.), *Carbon Cycle and Ecosystem Response to the Jenkyns Event in the Early Toarcian (Jurassic)*, Geological Society, London, Special Publications, vol. 514, pp. 269–289.
- Neumeister, S., Gratzer, R., Algeo, T.J., Bechtel, A., Gawlik, H.-J., Newton, R.J., Sachsenhofer, R.F., 2015. Oceanic response to Pliensbachian and Toarcian magmatic events: Implications from an organic-rich basinal succession in the NW Tethys. *Glob. Planet. Chang.* 126, 62–83.
- Neumeister, S., Algeo, T.J., Bechtel, A., Gawlik, H.-J., Gratzer, R., Sachsenhofer, R.F., 2016. Redox conditions and depositional environment of the lower Jurassic Bächental bituminous marls (Tyrol, Austria). *Aust. J. Earth Sci.* 109, 142–159. <https://doi.org/10.11773/ajes.2016.0010>.
- Nikitenko, B., Shurygin, B., Mickey, M., 2008. High resolution stratigraphy of the lower Jurassic and Aalenian of Arctic regions as the basis of detailed paleobiogeographic reconstructions. *Nor. J. Geol.* 88, 267–277.
- Page, K.N., 2003. The lower Jurassic of Europe: its subdivision and correlation. *Geol. Surv. Denmark Greenl. Bull.* 1, 23–59.
- Pálfy, J., Smith, P.L., 2000. Synchrony between early Jurassic extinction, oceanic anoxic event, and the Karoo-Ferrar flood basalt volcanism. *Geology* 28, 747–750.
- Pearce, C.R., Cohen, A.S., Coe, A.L., Burton, K.W., 2008. Molybdenum isotope evidence for global ocean anoxia coupled with perturbations to the carbon cycle during the early Jurassic. *Geology* 36, 231–234.
- Pedersen, T.F., Price, N.B., 1982. The geochemistry of manganese carbonate in Panama Basin sediments. *Geochim. Cosmochim. Acta* 46, 59–68.
- Percival, I.M.E., Witt, M.L.I., Mather, T.A., Hermoso, M., Jenkyns, H.C., Hesselbo, S.P., Al-Suwaidi, A.H., Storm, M.S., Xu, W., Ruhl, M., 2015. Globally enhanced mercury deposition during the end-Pliensbachian extinction and Toarcian OAE: A link to the Karoo-Ferrar Large Igneous Province. *Earth Planet. Sci. Lett.* 428, 267–280.

- Percival, L.M.E., Cohen, A.S., Davies, M.K., Dickson, A.J., Hesselbo, S.P., Jenkyns, H.C., Leng, M.J., Mather, T.A., Storm, M.S., Xu, W., 2016. Osmium isotope evidence for two pulses of increased continental weathering linked to early Jurassic volcanism and climate change. *Geology* 44, 759–762.
- Pienkowski, G., Hodbod, M., Ullmann, C.V., 2016. Fungal decomposition of terrestrial organic matter accelerated early Jurassic climate warming. *Sci. Rep.* 6, 31930. <https://doi.org/10.1038/srep31930>.
- Pittet, B., Suan, G., Lenoir, F., Duarte, L.V., Mattioli, E., 2014. Carbon isotope evidence for sedimentary discontinuities in the lower Toarcian of the Lusitanian Basin (Portugal): Sea level change at the onset of the Oceanic Anoxic Event. *Sediment. Geol.* 303, 1–14.
- Polgári, M., Okita, P.M., Hein, J.R., 1991. Stable isotope evidence for the origin of the Úrkút manganese ore deposit, Hungary. *J. Sediment. Res.* 61, 384–393.
- Polgári, M., Hein, J.R., Vigh, T., Szabó-Drubina, M., Fórész, I., Bíró, L., Müller, A., Tóth, A.L., 2012. Microbial processes and the origin of the Úrkút manganese deposit, Hungary. *Ore Geol. Rev.* 47, 87–109.
- Posenato, R., Bassi, D., Trecalli, A., Parente, M., 2018. Taphonomy and evolution of lower Jurassic lithiotid bivalve accumulations in the Apennine Carbonate Platform (southern Italy). *Palaeogeogr. Palaeoclimatol. Palaeoecol.* 489, 261–271.
- Raiswell, R., Canfield, D.E., 2012. The iron biogeochemical cycle past and present. *Geochem. Perspect.* 1, 1–220.
- Rajendran, A., Dileepkumar, M., Bakker, J.F., 1992. Control on manganese and iron in Skagerrak sediment (northeastern North-Sea). *Chem. Geol.* 98, 111–129.
- Remirez, M.N., Algeo, T.J., 2020a. Paleosalinity determination in ancient epicontinental seas: a case study of the T-OAE in the Cleveland Basin (UK). *Earth Sci. Rev.* 201, 103072.
- Remirez, M.N., Algeo, T.J., 2020b. Carbon-cycle change during the Toarcian (early Jurassic) and implications for regional versus global drivers of the Toarcian oceanic anoxic event. *Earth Sci. Rev.* 209, 103283.
- Reolid, M., 2014. Stable isotopes on foraminifera and ostracods for interpreting incidence of the Toarcian Oceanic Anoxic Event in Westernmost Tethys: role of water stagnation and productivity. *Palaeogeogr. Palaeoclimatol. Palaeoecol.* 395, 77–91.
- Reolid, M., Rodríguez-Tovar, F.J., Marok, A., Sébâne, A., 2012. The Toarcian oceanic anoxic event in the Western Saharan Atlas, Algeria (North African paleomargin): Role of anoxia and productivity. *Geol. Soc. Am. Bull.* 124, 1646–1664.
- Reolid, M., Mattioli, E., Nieto, L.M., Rodríguez-Tovar, F.J., 2014a. The early Toarcian Oceanic Anoxic Event in the External Subtetic (Southibrian Palaeomargin, Westernmost Tethys): Geochemistry, nannofossils and ichnology. *Palaeogeogr. Palaeoclimatol. Palaeoecol.* 411, 79–94.
- Reolid, M., Marok, A., Sébâne, A., 2014b. Foraminiferal assemblages and geochemistry for interpreting the incidence of early Toarcian environmental changes in North Gondwana palaeomargin (Traras Mountains, Algeria). *J. Afr. Earth Sci.* 95, 105–122.
- Reolid, M., Molina, J.M., Nieto, L.M., Rodríguez-Tovar, F.J., 2018. The Toarcian Oceanic Anoxic Event in the South Iberian Palaeomargin. *SpringerBriefs Earth Sci.* 122 p.
- Reolid, M., Iwanickzuk, J., Mattioli, E., Abad, I., 2020a. Integration of gamma ray spectrometry, magnetic susceptibility and calcareous nannofossils for interpreting environmental perturbations: an example from the Jenkyns Event (lower Toarcian) from South Iberian Palaeomargin (median Subbetic, SE Spain). *Palaeogeogr. Palaeoclimatol. Palaeoecol.* 560, 110031.
- Reolid, M., Mattioli, E., Duarte, L.V., Marok, A., 2020b. The Toarcian Oceanic Anoxic Event and the Jenkyns Event (IGCP-655 final report). *Episodes* 43, 833–844.
- Reolid, M., Mattioli, E., Duarte, L.V., Ruebsam, W., 2021a. The Toarcian Oceanic Anoxic Event: Where do we stand? In: Reolid, M., Duarte, L.V., Mattioli, E., Ruebsam, W. (Eds.), *Carbon Cycle and Ecosystem Response to the Jenkyns Event in the Early Toarcian (Jurassic)*, Geological Society, London, Special Publications, vol. 514, pp. 1–11.
- Reolid, M., Soussi, M., Reolid, J., Ruebsam, W., Taher, I.B., Mattioli, E., Saidi, M., Schwark, L., 2021b. The onset of the early Toarcian flooding of the Pliensbachian carbonate platform of Central Tunisia (north-south axis) as inferred from trace fossils and geochemistry. In: Reolid, M., Duarte, L.V., Mattioli, E., Ruebsam, W. (Eds.), *Carbon Cycle and Ecosystem Response to the Jenkyns Event in the Early Toarcian (Jurassic)*, Geological Society, London, Special Publications, vol. 514, pp. 213–238.
- Reolid, M., Soussi, M., Ruebsam, W., Taher, I.B.H., Mattioli, E., Saidi, M., Schwark, L., 2023. Ecosystem recovery in the Châabat El Attaris section of the Tunisian Atlas. *Palaeogeogr. Palaeoclimatol. Palaeoecol.* 111832.
- Rodrigues, B., Silva, R.L., Reolid, M., Filho, J.G.M., Duarte, L.V., 2019. Sedimentary organic matter and $\delta^{13}\text{C}_{\text{Kerogen}}$ variation on the southern Iberian palaeomargin (Betis Cordillera, SE Spain) during the latest Pliensbachian-Early Toarcian. *Palaeogeogr. Palaeoclimatol. Palaeoecol.* 534, 109342.
- Rodrigues, B., Duarte, L.V., Silva, R.L., Filho, J.G.M., 2020a. Sedimentary organic matter and early Toarcian environmental changes in the Lusitanian Basin (Portugal). *Palaeogeogr. Palaeoclimatol. Palaeoecol.* 554, 109781.
- Rodrigues, B., Silva, R.L., Filho, J.G.M., Comas-Rengifo, Goy, A., Duarte, L.V., 2020b. Kerogen assemblages and $\delta^{13}\text{C}_{\text{Kerogen}}$ of the uppermost Pliensbachian-lower Toarcian succession of the Asturian Basin (northern Spain). *Int. J. Coal Geol.* 229, 103573.
- Rodrigues, B., Silva, R.L., Filho, J.G.M., Reolid, M., Sadki, D., Comas-Rengifo, M.J., Goy, A., Duarte, L.V., 2021. The Phytoclast Group as a tracer of palaeoenvironmental changes in the early Toarcian. In: Reolid, M., Duarte, L.V., Mattioli, E., Ruebsam, W. (Eds.), *Carbon Cycle and Ecosystem Response to the Jenkyns Event in the Early Toarcian (Jurassic)*, Geological Society, London, Special Publications, vol. 514, pp. 291–307.
- Rodríguez-Tovar, F.J., 2021. Ichnology of the Toarcian Oceanic Anoxic Event: an underestimated tool to reassess palaeoenvironmental interpretations. *Earth Sci. Rev.* 216, 103579.
- Röhl, H.-J., Schmid-Röhl, A., 2005. Lower Toarcian (Upper Liassic) black shales of the central European epicontinental basin: A sequence stratigraphic case study from the SW German Posidonia Shale. In: Harris, N.B. (Ed.), *The Deposition of Organic Carbon-Rich Sediments: Models, Mechanisms, and Consequences*, vol. 82. Society for Sedimentary Geology, Tulsa, Oklahoma, pp. 165–189.
- Röhl, H.-J., Schmid-Röhl, A., Oschmann, W., Frimmel, A., Schwark, L., 2001. The Posidonia Shale (lower Toarcian) of SW-Germany: an oxygen-depleted ecosystem controlled by sea level and palaeoclimate. *Palaeogeogr. Palaeoclimatol. Palaeoecol.* 165, 27–52.
- Rosales, I., Robles, S., Quesada, S., 2004. Elemental and oxygen isotope composition of early Jurassic belemnites: Salinity vs. temperature signals. *J. Sediment. Res.* 74, 342–354.
- Rosales, I., Barnolas, A., Goy, A., Sevillano, A., Armendáriz, M., López-García, J.M., 2018. Isotope records (C-O-Sr) of late Pliensbachian-early Toarcian environmental perturbations in the westernmost Tethys (Majorca Island, Spain). *Palaeogeogr. Palaeoclimatol. Palaeoecol.* 497, 168–185.
- Ruebsam, W., Al-Husseini, M., 2020. Calibrating the early Toarcian (early Jurassic) with stratigraphic black holes (SBH). *Gondwana Res.* 82, 317–336.
- Ruebsam, W., Münzberger, P., Schwark, L., 2014. Chronology of the early Toarcian environmental crisis in the Lorraine Sub-Basin (NE Paris Basin). *Earth Planet. Sci. Lett.* 404, 273–282.
- Ruebsam, W., Müller, T., Kovács, J., Pálfy, J., Schwark, L., 2018. Environmental response to the early Toarcian carbon cycle and climate perturbations in the northeastern part of the West Tethys shelf. *Gondwana Res.* 59, 144–158.
- Ruebsam, W., Mayer, B., Schwark, L., 2019. Cryosphere carbon dynamics control early Toarcian global warming and sea level evolution. *Glob. Planet. Chang.* 172, 440–453.
- Ruebsam, W., Reolid, M., Schwark, L., 2020a. $\delta^{13}\text{C}$ of terrestrial vegetation records Toarcian CO₂ and climate gradients. *Sci. Rep.* 10, 117. <https://doi.org/10.1038/s41598-019-56710-6>.
- Ruebsam, W., Reolid, M., Marok, A., Schwark, L., 2020b. Drivers of benthic extinction during the early Toarcian (early Jurassic) at the northern Gondwana paleomargin: Implications for paleoceanographic conditions. *Earth Sci. Rev.* 203, 103117.
- Ruebsam, W., Pienkowski, G., Schwark, L., 2020c. Toarcian climate and carbon cycle perturbations – its impact on sea-level changes, enhanced mobilization and oxidation of fossil organic matter. *Earth Planet. Sci. Lett.* 546, 116417.
- Ruebsam, W., Reolid, M., Sabatino, N., Masetti, D., Schwark, L., 2020d. Molecular paleothermometry of the early Toarcian climate perturbation. *Glob. Planet. Chang.* 195, 103351. <https://doi.org/10.1016/j.gloplacha.2020.103351>.
- Ruebsam, W., Thibault, N., Al-Husseini, M., 2020e. Chapter 12 - Early Toarcian glacio-eustatic unconformities and chemostratigraphic black holes. In: Montenari, M. (Ed.), *Stratigraphy & Timescales*, vol. 5. Elsevier-Inc., pp. 629–676.
- Ruebsam, W., Reolid, M., Mattioli, E., Schwark, L., 2022a. Organic carbon accumulation at the northern Gondwana paleomargin (Tunisia) during the Toarcian Oceanic Anoxic Event: Sedimentological and geochemical evidence. *Palaeogeogr. Palaeoclimatol. Palaeoecol.* 586, 110781.
- Ruebsam, W., Mattioli, E., Schwark, L., 2022b. Weakening of the biological pump induced by a biocalcification crisis during the early Toarcian Oceanic Anoxic Event. *Glob. Planet. Chang.* 217, 103954.
- Ruhl, M., Hesselbo, S.P., Jenkyns, H.C., Xu, W., Silva, R.L., Matthews, K.J., Mather, T.A., Mac Niocaill, C., Riding, J.B., 2022. Reduced plate motion controlled timing of early Jurassic Karoo-Ferrar large igneous province volcanism. *Sci. Adv.* 8, eab00866.
- Sabatino, N., Neri, R., Bellanca, A., Jenkyns, H.C., Baudin, F., Parisi, G., Masetti, D., 2009. Carbon-isotope records of the early Jurassic (Toarcian) oceanic anoxic event from the Valdorbia (Umbria-Marche Apennines) and Monte Mangart (Julian Alps) sections: palaeoceanographic and stratigraphic implications. *Sedimentology* 56, 1307–1328.
- Sabatino, N., Neri, R., Bellanca, A., Jenkyns, H.C., Masetti, D., Scopelliti, G., 2011. Petrography and high-resolution geochemical records of lower Jurassic manganese-rich deposits from Monte Mangart, Julian Alps. *Palaeogeogr. Palaeoclimatol. Palaeoecol.* 299, 97–109.
- Sabatino, N., Vlahovic, I., Jenkyns, H.C., Scopelliti, G., Neri, R., Prtoljan, B., Velić et al., 2013. Carbon-isotope record and palaeoenvironmental changes during the early Toarcian oceanic anoxic event in shallow-marine carbonates of the Adriatic Carbonate Platform in Croatia. *Geol. Mag.* 150, 1085–1102.
- Sælen, G., Doyle, P., Talbot, M.R., 1996. Stable isotope analysis of belemnite rostra from the Whitby Mudstone Formation, England: surface water conditions during deposition of a marine black shale. *Palaios* 11, 97–117.
- Sælen, G., Tyson, R.V., Telnes, N., Talbot, M.R., 2000. Contrasting watermass conditions during deposition of the Whitby Mudstone (lower Jurassic) and Kim-meridge Clay (Upper Jurassic) formations, UK. *Palaeogeogr. Palaeoclimatol. Palaeoecol.* 163, 163–196.
- Schettino, A., Turco, E., 2011. Tectonic history of the western Tethys since the late Triassic. *GSA Bull.* 123, 89–105.
- van de Schootbrugge, B., Bailey, T.R., Rosenthal, Y., Katz, M.E., Wright, J.D., Miller, K.G., Feist-Burkhardt, S., Falkowski, P.G., 2005. Early Jurassic climate change and the radiation of organic-walled phytoplankton in the Tethys Ocean. *Paleobiology* 31, 73–97.
- van de Schootbrugge, B., Richoz, S., Pross, J., Luppold, F.W., Hunze, S., Wonik, T., Blau, J., Meister, C., van der Weijst, C.M.H., Suan, G., Fraguas, A., Fiebig, J., Herrelle, J.O., Guex, J., Little, C.T.S., Wignall, P.B., Püttmann, W., Oschmann, W., 2019. The Schandelah Scientific Drilling Project: a 25-million year record of early

- Jurassic palaeoenvironmental change from northern Germany. *Newsl. Stratigr.* 52, 249–296.
- van de Schootbrugge, B., Houben, A.J.P., Ercan, F.E.Z., Verreussel, R., Kerstholt, S., Janssen, N.M.M., Nikitenko, B., Suan, G., 2020. Enhanced Arctic-Tethys connectivity ended the Toarcian Oceanic Anoxic Event in NW Europe. *Geol. Mag.* 157, 1593–1611.
- Schouten, S., van Kaam-Peters, H.M.E., Rijpstra, W.I.C., Schoell, M., Sinnighe Damsté, J.S., 2000. Effects of an oceanic anoxic event on the stable carbon isotopic composition of early Toarcian carbon. *Am. J. Sci.* 300, 1–22.
- Schwarz, L., Frimmel, A., 2004. Chemostratigraphy of the Posidonia Black Shale, SW-Germany II. Assessment of extent and persistence of photic-zone anoxia using aryl isoprenoid distributions. *Chem. Geol.* 206, 185–211.
- Silva, R.L., Duarte, L.V., 2015. Organic matter production and preservation in the Lusitanian Basin (Portugal) and Pliensbachian climatic hot snaps. *Glob. Planet. Chang.* 131, 24–34.
- Silva, R.L., Duarte, L.V., Wach, G.D., Ruhl, M., Sadki, D., Gómez, J.J., Hesselbo, S.P., Xu, W., O'Connor, D., Rodrigues, B., Mendonça Filho, J.G., 2021a. An early Jurassic (Sinemurian–Toarcian) stratigraphic framework for the occurrence of Organic Matter Preservation Intervals (OMPIs). *Earth Sci. Rev.* 221, 103780.
- Silva, R.L., Ruhl, M., Barry, C., Reolid, M., Ruebsam, W., 2021b. Pacing of late Pliensbachian and early Toarcian carbon cycle perturbations and environmental change in the westernmost Tethys (La Cerradura Section, Subbetic zone of the Betic Cordillera, Spain). In: Reolid, M., Duarte, L.V., Mattioli, E., Ruebsam, W. (Eds.), *Carbon Cycle and Ecosystem Response to the Jenkyns Event in the Early Toarcian (Jurassic)*. Geological Society, London, Special Publications, vol. 514, pp. 387–408.
- Simo, V., Reolid, M., 2021. Palaeogeographical homogeneity of trace-fossil assemblages in lower Jurassic spotted marls and limestones: Comparison of the Western Carpathians and the Betic Cordillera. In: Reolid, M., Duarte, L.V., Mattioli, E., Ruebsam, W. (Eds.), *Carbon Cycle and Ecosystem Response to the Jenkyns Event in the Early Toarcian (Jurassic)*. Geological Society, London, Special Publications, vol. 514, pp. 121–152.
- Sinnighe Damsté, J., Kenig, F., Koopmans, M., Köster, J., Schouten, S., Hayes, J., de Leeuw, J., 1995. Evidence for gammacerane as an indicator of water column stratification. *Geochim. Cosmochim. Acta* 59, 1895–1900.
- Sinnighe Damsté, J.S., Wakeham, S.G., Kohnen, M.E.L., Hayes, J.M., de Leeuw, J.W., 1993. A 6,000-year sedimentary molecular record of chemocline excursions in the Black Sea. *Nature* 362, 827–829.
- Storm, M.S., Hesselbo, S.P., Jenkyns, H.C., Ruhl, M., Ullmann, C.V., Xu, W., Leng, M.J., Riding, J.B., Gorbanenko, O., 2020. Orbital pacing and secular evolution of the early Jurassic carbon cycle. *Proc. Natl. Acad. Sci.* 117, 3974–3982.
- Suan, G., Mattioli, E., Pittet, B., Lécuyer, C., Stuchéras-Marx, B., Duarte, L.V., Philippe, M., Reggiani, L., Martineau, F., 2010. Secular environmental precursors to early Toarcian (Jurassic) extreme climate changes. *Earth Planet. Sci. Lett.* 290, 448–458.
- Suan, G., van de Schootbrugge, B., Adatte, T., Fiebig, J., Oschmann, W., 2015. Calibrating the magnitude of the Toarcian carbon cycle perturbation. *Paleoceanography* 30, 495–509.
- Suan, G., Schlögl, J., Mattioli, E., 2016. Bio- and chemostratigraphy of the Toarcian organic-rich deposits of some key successions of the Alpine Tethys. *Newsl. Stratigr.* 49 (3), 401–419.
- Suan, G., Schöllhorn, I., Schlögl, J., Segit, T., Mattioli, E., Lécuyer, C., Fourel, F., 2018. Euxinic conditions and high sulfur burial near the European shelf margin (Pieniny Klippen Belt, Slovakia) during the Toarcian oceanic anoxic event. *Glob. Planet. Chang.* 170, 246–259.
- Summons, R.E., Powell, T.G., 1986. Chlorobiaceae in Phanerozoic seas revealed by biological markers, isotopes and geology. *Nature* 319, 763–765.
- Svensen, H.H., Planke, S., Chevallier, L., Malthe-Sørensen, A., Corfu, F., Jamtveit, B., 2007. Hydrothermal venting of greenhouse gases triggering early Jurassic global warming. *Earth Planet. Sci. Lett.* 256, 554–566.
- Them II, T.R., Gill, B.C., Caruthers, A.H., Gröcke, D.R., Tulsky, E.T., Martindale, R.C., Poult, T.P., Smith, P.L., 2017. High-resolution carbon isotope records of the Toarcian Oceanic Anoxic Event (early Jurassic) from North America and implications for the global drivers of the Toarcian carbon cycle. *Earth Planet. Sci. Lett.* 459, 118–126.
- Them, T.R., Gill, B.C., Selby, D., Gröcke, D.R., Friedman, R.M., Owens, J.D., 2017. Evidence for rapid weathering response to climatic warming during the Toarcian Oceanic Anoxic Event. *Sci. Rep.* 7, 5003. <https://doi.org/10.1038/s41598-017-05307-y>.
- Thibault, N., Ruhl, M., Ullmann, C.V., Korte, C., Kemp, D.B., Gröcke, D.R., Hesselbo, S.P., 2018. The wider context of the lower Jurassic Toarcian oceanic anoxic event in Yorkshire coastal outcrops, UK. *Proc. Geol. Assoc.* 129, 372–391.
- Trabucho-Alexandre, J., Dirkx, R., Veld, H., Klaver, G., De Boer, P., 2012. Toarcian black shales in the Dutch Central Graben: record of energetic, variable depositional conditions during an oceanic anoxic event. *J. Sediment. Res.* 82, 104–120.
- Trecalli, A., Spangenberg, J., Adatte, T., Föllmi, K.B., Parente, M., 2012. Carbonate platform evidence of ocean acidification at the onset of the early Toarcian oceanic anoxic event. *Earth Planet. Sci. Lett.* 357–358, 214–225.
- Tremolada, F., van de Schootbrugge, B., Erba, E., 2005. Early Jurassic schizophaerellid crisis in Cantabria, Spain: Implications for calcification rates and phytoplankton evolution across the Toarcian oceanic anoxic event. *Paleoceanography* 20, PA2011. <https://doi.org/10.1029/2004PA001120>.
- Tribouillard, N., Algeo, T.J., Lyons, T., Ribouleau, A., 2006. Trace metals as paleoredox and paleoproductivity proxies: an update. *Chem. Geol.* 232, 12–32.
- Tyson, R.V., Pearson, T.H., 1991. Modern and ancient continental shelf anoxia: An overview. In: Tyson, R.V., Pearson, T.H. (Eds.), *Modern and Ancient Continental Shelf Anoxia*, vol. 58. Geological Society Special Publication. Geological Society of London Special Publication, London, UK, pp. 1–24.
- Ullmann, C.V., Hesselbo, S.P., Korte, C., 2013. Tectonic forcing of early to Middle Jurassic seawater Sr/ca. *Geology* 41, 211–214.
- Vető, I., Demény, A., Hertelendi, E., Hetényi, M., 1997. Estimation of primary productivity in the Toarcian Tethys—a novel approach based on TOC, reduced Sulphur and manganese contents. *Palaeogeogr. Palaeoclimatol. Palaeoecol.* 132, 355–371.
- Visentini, S., Erba, E., 2021. High-resolution calcareous nannofossil biostratigraphy 1 across the Toarcian Oceanic Anoxic Event in northern Italy: clues from the Sogno and Gajum Cores (Lombardy Basin, Southern Alps). *Riv. Ital. Paleontol. Stratigr.* 127, 539–556.
- Visentini, S., Erba, E., Mutterlose, J., 2021. Bio- and chemostratigraphy of the Posidonia Shale: a new database for the Toarcian Anoxic Event from northern Germany. *Newsl. Stratigr.* <https://doi.org/10.1127/nos/2021/0658>.
- Wang, Y., Ossa Ossa, F., Wille, M., Schurr, S., Saussele, M.-E., Schmid-Röhl, Schoenberg, R., 2020. Evidence for local carbon-cycle perturbations superimposed on the Toarcian carbon isotope excursion. *Geobiology* 18, 682–709.
- Wang, Y., Ossa Ossa, F., Spangenberg, J.E., Wille, M., Schoenberg, R., 2021. Restricted oxygen-deficient basins on the northern European epicontinental shelf across the Toarcian carbon isotope excursion interval. *Paleoceanogr. Paleoclimatol.* 36 <https://doi.org/10.1029/2020PA004207> e2020PA004207.
- Wei, W., Algeo, T.J., 2020. Elemental proxies for paleosalinity analysis of ancient shales and mudrocks. *Geochim. Cosmochim. Acta* 287, 341–366.
- Wei, W., Algeo, T.J., Lu, Y., Lu, Y.G., Liu, H., Zhang, S., Peng, L., Zhang, J., Chen, L., 2018. Identifying marine incursions into the Paleogene Bohai Bay Basin lake system in northeastern China. *Int. J. Coal Geol.* 200, 1–17.
- Wiedenmayer, F., 1980. Die Ammoniten der Mittelrheinischen Provinz im Pliensbachian und unteren Toarcian aufgrund neuer Untersuchungen im Generoso-Becken (Lombardische Alpen). *Denkschriften Schweizerischen Nat. Gesellschaft* 93, 263 pp.
- Wijsman, J.W.M., Middelburg, J.J., Heip, C.H.R., 2001. Reactive iron in Black Sea sediments: implications for iron cycling. *Mar. Geol.* 172, 167–180.
- Wilkin, R.T., Barnes, H.L., 1996. Formation processes of frambooidal pyrite. *Geochim. Cosmochim. Acta* 61, 323–339.
- Wilkin, R.T., Barnes, H.L., Brantley, S.L., 1996. The size distribution of frambooidal pyrite in modern sediments: an indicator of redox conditions. *Geochim. Cosmochim. Acta* 60, 3897–3912.
- Winterer, E.L., 1998. Paleobathymetry of Mediterranean Tethyan Jurassic pelagic sediments. *Mem. Soc. Geol. Ital.* 53, 97–131.
- Woodfine, R.G., Jenkyns, H.C., Sarti, M., Baroncini, F., Violante, C., 2008. The response of two Tethyan carbonate platforms to the early Toarcian (Jurassic) oceanic anoxic event: environmental change and differential subsidence. *Sedimentology* 55, 1011–1028.
- Xu, W., Ruhl, M., Jenkyns, H.C., Hesselbo, S.P., Riding, J.B., Selby, D., Naafs, B.D.A., Weijers, J.W.H., Pancost, R.D., Tegelaar, E., Idiz, E., 2017. Carbon sequestration in an expanded lake system during the Toarcian oceanic anoxic event. *Nat. Geosci.* 10, 129–134.
- Xu, W., Ruhl, M., Jenkyns, H.C., Leng, M.J., Huggett, J.M., Minisini, D., Ullmann, C.V., Riding, J.B., Weijers, J.W., Storm, M.S., Percival, L.M., 2018. Evolution of the Toarcian (early Jurassic) carbon-cycle and global climatic controls on local sedimentary processes (Cardigan Bay Basin, UK). *Earth Planet. Sci. Lett.* 484, 396–411.
- Zimmermann, J., Franz, M., Schaller, A., Wolfgramm, M., 2017. The Toarcian–Bajocian deltaic system in the North German Basin: Subsurface mapping of ancient deltas-morphology, evolution and controls. *Sedimentology* 65, 897–930.